Abschlussbericht über das F+E Vorhaben

im BMBF-Verbundprojekt:

Spininjektion, Spintransport, und Spinkohärenz für neuartige Spintronik-Bauelemente bei Raumtemperatur

Teilvorhaben:

„Hybridstrukturen aus Halbleitern und ferromagnetischen Materialien“

Förderkennzeichen: 13N8255
Förderzeitraum: 01.02.2002 – 31.01.2005
Projektleiter: Prof. K. H. Ploog

zusammengestellt von
Dr. Jens Herfort und Prof. Klaus H. Ploog

Paul-Drude-Institut für Festkörperelektronik
Hausvogteiplatz 5-7, 10117 Berlin

Berlin, 31.07.2005

I. Kurze Darstellung

1. Aufgabenstellung

Ziel des Verbundprojektes war es, einen Beitrag zu den offenen technologischen und physikalischen Fragestellungen zur Realisierung eines Spintronik-Bauelementes bei Raumtemperatur zu leisten. Hierbei standen die elektrische Spininjektion vom Ferromagneten (FM) in den Halbleiter (HL) sowie der Spintransport und die Spinkontrolle innerhalb des Halbleiters im Mittelpunkt. Die Schwerpunkte der Arbeiten am Paul-Drude-Institut lagen in der gezielten Herstellung von FM/HL Hybridstrukturen mittels Molekularstrahlepitaxie (MBE) und deren strukturellen Charakterisierung mittels hochauflösender Methoden, der Bestimmung der magnetischen Eigenschaften mittels Kerr-Effekts-, SQUID- und Magnetotransportmagnetometrie, sowie der Bestimmung der Spininjektionseffizienz im Halbleiter. Weiterhin sollten geeignete Strukturierungsverfahren (Ätzverfahren, Lift-Off, Kontaktieren) entwickelt werden, um die Bestimmung des injizierten Spinzustandes zu ermöglichen.

2. Voraussetzungen

Zu den Voraussetzungen, unter denen das Vorhaben durchgeführt wurde gehört, dass international sehr intensiv sowohl an der möglichen Realisierung von Bauelementen, die den Spin der Elektronen ausnutzen als auch an der Weiterentwicklung und Verbesserung von Ferromagnet/Halbleiter-Hybridstrukturen gearbeitet wird. Dazu war es notwendig, ständig den Vergleich mit dem internationalen Stand der Forschung zu ziehen und die gezielten Ergebnisse zeitnah, d.h. bereits vor Projektablauf, in einschlägigen Fachzeitschriften und auf internationalen Konferenzen zu veröffentlichen. Das Wachstum der FM/HL-Hybridstrukturen wurde in einer vorhandenen Mehrkammer-Molekularstrahlepitaxie-Anlage (III-V-HL-MBE, FM-MBE, Schleusen- und Ladekammer) durchgeführt. Die FM-MBE-Kammer wurde entsprechend des Investitionsplans um zwei Hochtemperatureffisionszellen erweitert. Gezielte Investitionen (finanziert aus dem Projekt 01BM907) schufen im Vorfeld des Projektes die experimentellen Voraussetzungen, die magnetischen Eigenschaften der Schichten sowohl *in-situ* (Kerr-Effekt-Meßaufbau in der Molekularstrahlepitaxie-Kammer) als auch *ex-situ* mittels eines SQUID-Magnetometers zu untersuchen. Weitere Investitionen wurden nicht getätigt.

3. Planung und Ablauf

Planung und Verlauf des Vorhabens erfolgte gemäß des in der Antragsformulierung aufgestellten Balkenplans (Meilensteinplanung). Der Zeitplan wurde eingehalten. Die Untersuchungen wurden mit dem Fe/GaAs-Materialsystem begonnen. Die ursprünglich vorgesehene Erweiterung auf das Fe/Co-Materialsystem wurde in Abstimmung mit den Verbundpartner nicht durchgeführt. Stattdessen wurde bereits wenige Monate nach Projektstart intensiv mit der Herstellung und Charakterisierung von Fe_3Si/GaAs-Hybridstrukturen begonnen und im gesamten Verlauf des Projekts fortgeführt. Dabei erwiesen sich die höhere thermische Stabilität dieser Schichten (insbesondere der Grenzflächen), die bessere Gitteranpassung und die hohe Schichtqualität als vorteilhaft für die weitere Anwendung dieses Materialsystems zur Realisierung spintronischer Bauelemente und rechtfertigen somit die Modifizierung des Ablaufplanes. Die Ergebnisse zum Fe/GaAs-Materialsystem, die zu Beginn des Projektes erzielt wurden, sind in den Abschlußbericht des vom BMBF geförderten Vorhabens 01BM907, das teilweise zeitlich parallel verlief, thematisch integriert wurden. Die wesentlichen Ergebnisse dieses Vorhabens, die Untersuchungen der Fe_3Si/GaAs-Hybridstrukturen, werden im Abschnitt II ausführlich dargestellt.

4. Wissenschaftlich technischer Stand an den angeknüpft wurde

Das Vorhaben knüpfte an den wissenschaftlich technischen Stand, der in einem vom BMBF geförderten Vorhaben 01BM907 erreicht wurde an. Der experimentelle Aufbau wurde mit den unter den Voraussetzungen genannten Apparaturen realisiert. An Fachliteratur wurden die einschlägigen Fachzeitschriften, der Informations- und Dokumentationsdienst INSPEC genutzt.

5. Zusammenarbeit mit anderen Stellen

Die Untersuchungen wurden im Rahmen des Verbundprojektes in enger Zusammenarbeit mit der Gruppe von Prof. G. Güntherodt und Dr. B. Beschoten (Rheinisch-Westfälische Technische Hochschule Aachen) durchgeführt. Dabei standen die Bestimmung Ladungsträgerrekombinationszeiten als auch Spinrelaxationszeiten von LED-Strukturen mittels zeitaufgelöster Transmissions-Spektroskopie im Mittelpunkt. Einige Untersuchungen zu den magnetischen Eigenschaften der Fe_3Si/GaAs-Schichten mittel ferromagnetischer Resonanzspektroskopie wurde in Zusammenarbeit mit der Gruppe von Prof. K. Baberschke an der Freien Universität Berlin durchgeführt. Eine enge Zusammenarbeit gab es auch innerhalb des Paul-Drude Instituts mit der Gruppe von Dr. W. Braun und Dr. B. Jenichen am Röntgen-Diffraktometer des PDI-Strahlrohrs bei BESSY II (BMBF-Vorhaben 01BM159).

6. Verwertung

Es wurden keine Schutzrechte beantragt.

II. Eingehende Darstellung

Im folgenden werden einige der wichtigsten Ergebnisse, die im Verlauf des Projekts erzielt wurden, ausführlicher dargestellt. Für eine umfassende und tiefergreifende Darstellung der Ergebnisse wird auf die im Anhang zusammengestellten Originalarbeiten verwiesen.

1. Motivation

Bei der Epitaxie von Ferromagnet/Halbleiter-Hybridstrukturen wie z. B. Fe, Co, und Fe_xCo_{1-x}, auf GaAs(001)-Substraten muss die Wachstumstemperatur sehr niedrig gehalten werden (ca. Raumtemperatur), um die Ausbildung von Grenzflächenreaktionen an der Ferromagnet/Halbleiter-Grenzfläche zu unterdrücken. Da diese Grenzflächenverbindungen zu einer Verringerung oder Unterdrückung der Spin-Injektion von Elektronen aus einen ferromagnetischen Metall in einen Halbleiter führen können, ist es wichtig, alternative Materialien zu finden, die sowohl eine verbesserte Grenzflächenqualität als auch eine bessere thermische Stabilität der Ferromagnet/Halbleiter-Grenzfläche aufweisen.

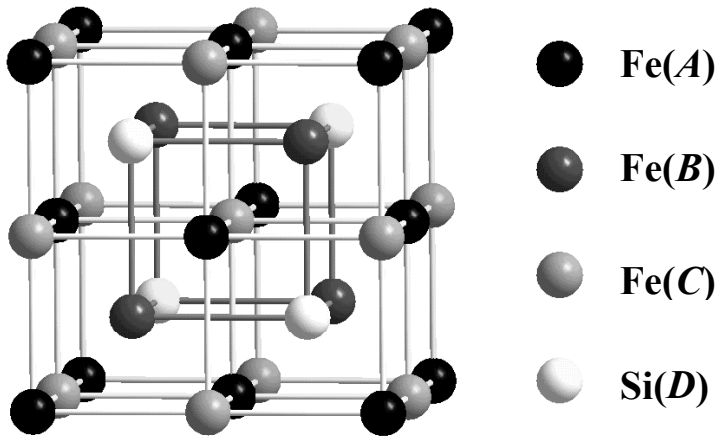

Abb. 1: *Einheitszelle der $D0_3$-Struktur der intermetallischen Verbindung Fe_3Si. Die Gitterplätze sind mit A, B, C, und D bezeichnet.*

Bisher gibt es in der Literatur nur wenige Studien zum Wachstum von Fe_3Si auf GaAs(001)-Substraten, obwohl es nahezu gitterangepasst zu GaAs(001) ist. Weiterhin ist Fe_3Si ferromagnetisch bis 840 K. Fe_3Si hat eine kubische $D0_3$-Struktur und die Einheitszelle besteht aus vier ineinander verschachtelten, kubisch flächenzentrierten Untergittern (Siehe Abb. 1). Die Gitterplätze *A*, *B*, und *C* sind im perfekt geordneten Gitter mit Fe-Atomen und die *D*-Gitterplätze mit Si-Atomen besetzt. Die Fe(*A,C*)-Gitterplätze sind äquivalent und besitzen jeweils vier Fe- und vier Si-Atome als nächste Nachbarn und tragen ein magnetisches Moment von 1.35 μ_B. Die Fe(*B*)-Atome besitzen 8 Fe-Atome als nächste Nachbarn und tragen ein magnetisches Moment von 2.2 μ_B. Fe_3Si kann somit als binäre Heusler-Legierung Fe_2FeSi betrachtet werden, da es analog zu den klassischen Heusler-Legierungen zwei unterschiedliche strukturelle und magnetische Fe-Gitterplätze aufweist. Hinzu kommt, dass für einige Heusler-Legierungen eine 100%-ige Spin-Polarisation an der Fermi-Energie theoretisch vorhergesagt sind, d. h. sie sind halbmetallisch. Allerdings gilt Fe_3Si bisher nicht als halbmetallisch.

2. Wachstum und strukturelle Charakterisierung von Fe_3Si/GaAs(001)-Hybridstrukturen

GaAs(001)-Templates wurden in einer separaten III-V-MBE-Wachstumskammer unter Standard-Wachstumsbedingungen bei 570°C hergestellt. As-reiche GaAs-Ausgangsoberflächen (jeweils mit mit (2×1)- oder c(4×4)-Oberflächenrekonstruktion) wurden präpariert, um die Ausbildung von makroskopischen Defekten zu verhindern. Die GaAs-Schichten wurden dann im UHV in die Wachstumskammer für ferromagnetische Metalle transferiert.

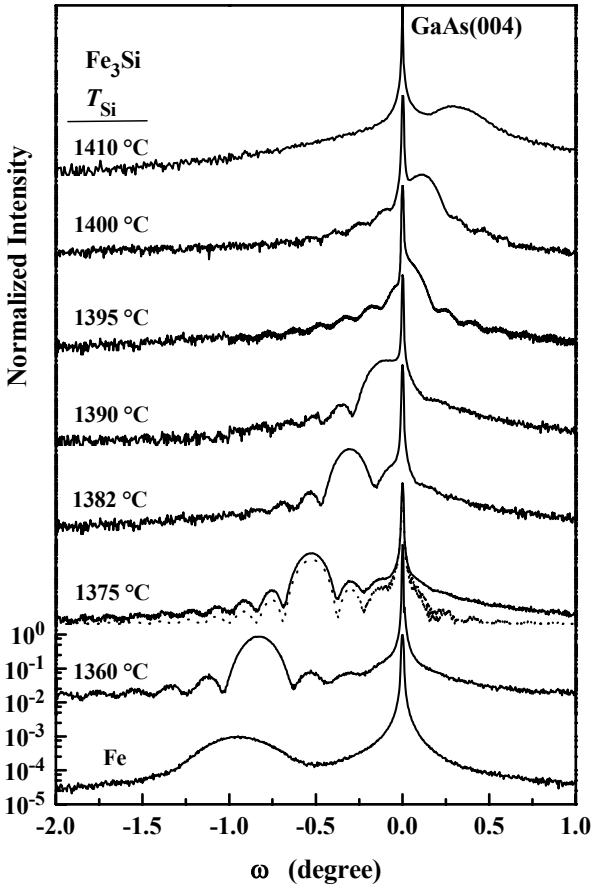

Abb. 2: *Logarithmische Darstellung der normierten Intensität von Röntgenbeugungs-Rocking-Kurven verschiedener Fe_3Si/GaAs(001)-Schichten. Die Wachstumstemperatur beträgt 200 °C. Variiert wurde die Si-Zellentemperatur T_{Si}. Die unterste Rocking-Kurve ist für eine Fe/GaAs(001)-Schicht, die bei 50 °C (optimale Wachstumstemperatur) gewachsen wurde. Die Rocking-Kurven sind auf den GaAs(004)-Reflex des Substrats normiert. Die Kurven sind zur Veranschaulichung untereinander verschoben. Die gestrichelte Linie zeigt eine Simulation der Rocking-Kurve für T_{Si} = 1375 °C.*

Eine Serie von Fe_3Si/GaAs(001)-Hybridstrukturen wurden mittels Molekularstrahlepitaxie (MBE) hergestellt. Dabei wurde Fe und Si gleichzeitig aus Hochtemperatur-Effusionszellen verdampft. Die Wachstumstemperatur der einzelnen Schichten wurde zwischen 50 und 500 °C variiert. Die Komposition der Fe_3Si-Schichten wurde durch eine Änderung der Si-Zellentemperatur bei fester Fe-Zellentemperatur geändert. Abbildung 2 zeigt Ergebnisse von Röntgenbeugungsexperimenten für eine Serie von Fe_3Si/GaAs(001)-Hybridstrukturen. Mit Erhöhung der Si-Zellentemperatur T_{Si} verschiebt sicht der entsprechende Fe_3Si-Peak systematisch bezüglich des GaAs(004)-Reflexes infolge der unterschiedlichen Komposition der Fe_3Si-Schichten. Die strukturelle Perfektion der Schichten als auch die

Grenzflächen-Abruptheit der Schichten erhöhen sich anfangs mit ansteigendem T_{Si}. Oberhalb von $T_{Si} = 1400$ °C nimmt die strukturelle Perfektion stark ab. Das wird deutlich im Auftreten von Interferenz-Oszillationen (bis zur 5. Ordnung) und sehr schmalen Fe_3Si-Peaks. Zum Vergleich haben wir in Abb. 2 eine Simulation der Rocking-Kurve für $T_{Si} = 1375$ °C unter Verwendung des Takagi-Taupin-Formalismus eingefügt. Fit-Parameter sind die Gitterverspannung und die Dicke der Schichten, wobei nur die apparative Verbreiterung des Diffraktometers berücksichtigt wurde. Die Übereinstimmung mit den experimentellen Rocking-Kurven ist ausgezeichnet. Das demonstriert die hohe strukturelle Perfektion der Schichten als auch die Schärfe der Grenzflächen. Es sei darauf hingewiesen, dass Interferenz-Oszillationen in reinen Fe-Schichten nicht beobachtet werden konnten (Siehe Abb. 2).

Es zeigt sich auch, dass die Fe_3Si-Phase (zwischen 10 und 26 at.% Si) mit dem Bereich hoher Kristall- und Grenzflächenperfektion korreliert ist, d. h. für den Bereich $1360 < T_{Si} < 1395$ °C in Abb. 2. Das ist in Abb. 3 verdeutlicht, wo die relaxierte Gitterkonstante als Funktion des Si-Anteils aufgetragen wurde. Die relaxierte Gitterkonstante wurde dabei aus den Röntgenbeugungsexperimenten unter Berücksichtigung der elastischen Konstanten von bulk Fe_3Si bestimmt. Die Komposition der Schichten wird aus dem Vergleich der relaxierten Gitterkonstanten mit den Literaturwerten für bulk $Fe_{3+x}Si_{1-x}$ bestimmt. Der Parameter x beschreibt hier die Abweichung der Komposition von der exakten Stöchiometrie und wird im Folgendem zur Angabe der Komposition verwendet. Es zeigt sich, dass die exakte Stöchiometrie, d. h. $x = 0$, für Schichten, die nahezu gitterangepasst sind, erzielt wird. Für $T_{Si} > 1400$ °C ($x > -0.07$) bildet sich eine neue Fe_xSi_y-Phase aus, die sich auch in den RHEED-Beugungsbildern während des Schicht-Wachstums manifestiert.

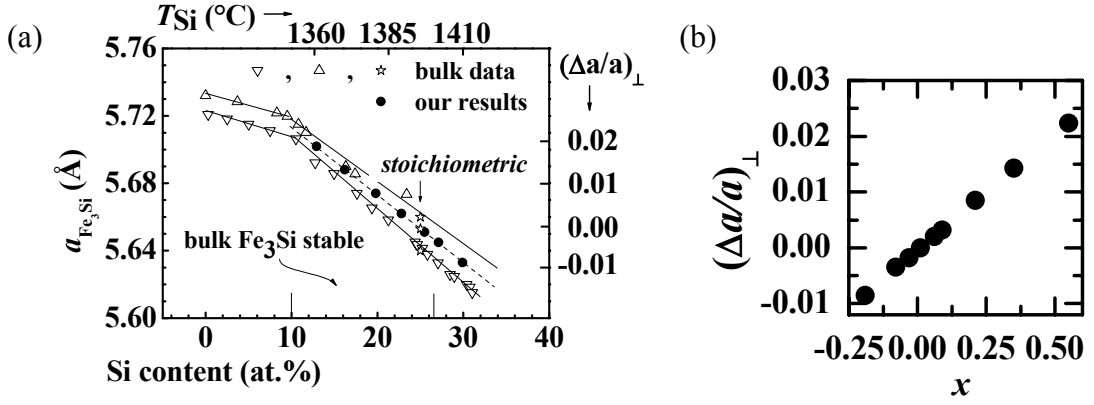

Abb. 3: *(a) Abhängigkeit der relaxierten Gitterkonstante a_{Fe3Si} vom Si-Anteil innerhalb der Fe_3Si-Phase. Die durchgezogenen Linien dienen zur Orientierung, die gestrichelte Linie repräsentiert den Mittelwert der Literaturwerte im Bereich 10 bis 30 at.% Si. Die schwarzen Punkte sind die Ergebnisse der Röntgenbeugungsexperimente (Abb. 2). Zu beachten ist, dass ein größerer Wert für a_{Fe3Si} zu einem niedrigeren T_{Si} in Abb. 2 gehört. (b) Korrelation zwischen der vertikalen Gitterfehlanpassung und der Abweichung von der exakten Stöchiometrie x.*

Weiterhin finden wir einen optimalen Wachstumstemperaturbereich, d. h. $150\ °C < T_G < 250\ °C$. Das ist in Abb. 4 im Ergebnis der Röntgenbeugungsexperimente verdeutlicht. Wichtig ist, dass die optimale Wachstumstemperatur für Fe_3Si/GaAs(001)-Hybridstrukturen wesentlich höher ist als die für das Wachstum von Fe, Co, und Fe_xCo_{1-x} auf GaAs(001)-Substraten. Deshalb ist Fe_3Si für technologische Prozessschritte viel besser geeignet, in denen oftmals Temperaturzyklen notwendig sind, die viel höher als Raumtemperatur sind.

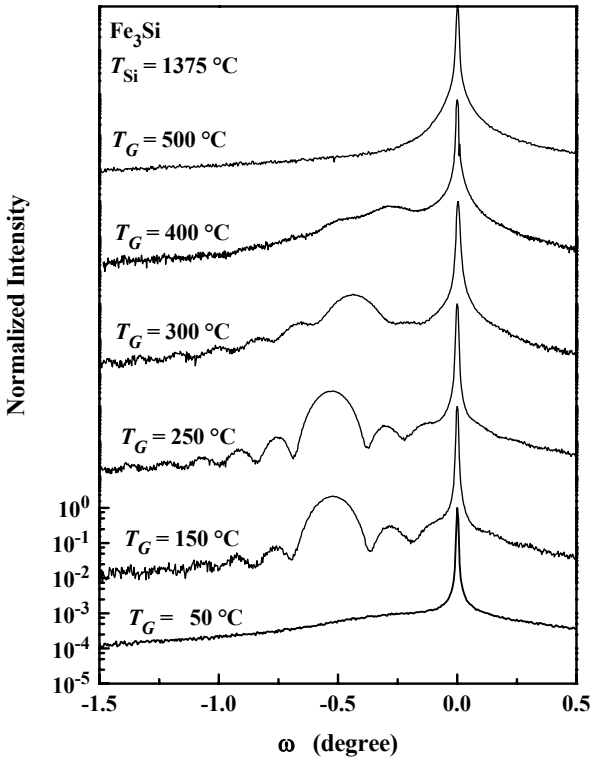

Abb. 4: *Logarithmische Darstellung der normierten Intensität von Röntgenbeugungs-Rocking-Kurven verschiedener Fe_3Si/GaAs(001)-Schichten, die bei unterschiedlichen Wachstumstemperaturen T_G aber bei konstanter Si-Zellentemperatur T_{Si} = 1375 °C hergestellt worden sind. Die Rocking-Kurven sind auf den GaAs(004)-Reflex des Substrats normiert. Die Kurven sind zur Veranschaulichung untereinander verschoben.*

Die Grenzfläche Fe_3Si/GaAs(001) ist weiterhin mittels Transmissionselektronenmikroskopie (TEM) in Abhängigkeit von der Wachstumstemperatur untersucht worden. Typische Ergebnisse sind in Abb. 5 für zwei stöchiometrische Fe_3Si/GaAs(001)-Hybridstrukturen, die bei 250 °C (a) und bei 400 °C (b) gewachsen wurden, dargestellt. Die höhere Grenzflächenperfektion im Falle der niedrigeren Wachstumstemperatur ist klar erkennbar. Die Unterschiede im Interferenzbild zwischen GaAs und Fe_3Si in der [110]-Richtung ermöglichen es, die Position der Grenzfläche genau zu bestimmen. Die Grenzfläche im Fall der niedrigeren Wachstumstemperatur (250 °C) ist abrupt innerhalb von 2 bis 3 Monolagen. Die Schicht ist kohärent verspannt, was sich in der perfekten Übereinstimmung der Fe_3Si(220) und der GaAs(220) atomaren Ebenen an der Grenzfläche dokumentiert. Weiterhin finden wir keine Reaktionsschicht an der Grenzfläche über die gesamte Schichtfläche (mehrere μm gerastert). Das ist auch im niedrigauflösenden Hellfeldbild (Einschub von Abb. 5(a)) erkennbar. Die dunkle Linie identifiziert die Grenzfläche, stellt jedoch keine Reaktionsschicht dar. Im Gegensatz dazu kann bei höheren Wachstumstemperaturen eine ausgedehnte Reaktionsschicht nachgewiesen werden (Abb. 5(b)). Die Reaktionsschicht besteht aus verschiedenen, flachen Präzipitaten unterschiedlicher kristalliner Phasen. In diesem Fall finden wir eine wesentlich rauere Grenzfläche mit einer hohen Stufendichte zwischen den einzelnen Phasen. Die Ergebnisse spiegeln sich auch im Beugungsbild wider, in dem zusätzliche Spots auftreten, die zu den verschiedenen Phasen gehören (Siehe Pfeile im SAD-Bild der Abb. 5(b)).

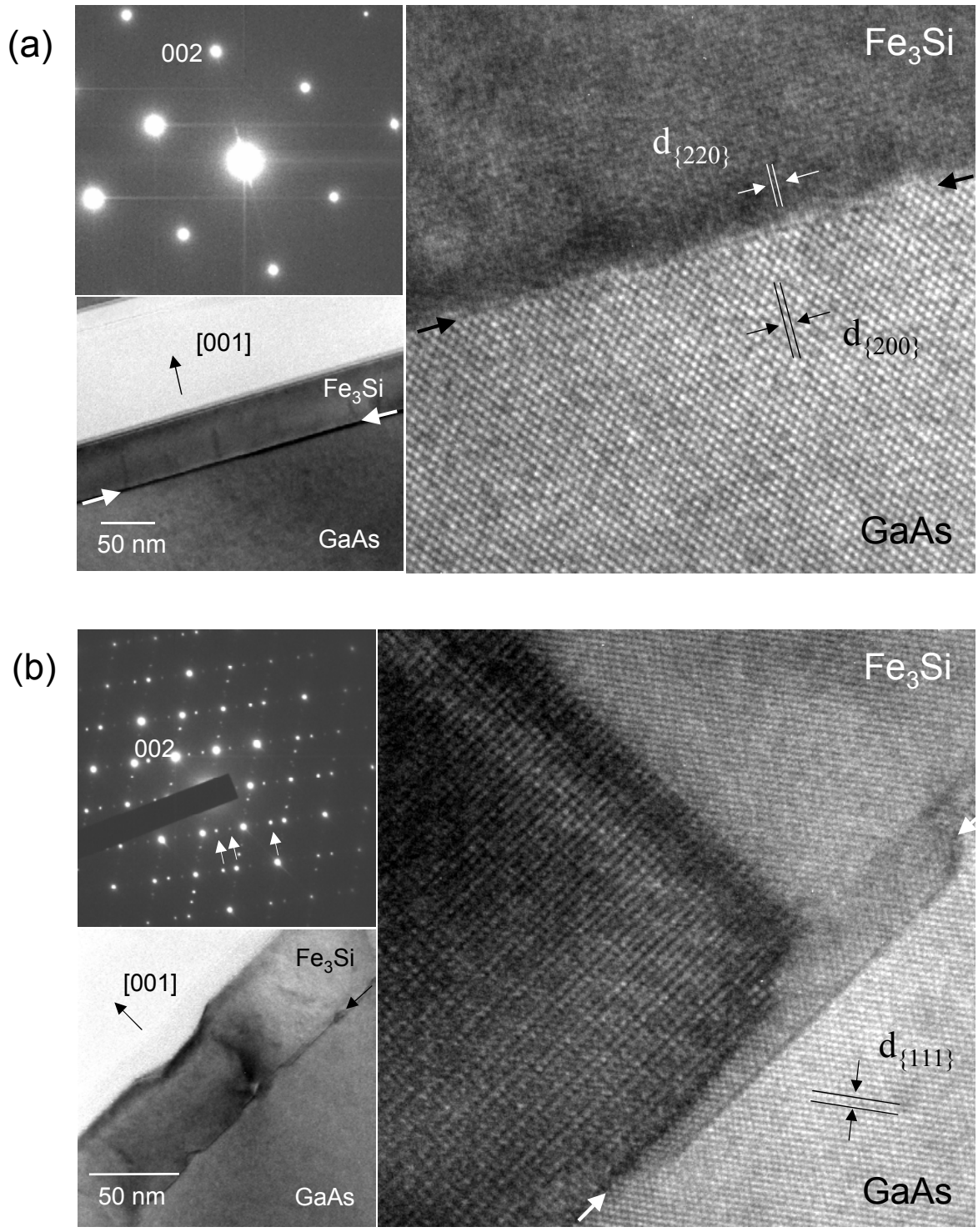

Abb. 5: *Hochauflösende Querschnitts-TEM-Bilder von zwei stöchiometrischen Fe_3Si/GaAs-Hybridstrukturen, die bei (a) 250 °C und (b) bei 400 °C gewachsen wurden. Die jeweiligen oberen Einschübe zeigen Beugungsbilder ausgewählter Bereiche (SAD), die Spots vom GaAs und Fe_3Si beinhalten. Die zusätzlichen Spots (Pfeile) in (b) sind auf die Reaktionsschicht zurückzuführen. Die unteren Einschübe zeigen Hellfeld-TEM-Aufnahmen. Die Schichtdicke beträgt 45 nm.*

3. Elektrische Eigenschaften und atomare Ordnung von Fe_3Si/GaAs(001)-Hybridstrukturen

Abb. 6 zeigt die Abhängigkeit des Schichtwiderstandes verschiedener Fe_3Si/GaAs(001)-Hybridstrukturen von der Komposition der $Fe_{3+x}Si_{1-x}$–Schichten. Der Schichtwiderstand wurde dabei mittels van-der-Pauw- und Hallbarstrukturen bei 300 K und 77 K gemessen. Für tiefere Temperaturen ändert sich der Schichtwiderstand nicht wesentlich. Unabhängig von der Temperatur erhöht sich der Schichtwiderstand anfangs mit Erhöhung des Si-Anteils, um dann drastisch abzufallen. Es bildet sich ein ausgeprägtes Mimimum des Schichtwiderstands im Bereich der exakten Stöchiometrie heraus. Für höhere Si-Anteile steigt der Schichtwiderstand wieder stark an. Der Einschub in Abb. 6 zeigt das Verhältnis der Schichtwiderstände *r* bei 300 und 77 K als Funktion der Komposition. Dabei zeigt *r* ein Maximum in Übereinstimmung mit dem Minimum im Schichtwiderstand., was auf eine Änderung des dominanten Streumechanismus hinweist.

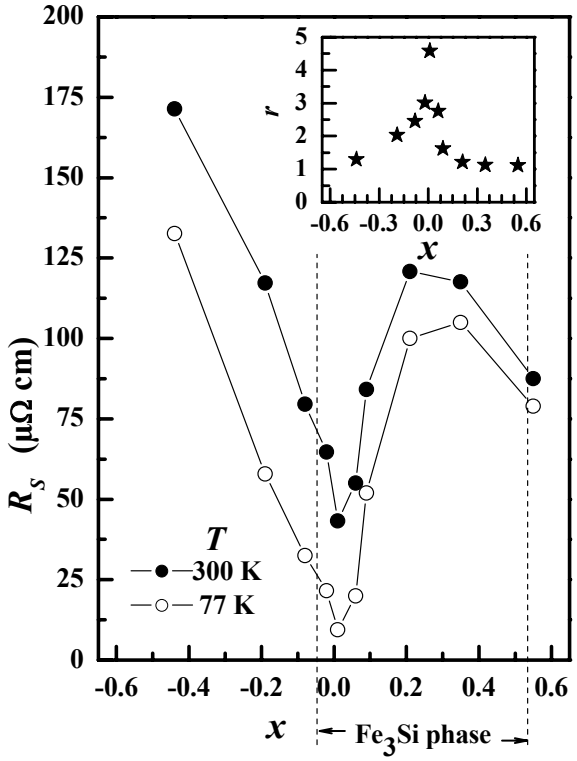

Abb. 6: *Schichtwiderstand R_S verschiedener Fe_3Si/GaAs(001) Hybridstrukturen in Abhängigkeit von der Komposition der Schichten x für zwei verschiedene Temperaturen. Die Schichten wurden bei 200 °C gewachsen. Der Einschub zeigt das Verhältnis $r = R_S^{300K}/R_S^{77K}$ in Abhängigkeit der Komposition.*

Diese Ergebnisse können qualitativ verstanden werden, wenn man die atomare Ordnung der Si-Atome innerhalb der Fe_3Si-Phase betrachtet. Der Schichtwiderstand reinen Eisens erhöht sich stark mit dem zusätzlichen, ungeordneten Einbau von Si in Folge der erhöhten Kompositionsfluktuationsstreuung. Dieser Streumechanismus ist nur schwach von der Temperatur abhängig. Sobald atomare Ordnung einsetzt, nimmt der Schichtwiderstand ab. Im Bereich höchster Ordnung (für stöchiometrische Schichten) finden wir den geringsten Schichtwiderstand. In diesem Bereich dominieren andere Streumechanismen (wie z. B. Phononenstreuung), die stärker temperaturabhängig sind. Ursache des starken Anstiegs des

Schichtwiderstandes für sehr hohe Si-Konzentrationen ist das Auftreten neuer Fe_xSi_y-Phasen zusätzlich zur Abweichung von der Stöchiometrie.

Um die atomare Ordnung der $Fe_{3+x}Si_{1-x}$–Schichten zu bestimmen, wurden Röntgenbeugungsuntersuchungen verschiedener Beugungsreflexe am Röntgen-Diffraktometer des PDI-Strahlrohrs bei BESSY II durchgeführt. Aus dem Vergleich verschiedener Reflexe, die unterschiedlich empfindlich für bestimmte Fehlordnungen (Austausch von Fe und Si Atomen) auf den verschiedenen Untergittern des Fe_3Si sind, lässt sich der Ordnungszustand der Schicht charakterisieren.

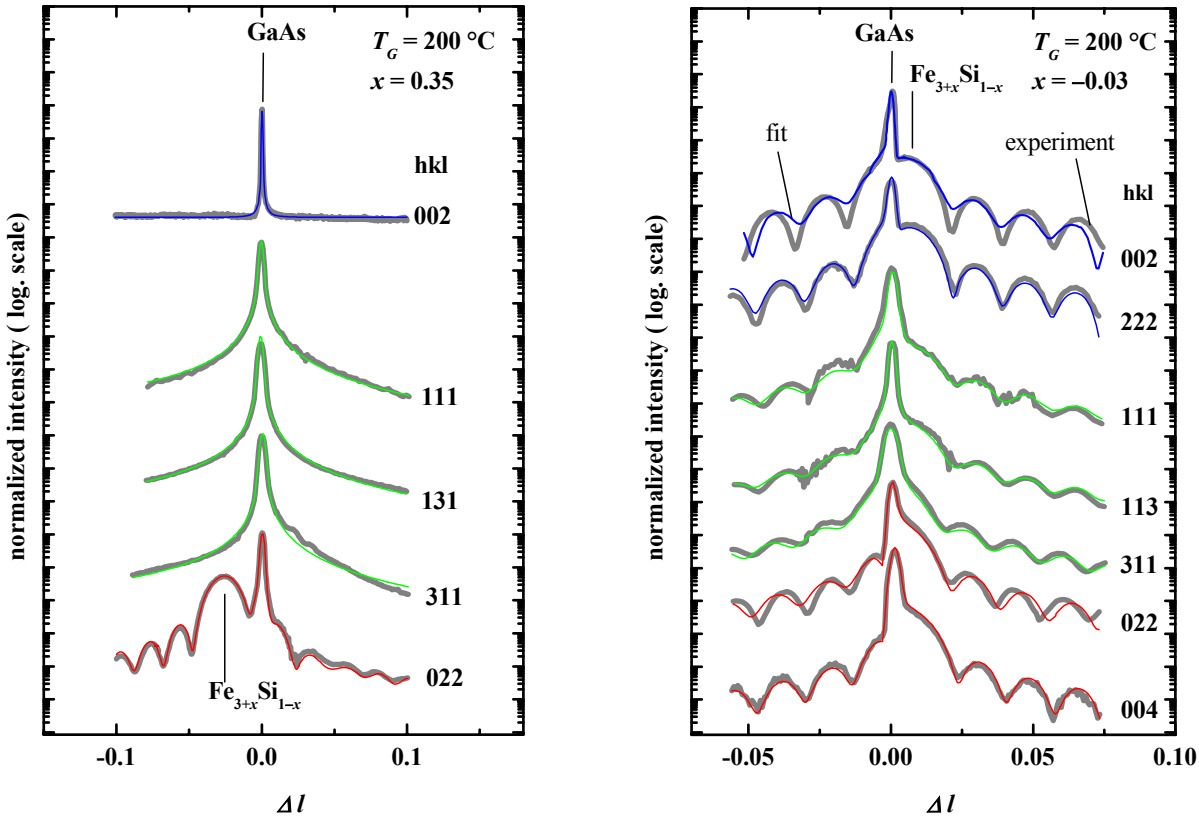

Abb. 7: *Gemessene (dicke Linien) und simulierte (dünne Linien) Röntgenbeugungsmessungen in der Umgebung verschiedener reziproker Gitterpunkte für zwei verschiedene $Fe_{3+x}Si_{1-x}$–Schichten. Die Wachstumstemperatur beträgt 200 °C. Die Kurven sind auf den entsprechenden GaAs-Reflex normiert und gegeneinander verschoben.*

Abb. 7 vergleicht verschiedene gemessene und berechnete Reflexprofile, die alle mit einem gemeinsamen Satz an Parametern für die Berechnung der Kurven angepasst worden sind. Das Auftreten des Fe_3Si-Schichtreflexes in allen Reflexprofilen im Falle der nahezu stöchiometrischen Schicht ($x = -0.03$) in Abb. 7 spiegelt den hohen Ordnungszustand wider und zeigt, dass die Schicht in der $D0_3$-Struktur kristallisiert. Die quantitative Analyse ergibt eine verbleibende leichte Unordnung aufgrund des Einbaus von Si auf Fe-Gitterplätzen des Fe(*A,C*)-Untergitters. Im Gegensatz dazu zeigt die nichtstöchiometrische Schicht ($x = 0.35$) eine starke Unordnung, was sich im Fehlen der entsprechenden Schichtreflexe in den meisten Reflexprofilen (jene die empfindlich auf die atomare Ordnung sind) widerspiegelt.

Die leichte verbleibende Unordnung ist wahrscheinlich auf die relativ niedrige Wachstumstemperatur der Schichten zurückzuführen. Das zeigt sich deutlich in der Abhängigkeit des Schichtwiderstandes für stöchiometrische Schichten von der Wachstumstemperatur (Abb. 8). Unabhängig von der Messtemperatur verringert sich der Schichtwiderstand mit Er-

höhung der Wachstumstemperatur bis 325 °C. Das demonstriert die Erhöhung der langreichweitigen, atomaren Ordnung in den Schichten. Anderseits verschlechtert sich die Grenzflächenqualität drastisch für Wachstumstemperaturen über 250 °C (Abschnitt 2), so dass die optimale Wachstumstemperatur für Schichten sowohl mit hoher Kristall- und Grenzflächenperfektion als auch mit einem hohen Ordnungsgrad bei dieser Temperatur liegt.

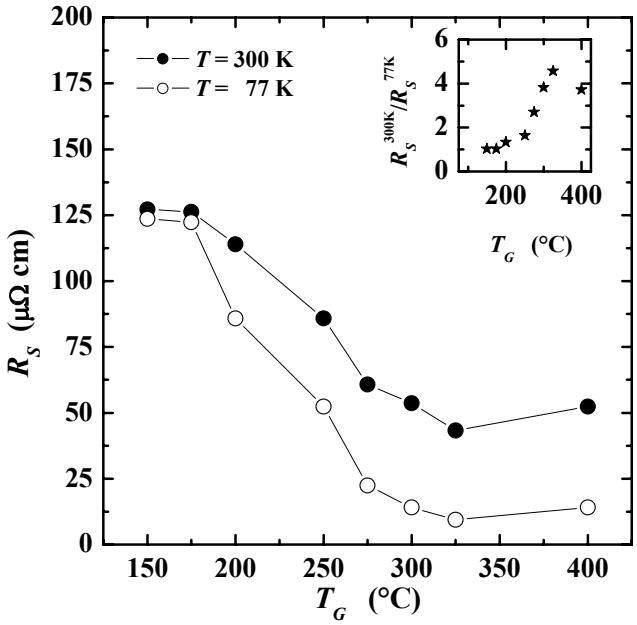

Abb. 8: *Schichtwiderstand R_S verschiedener, stöchiometrischer Fe_3Si/GaAs(001) Hybridstrukturen in Abhängigkeit von der Wachstumstemperatur T_G der Schichten für zwei verschiedene Temperaturen. Der Einschub zeigt das Verhältnis $r = R_S^{300K}/R_S^{77K}$ in Abhängigkeit der Wachstumstemperatur.*

4. Magnetische Eigenschaften

Die magnetischen Eigenschaften der Schichten wurden mittels SQUID-Magnetometrie gemessen. Wie man in Abb. 9 erkennen kann, sind die Schichten ferromagnetisch bei Raumtemperatur, wobei die leichte Achse der Magnetisierung in der Schichtebene entlang der <100>-Richtungen liegt. Die magnetischen Eigenschaften sind nur schwach von der Temperatur abhängig (Abb. 9), was erwartet werden kann, da die Curie-Temperatur viel höher als Raumtemperatur liegt.

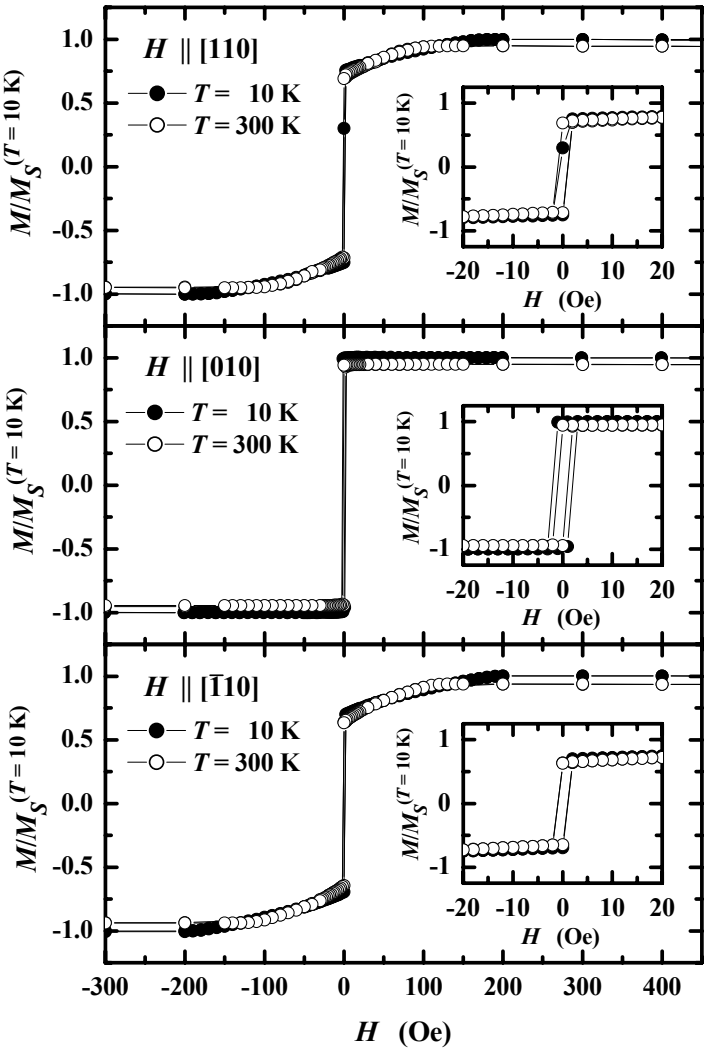

Abb. 9: *Magnetisierungskurven einer stöchiometrischen Fe_3Si/GaAs(001)-Schicht, wobei das Magnetfeld H in der Schichtebenen entlang verschiedener kristallographischer Orientierungen angelegt wurde. Die Messungen wurden bei Raumtemperatur (300 K) und bei tiefen Temperaturen (10 K) durchgeführt. Die Magnetisierung ist auf den Sättigungswert bei T = 10 K, $M_S^{(T=10K)}$, normiert. Die Einschübe zeigen die Magnetisierungskurven bei sehr niedrigen Magnetfeldern.*

Abbildung 10 fasst die Werte für die Sättigungsmagnetisierung und die Koerzitivfeldstärken verschiedener $Fe_{3+x}Si_{1-x}$/GaAs(001)-Hybdridstrukturen in Abhängigkeit von der Komposition der Schichten zusammen. Die Sättigungsmagnetisierung verringert sich nahezu linear mit steigendem Si-Anteil in den Schichten. Die Werte sind im Rahmen der experimen-

tellen Genauigkeit nahe an den Volumenwerten für $Fe_{3+x}Si_{1-x}$–Schichten. Weiterhin erkennt man, dass die Fe_3Si-Phase mit sehr kleinen Koerzitivfeldstärken verbunden ist. Abweichungen zu niedrigen oder höheren Si-Anteilen führen zu deutlich höheren Werten für die Koerzitivfeldstärke. Das ist ein weiteres Indiz für die hohe Kristall- und Grenzflächenperfektion im Bereich der Fe_3Si-Phase.

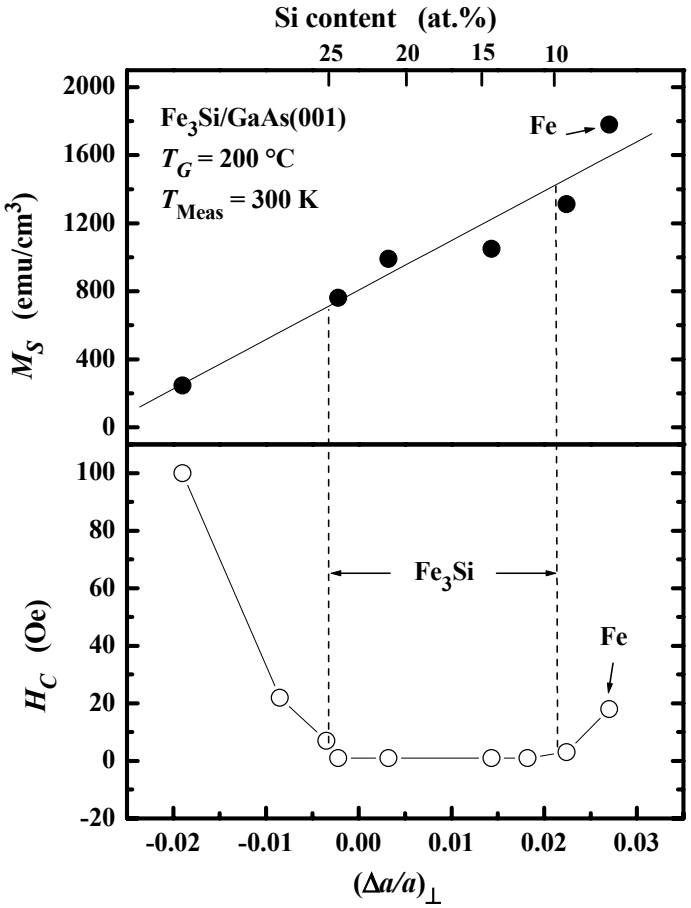

Abb. 10: *Sättigungsmagnetisierung M_S und Koerzitivfeldstärke H_C für verschiedene Fe_3Si(GaAs(001)-Schichten in Abhängigkeit von der Komposition der Schichten, die hier in Form der Gitterverspannung $(\Delta a/a)_\perp$ ausgedrückt ist. Die obere Skala repräsentiert die Komposition der Schichten wie sie in Abb. 3 abgeschätzt wurde.*

Die magnetische Anistropie-Energie und die Resonanz-Linienbreite von zwei ausgewählten $Fe_{3+x}Si_{1-x}$/GaAs(001)-Hybdridstrukturen sind zusätzlich mittels ferromagnetischer Resonanz-Spektroskopie untersucht wurden. Die Winkelabhängigkeit der angeregten Einheitsmoden gestattet die akkurate Bestimmung der magnetischen Anisotropiefelder. Für die stöchiometrische Schicht ($x = -0.03$) finden wir in Übereinstimmung mit den SQUID-Messungen eine vierfache Anistropie, die durch eine schwache uniaxiale Komponente moduliert wird. Der Anteil der uniaxialen magnetischen Anistropie (UMA) erhöht sich mit Verringerung des Si-Gehalts, wobei die leichte Achse der Magnetisierung der UMA um 45° gegenüber der leichten Achse der vierfachen Anistropie gedreht ist. Die Zunahme der UMA mit steigenden Fe-Anteil kann auf die veränderte Bindungsstruktur an der FM/HL-Grenzfläche zurückgeführt werden. Die Schichten zeigen außergewöhnlich schmale Resonanz-Linienbreiten von ca. 17 Oe bei einer Anregung von 9 GHz, was wiederum die sehr hohe, strukturelle Schichtqualität demonstriert.

5. Magnetotransportuntersuchungen

Der Halleffekt in dünnen, ferromagnetischen Schichten liefert eine zusätzliche, leistungsstarke Methode, die magnetischen Eigenschaften von Ladungsträgern zu studieren. Die Mischung von Spin-up und Spin-down Zuständen, die zu einer unterschiedlichen Streuung von Elektronen mit den Impulsen $k \parallel H$ und $k \perp H$ führt, sind eine Folge der Spin-Bahn-Wechselwirkung. Es ergeben sich anisotrope Schichtwiderstände ρ_{xx} und ρ_{xy} für Ströme parallel oder senkrecht zur Magnetisierung der Schicht. Der transversale Magnetowiderstand ρ_{xy} für Magnetfelder in der Schichtebene wird dabei als *planarer* Hallwiderstand bezeichnet.

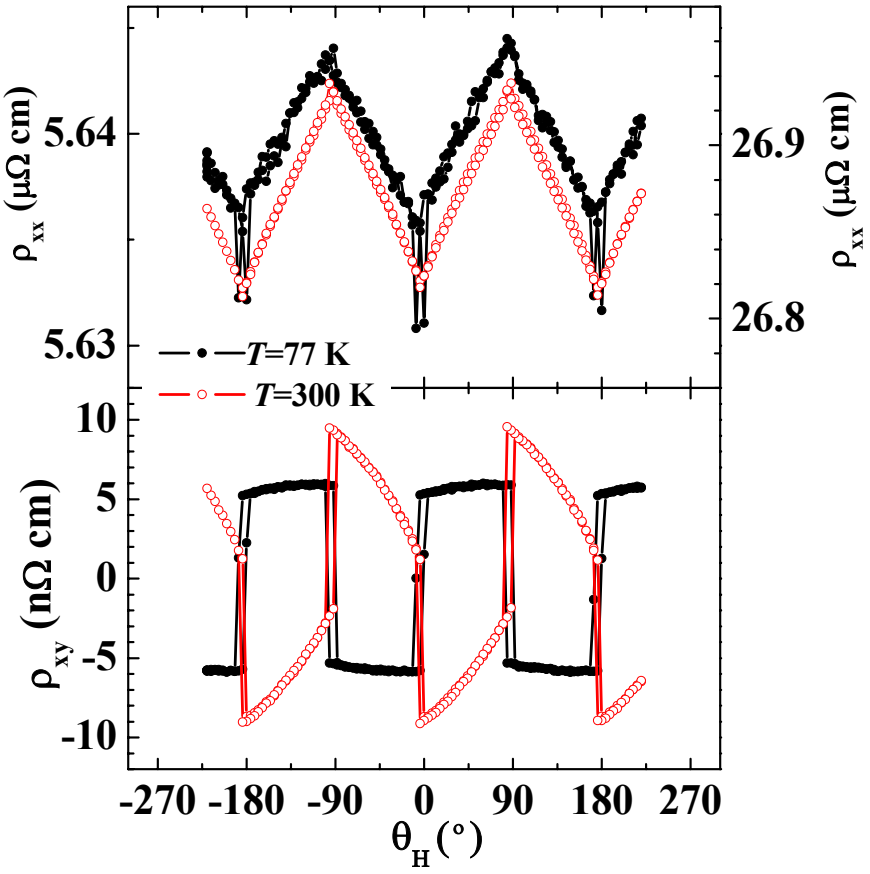

***Abb. 11**: Abhängigkeit der Komponenten der Widerstandstensors ρ_{xx} und ρ_{xy} vom Winkel bezüglich der Richtung des angelegten Magnetfeldes für eine Schicht mit einer nahezu exakten Stoichiometrie (x = +0.01). Das angelegte Magnetfeld beträgt 25 Oe.*

In Abb. 11 sind ρ_{xy} und ρ_{xx} für eine Probe mit nahezu exakter Stöchiometrie ($x = 0.01$) in Abhängigkeit vom Winkel für sehr kleine Magnetfelder in der Schichtebene gezeigt. Hierbei wurde der Strom parallel zur [110]-Richtung eingespeist, die einer schweren Magnetisierungsrichtung in der Schichtebenen entspricht (Abschnitt 4). Wird das Magnetfeld entlang einer leichten Achse ($\theta_H = 45°$) ausgerichtet, fallen die Richtungen der Magnetisierung und des Magnetfeldes zusammen. Dreht man die Probe weiter, bleibt die Richtung der Magnetisierung hinter der Magnetfeldrichtung zurück. Passiert man eine schwere Magnetisierungsachse springt die Magnetisierungsrichtung zur nächsten leichten Achse. Folglich entsteht ein Sprung in der Winkelabhängigkeit von ρ_{xy}. Überraschend tritt unterhalb einer kritischen Tem-

peratur jedoch eine Inversion der ρ_{xy}-Werte bei 45 und 135° auf, was einem Vorzeichenwechsel von ρ_{xy} entspricht. Bemerkenswerterweise tritt dieser Übergang nur in ρ_{xy} nicht aber in ρ_{xx} auf. Diese Inversion wird nur bei Schichten mit einer Komposition nahe der exakten Stöchiometrie ($-0.08 < x < 0.06$) beobachtet. Abbildung 12 zeigt die Abhängigkeit der planaren Hallleitfähigkeit vom temperaturabhängigen Längswiderstand verschiedener $Fe_{3+x}Si_{1-x}$/GaAs(001) Hybridstrukturen im Temperaturbereich 77 bis 300 K. Zwei Magnetotransportregime werden beobachtet. Bei hohen Temperaturen, d. h. oberhalb der Inversionstemperatur, ist σ_{xy} für alle Proben nahezu gleich (ca. +20 $(\Omega\ \mathrm{cm})^{-1}$), hat dasselbe Vorzeichen, und ist nur schwach temperaturabhängig. Für niedrigere Temperaturen als die Inversionstemperatur ändert σ_{xy} das Vorzeichen und nimmt für kleinere Werte von x und ρ_{xx} stark zu. Die Inversionstemperatur verringert sich stark bei zunehmender Abweichung von der exakten Stöchiometrie (Siehe Einschub von Abb. 12).

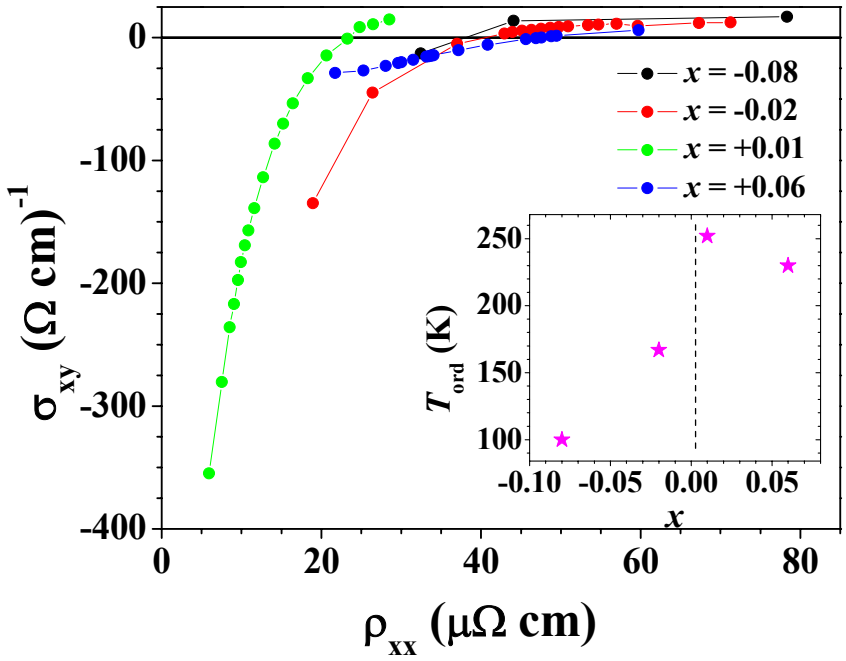

Abb. 12: *Planare Hallleitfähigkeit σ_{xy} für verschiedene $Fe_{3+x}Si_{1-x}$/GaAs(001) Hybridstrukturen als Funktion des longitudinalen Schichtwiderstands ρ_{xx}. Die Änderung von ρ_{xx} spiegelt hierbei die Temperaturabhängigkeit des longitudinalen Schichtwiderstands zwischen 77 und 300 K wider. Der Einschub zeigt die Abhängigkeit der Inversionstemperatur T_{Ord}, d. h. der Temperatur bei der das Vorzeichen wechselt, von der Komposition der Schichten.*

Die Ursache dieses Effekts ist bisher noch nicht vollständig verstanden. Ein mikroskopisches Modell, dass auf dem Einfluss der Berry-Phase basiert, ist in der Lage, einen zusätzlichen Term im Magnetowiderstandstensor abzuleiten, der die magnetische Wechselwirkung in Folge der reduzierten Kristallsymmetrie der unterschiedlichen Fe-Untergitter im geordneten Fe_3Si-Kristall berücksichtigt. Dabei zerstören sowohl strukturelle als auch thermische Unordnung oberhalb einer bestimmten Ordnungstemperatur die kohärenten Spindichtefluktuationen und es kommt zu einen Übergang von einem geordneten, intrinsischen in ein konventionellen Magnetotransport-Bereich.

6. Elektrische Spininjektion

Spin-Injektion vom Fe_3Si in GaAs wurde mittels der Analyse der Elektrolumineszenz (EL) einer in die Schichtfolge integrierten *n-i-p* GaAs/(In,Ga)As LED (Einschub von Abb. 13) nachgewiesen. Der zirkulare Polarisationsgrad *P* der EL bei 150 K ist in Abb. 13 als Funktion des Magnetfeldes *B* gezeigt. Im Unterschied zur Referenz-Probe, in der die Fe_3Si-Schicht durch das nicht-magnetische Ti ersetzt wurde, folgt der Polarisationsgrad der EL im Falle einer Fe_3Si-Schicht der „out-of-plane"-Magnetisierungskurve. Dabei erkennt man den starken Anstieg von *P* für Magnetfelder $|B| < 2$ T und die Sättigung bei ca. 3 % für $|B| > 2$ T. Die EL Polarisation in Folge des Zeeman-Effekts in der LED-Struktur ist vernachlässigbar bei $T = 150$ K. Für die Referenz-Probe konnte keine signifikante Polarisation beobachtet werden. Der beobachtete Polarisationsgrad von ca. 3 % ist vergleichbar mit den Werten, die wir zuvor für die Injektion von Fe und MnAs in eine vergleichbare LED-Struktur erhalten haben. Das deutet darauf hin, dass zusätzlich zu einer weiteren Optimierung der Ferromagnet/Halbleitergrenzfläche auch eine Optimierung der Halbleiterstruktur erforderlich ist, um zu deutlich höheren Werten für den Polarisationsgrad zu gelangen. Der Polarisationsgrad bei Raumtemperatur beträgt ca. 1 %.

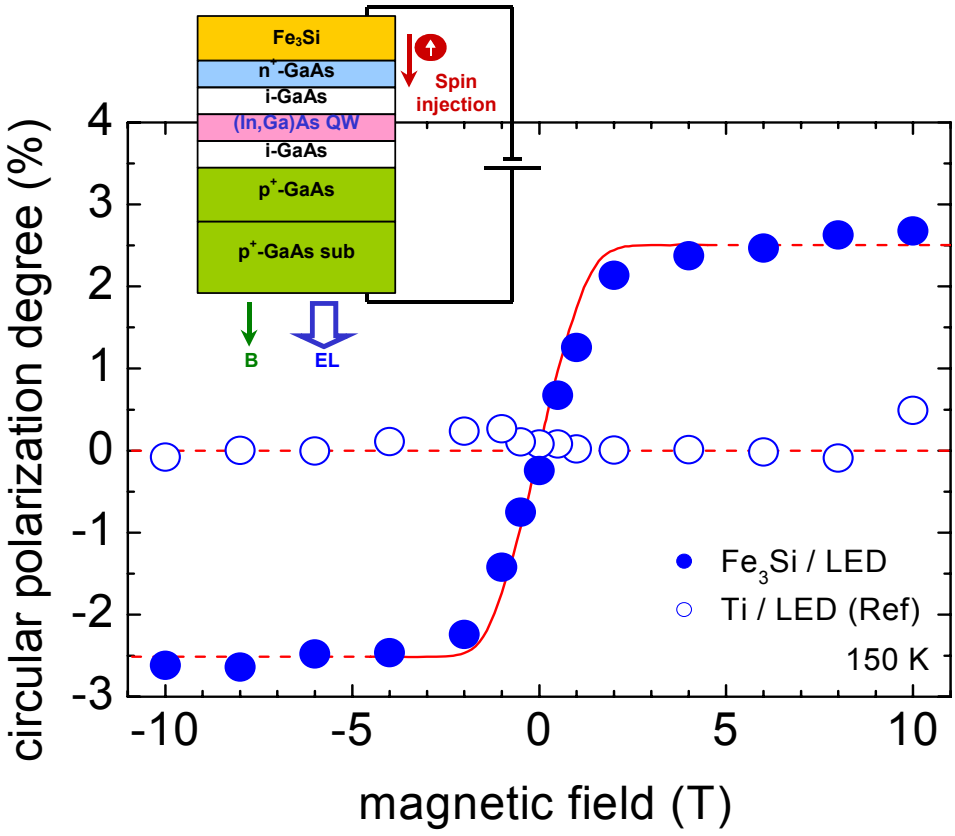

Abb. 13: *Zirkularer Polarisationsgrad P als Funktion des externen Magnetfelds für LED's mit Fe_3Si- (volle Symbole) und mit Ti- Injektionsschichten (offene Symbole). Die Messungen wurden bei 150 K durchgeführt, Die „Out-of-plane"-Magnetisierungkurve einer dünnen Fe_3Si-Schicht ist zum Vergleich als durchgezogene Linie hinzugefügt. Die gestrichelten Linien sind Orientierungshilfen für den Bereich hoher Magnetfelder.*

Um die tatsächliche Spininjektionseffizienz zu bestimmen, haben wir in Kooperation mit der Gruppe von Dr. B. Beschoten (RWTH Aachen) sowohl die Ladungsträgerrekombinationszeit als auch die Spinrelaxationszeit der LED-Struktur mittels zeitaufgelöster Transmissions-Spektroskopie in Abhängigkeit von der Temperatur gemessen. Die Ergebnisse sind in Abb. 14 dargestellt. Dabei zeigt sich eine starke Temperaturabhängigkeit insbesondere der Ladungsträgerrekombinationszeit. Mittels eines einfachen Ratengleichungsmodells lässt sich daraus eine Spininjektionseffizienz von 18% bei tiefen Temperaturen und von 10% bei Raumtemperatur für die untersuchten Spin-LEDs abschätzen.

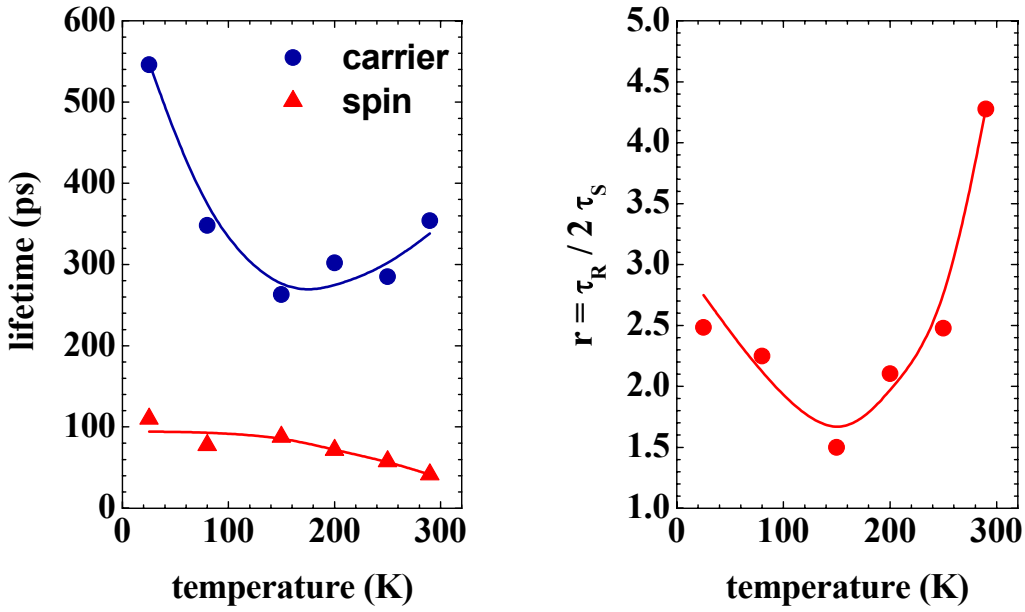

Abb. 14: *Temperaturabhängigkeit der Ladungsträger- und Spinlebensdauern in einem (In,Ga)As-Quantengraben. Hierbei wurde die komplette LED-Struktur gemessen. Weiterhin ist die Temperaturabhängigkeit des Verhältnisses r beider Lebensdauern dargestellt.*

7. Laterale Nanostrukturierung von Fe/GaAs(001) Hybridstrukturen

Neben der Herstellung von geeigneten Spin-LEDs mittels konventioneller Fotolithografie und Lift-off-Technik wurden die Strukturierungsverfahren derart weiterentwickelt und optimiert, dass große Flächen mit periodischen, ferromagnetischen Nanostrukturen (Nanomagneten) hergestellt werden können. Dabei beschränkten sich die Arbeiten bisher auf Fe/GaAs(001) Hybridstrukturen. Eine Ausdehnung auf Heusler-Legierungen ist prinzipiell möglich und in Vorbereitung.

Mehrere zweidimensionale Gitter von Nanomagneten im Submikrometerbereich wurden von einer 20 nm dicken Fe/GaAs(001) Hybridstruktur mittels Elektronenstrahllithografie und Trockenätz-Verfahren hergestellt. Die Fe/GaAs(001)-Schichten sind dabei mittels MBE bei 50 °C gewachsen worden. Da der Abstand zwischen den einzelnen Nanomagneten 900 nm beträgt, kann der Einfluss der Dipol-Dipol-Wechselwirkung auf die magnetischen Eigenschaften vernachlässigt werden. In diesem Fall stellt die gemessene Magnetisierung die statistische gemittelte Magnetisierung der einzelnen Nanomagneten dar.

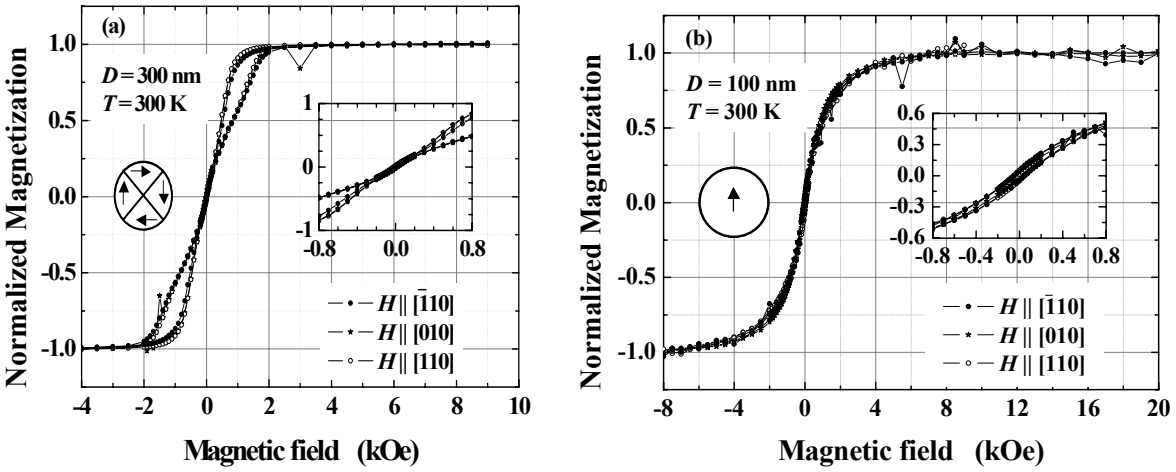

Abb. 15: *Magnetisierung von zwei verschiedenen Gittern von Fe Nanomagneten auf GaAs(001)-Substraten entlang verschiedener kristallografischer Richtungen bei 300 K. Die Magnetisierung ist auf die Sättigungsmagnetisierung normiert. Der diamagnetische Beitrag des GaAs-Substrats ist abgezogen worden. Der Durchmesser der Fe Nanomagneten betragt (a) 300 nm und (b) 100 nm. Die Einschübe zeigen den Bereich schwacher Magnetfelder.*

Die Magnetisierung wurde mittels SQUID-Magnetometrie für Magnetfelder entlang verschiedener kristallografischen Richtungen gemessen (Abb. 15). Dabei zeigt sich eine nahezu isotrope Magnetisierung. Das zeigt, dass die Formanisotropie sehr viel stärker als die magneto-kristalline Anisotropie ist. Die Form der Magnetisierungskurven zeigt, dass Fe Nanomagneten mit einem Durchmesser kleiner oder gleich 100 nm im gesamten Magnetfeldbereich durch eine Einzeldomänenstruktur gekennzeichnet sind. Dagegen weisen Fe Nanomagneten mit einen Durchmesser größer als 100 nm eine Vielfachdomänenstruktur im Bereich sehr kleiner Magnetfelder auf. Zweidimensionale Gitter von Nanomagneten wurden sowohl in regulärer als auch in zufälliger Anordnung der Fe Nanomagneten untersucht. Es konnten keine Unterschiede in den Magnetisierungskurven gefunden werden.

Die Sättigungsmagnetisierung der Nanomagneten zeigt eine sehr starke Temperaturabhängigkeit (Abb. 16). Die Reduzierung der Sättigungsmagnetisierung bei hohen Temperaturen ist bei kleineren Durchmessern der Nanomagneten stärker. Die Reduzierung ist dabei unabhängig von der Domänenstruktur im schwachen Magnetfeld. Bisher ist die Ursache der starken Temperaturabhängigkeit der Sättigungsmagnetisierung unverstanden. Jedoch können eine Reihe von Möglichkeiten wie z. B. eine Absenkung der Curie-Temperatur oder ein superparamagnetisches Verhalten ausgeschlossen werden. Hingegen kann der Einfluss der antiferromagnetische Kopplung durch das an der Oberfläche vorhandene Fe-Oxid nicht grundsätzlich ausgeschlossen werden.

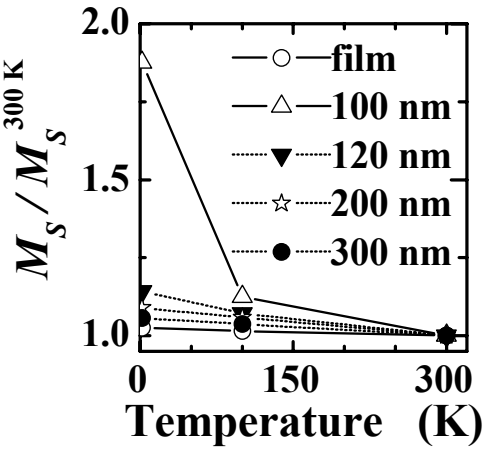

Abb. 16: *Temperaturabhängigkeit der Sättigungsmagnetisierung M_S für Fe Nanomagneten mit unterschiedlichen Durchmessern. Der Wert der Sättigungsmagnetisierung wurde auf den Wert bei 300 K, M_S^{300K}, normiert, da das absolute Volumen sämtlicher Nanomagneten nur sehr ungenau bestimmt werden kann. Die Werte wurden für ein Magnetfeld entlang der [110]-Richtung bestimmt, wobei keine klare Abhängigkeit von der Orientierung des Magnetfeldes bezüglich verschiedener kristallografischer Richtungen beobachtet wird.*

8. Veröffentlichungen

8.1. Manuskripte in Fachzeitschriften

[1] J. Herfort, H.-P. Schönherr, and K. H. Ploog
Epitaxial growth of Fe_3Si/GaAs(001) hybrid structures
Appl. Phys. Lett. **83**, 3912 – 3914 (2003).

[2] J. Herfort, H.-P. Schönherr, K.-J. Friedland, and K. H. Ploog
Structural and magnetic properties of Fe_3Si/GaAs(001) hybrid structures
J. Vac. Sci. Technol. B **22**, 2073 – 2078 (2004).

[3] A. Kawaharazuka, M. Ramsteiner, J. Herfort, H.-P. Schönherr, H. Kostial, and K. H. Ploog
Spin injection from Fe_3Si into GaAs
Appl. Phys. Lett. **85**, 3492 – 3494 (2004).

[4] J. Herfort, H.-P. Schönherr, A. Kawaharazuka, M. Ramsteiner, and K. H. Ploog
Epitaxial growth of Fe_3Si/GaAs(001) hybrid structures for spintronic application
J. Cryst. Growth, **278**, 666 – 670 (2005).

[5] M. Bowen, K.-J. Friedland, J. Herfort, H.-P. Schönherr, and K. H. Ploog
Order-driven contribution to the planar Hall effect in Fe_3Si thin films
Phys. Rev. B **71**, 172401 *4 pages* (2005).

[6] B. Jenichen, V. M. Kaganer, J. Herfort, D. K. Satapathy, H.-P. Schönherr, W. Braun, and K. H. Ploog
Long-range order in thin epitaxial Fe_3Si films grown on GaAs(001)
Phys. Rev. B **72**, 075329 *5 pages* (2005).

[7] K. Lenz, E. Kosubek, K. Baberschke, J. Herfort, H.-P. Schönherr, and K. H. Ploog
Magnetic Anisotropy and resonance linewidth of Fe_3Si/GaAs(001)
Phys. Stat. Solidi (c), in press (2005).

8.2. Eingeladene Vorträge auf internationalen Konferenzen

[1] K. H. Ploog
Growth and properties of ferromagnet-semiconductor heterostructures for spin injection at room temperature
12th International Conference on Molecular Beam Epitaxy (MBE-XII), San Francisco (USA), September 15 – 20 (2002).

[2] K. H. Ploog
Ferromagnet-semiconductor heterostructures
Advanced Heterostructure Workshop (AHW2002), Kauna (USA), December 1 – 6 (2002).

[3] K. H. Ploog
Growth and properties of ferromagnet-semiconductor heterostructures for spin injection
International Symposium on Quantum Nanoelectronics for Meme-Media-Based Information Technologies, Sapporo (Japan), February 12 – 14 (2003).

[4] K. H. Ploog
Growth and properties of ferromagnet-semiconductor heterostructures for spin injection at room temperature
International Symposium on Carrier Interaction and Spintronics in Nanostructures (CISN2003), Atsugi (Japan), March 10 – 12 (2003).

[5] K. H. Ploog
Ferromagnet-semiconductor heterostructures for spin injection
International Symposium on Inter-Nano-Science (INS-2003), Osaka (Japan), March 11 – 13 (2003).

[6] K. H. Ploog
Epitaxial ferromagnet-semiconductor heterostructures for electrical spin injection
61st International Device Research Conference (DRC2003), Salt Lake City (USA), June 23 – 25 (2003).

[7] K. H. Ploog
Epitaxial ferromagnetic-semiconductor heterostructures for electrical spin injection
International Conference on Materials for Advanced Technologies (ICMAT2003), Singapore (Singapore) , December 7 - 12 (2003).

[8] K. H. Ploog
Ferromagnetic/Semiconductor heterostructures – From electrical spin injection to new magnetologic concepts
Spring Meeting of the Materials Research Society (MRS-2004), San Franzisco (USA), April 12 – 16 (2004).

[9] K. H. Ploog
Ferromagnetic/Semiconductor nanostructures for spintronics and new magnetologic concepts
First Taiwan International Conference on Nanoscience and Technology (TICON-2004), Taipeh (Taiwan), June 30 – July 3 (2004).

[10] K. H. Ploog
Ferromagnetic/Semiconductor nanostructures for spintronics and new magnetologic concepts
International Symposium on Quantum Hall Systems and Quantum Materials, Hamburg (Germany), September 22 – 24 (2004).

[11] K. H. Ploog
Ferromagnetic/Semiconductor nanostructures for spintronics and new magnetologic concepts
International Workshop: Spin Injection, Transport, and Manipulation, Bochum (Germany), October 10 – 12 (2004).

[12] K. H. Ploog
Ferromagnetic/Semiconductor nanostructures for spintronics
International Symposium on Waseda University COE Nanotechnology, Tokyo (Japan), December 21 – 22 (2004).

8.3. Vorträge und Poster auf internationalen Konferenzen

[1] J. Herfort, H.-P. Schönherr, and K. H. Ploog
Structural and magnetic properties of Fe_3Si/GaAs(001) hybrid structures
31st International Conference on the Physics and Chemistry of Semiconductor Interfaces (PCSI-31), Kailua-Kona, Hawaii (USA), January 18 – 22 (2004).

[2] A. Kawaharazuka, M. Ramsteiner, J. Herfort, H.-P. Schönherr, H. Kostial, and K. H. Ploog
Spin injection from Fe_3Si into GaAs
46th Electronic Materials Conference (EMC2004), Notre Dame (USA), June 23 – 25 (2004).

[3] M. Ramsteiner, A. Kawaharazuka, J. Herfort, H.-P. Schönherr, H. Kostial, and K. H. Ploog
Spin injection from Fe_3Si into GaAs studied by temperature-dependent electroluminescence spectroscopy
3rd International Conference on the Physics and Application of Spin-related phenomena in Semiconductors (PASPS-III), Santa Barbara (USA), July 21 – 23 (2004).

[4] M. Bowen, K.-J. Friedland, J. Herfort, H.-P. Schönherr, and K. H. Ploog
Disorder-driven contribution to the planar Hall effect in Fe_3Si thin films
Gordon Research Conference on Magnetic Nanostructures, Big Sky (USA), August 22 – 27 (2004).

[5] J. Herfort, H.-P. Schönherr, A. Kawaharazuka, M. Ramsteiner, and K. H. Ploog
Epitaxial growth of Fe_3Si/GaAs(001) hybrid structures for spintronic applications
13th International Conference on Molecular Beam Epitaxy (MBE2004), Edinburgh (UK), August 23 – 27 (2004).

[6] K.-J. Friedland, M. Bowen, J. Herfort, and K. H. Ploog
Intrinsic contributions to the planar Hall effect in Fe and Fe_3Si films on GaAs substrates
11th Advanced Heterostructure Workshop, Kohala-Coast (USA), December 5 – 10 (2004).

[7] P. K. Muduli, J. Herfort, H.-P. Schönherr, and K. H. Ploog
Epitaxial growth, structural and magnetic properties of Fe and Fe_3Si films on GaAs(113)A substrates
338th Hereaus-Seminar Nanomagnetism: New Insights with Synchrotron Radiation , Bad Honnef (Germany), January 5 – 7 (2005).

[8] J. Herfort, H.-P. Schönherr, M. Bowen K.-J. Friedland, and K. H. Ploog
Epitaxial Fe_3Si/GaAs(001) hybrid structures with nearly exact stoichiometry
32nd International Conference on the Physics and Chemistry of Semiconductor Interfaces (PCSI-32), Bozeman (USA), January 23 – 27 (2005).

Anhang der Publikationen

Epitaxial growth of Fe_3Si/GaAs(001) hybrid structures

Jens Herfort,[a] Hans-Peter Schönherr, and Klaus H. Ploog
Paul-Drude-Institut für Festkörperelektronik, Hausvogteiplatz 5-7, 10117 Berlin, Germany

(Received 5 August 2003; accepted 12 September 2003)

We have established an optimized growth temperature range, namely, 150 °C$<T_G<$250 °C, where ferromagnetic Fe_3Si/GaAs(001) hybrid structures with high crystalline and interfacial quality can be fabricated by molecular-beam epitaxy. The composition of the Fe_3Si layers, which can be regarded as a Heusler alloy, was tuned within the stable Fe_3Si phase. The layers show high magnetic moments with a value of 1050 emu/cm^3, which is close to that of bulk Fe_3Si. © *2003 American Institute of Physics.* [DOI: 10.1063/1.1625426]

Epitaxial ferromagnet/semiconductor (FM/SC) heterostructures have attracted considerable attention due to their possible application in future magnetoelectronics.[1] Most of the work so far has been concentrated on the elements Fe,[2,3] Co,[4] and the binary alloy Fe_xCo_{1-x},[5] which grow epitaxially on GaAs(001) substrates and are ferromagnetic at room temperature. However, the growth temperature has to be kept very low, that is, close to room temperature, to prevent the formation of interfacial compounds at the FM/SC interface, which are detrimental for the realization of spin injection from a FM metal into a SC.[3–6] Nevertheless, using optimized growth conditions of the Fe/GaAs(001) interface, we recently demonstrated spin injection at room temperature, although the spin injection efficiency remained low.[7] Therefore, it is highly desirable to obtain alternative materials that show improved interfacial quality as well as a higher thermal stability of the FM/SC interface.

Surprisingly, only a little work has been done on the growth of Fe_3Si on GaAs(001), despite the fact that it is almost lattice matched to GaAs and is ferromagnetic up to 840 K.[8] Fe_3Si has the cubic DO_3 structure and can be regarded as a Heusler alloy Fe_2FeSi as there are two distinct crystallographic and magnetic Fe sites.[9] Moreover, certain Heusler alloys are predicted to be 100% spin polarized at the Fermi level (i.e., they exhibit half-metallic behavior[10]), hence making Fe_3Si an attractive alternative material for electrical spin injection.

In this report, we present our results on the fabrication and characterization of epitaxial single-crystal Fe_3Si films grown by molecular-beam epitaxy (MBE) on GaAs(001) substrates. As evidenced by double-crystal x-ray diffraction measurements (DCXRD), an optimized growth temperature regime is established in which ferromagnetic Fe_3Si/GaAs(001) layers with high crystalline and interfacial quality can be obtained.

The GaAs templates are prepared in a separate III–V growth chamber using standard GaAs growth techniques. For the Fe_3Si growth, the substrate is then transferred into a As-free metal deposition chamber through UHV. Fe and Si are codeposited from high-temperature effusion cells at growth temperatures varied between 50 and 500 °C, at a growth rate of 0.4 nm/min with a base pressure of 1×10^{-10} Torr. The thickness for all layers is between 30 and 40 nm. The evaporation rates are controlled by the cell temperatures and are adjusted by measuring the beam-equivalent pressure using a Bayard–Alpert ionization gauge. To change the composition, we kept the Fe cell temperature $T_{Fe}=1350$ °C constant, and changed the Si cell temperature T_{Si} in the range between 1360 and 1410 °C. The growth of Fe_3Si is initiated on an As-rich (2×1) reconstructed GaAs(001) surface similar to our previous work[3] on Fe/GaAs(001) in order to avoid the formation of macroscopic defects. The growth was monitored *in situ* using reflection high-energy electron diffraction (RHEED). Immediately upon deposition of about 1 monolayer (ML) Fe_3Si, a sharp, streaky (2×2) RHEED pattern is established that does not significantly change during further growth. After a few monolayers, sharp Kikuchi lines are observed. This is a clear indication of a two-dimensional growth mode and a rather smooth surface of the films. However, the RHEED pattern changes from a $2\times$ to a more complex $5\times$ pattern along the [110] direction for T_{Si} above 1400 °C, indicating the appearance of a different Fe_xSi_y phase.

Figures 1 and 2 show the results of DCXRD measurements on Fe_3Si films having different composition (i.e., different T_{Si}), and grown at different growth temperatures T_G, respectively. The rocking curves are recorded with a wide-open detector and normalized to the symmetric GaAs(004) reflection of the substrate. The second reflection is due to the Fe_3Si layer. For comparison, we have included in Fig. 1 the rocking curve of a pure Fe film grown at 50 °C, which is the optimized T_G for Fe epitaxy on GaAs(001).[3] Three main results can be deduced from Figs. 1 and 2.

First, with increasing T_{Si}, the Fe_3Si peak systematically shifts with respect to the GaAs main peak due to the different composition of the layers. Note that the Fe_3Si phase covers a range from 10 to 26.6 at. % Si.[11] As the Fe/Si ratio is varied around stoichiometry, any excess Fe will substitute into Si lattice sites and vice versa, leading to different lattice constants of the layers.[12] From the peak separation, the perpendicular lattice mismatch $(\Delta a/a)_\perp$ of the layers is determined, and it varies between $+2$ and -0.85% for T_{Si} between 1360 and 1410 °C, respectively. The layers are tetragonally distorted with a parallel lattice mismatch smaller than 0.01%, as evidenced by DCXRD profiles of asymmetric Bragg reflections (not shown here).

[a]Electronic mail: herfort@pdi-berlin.de

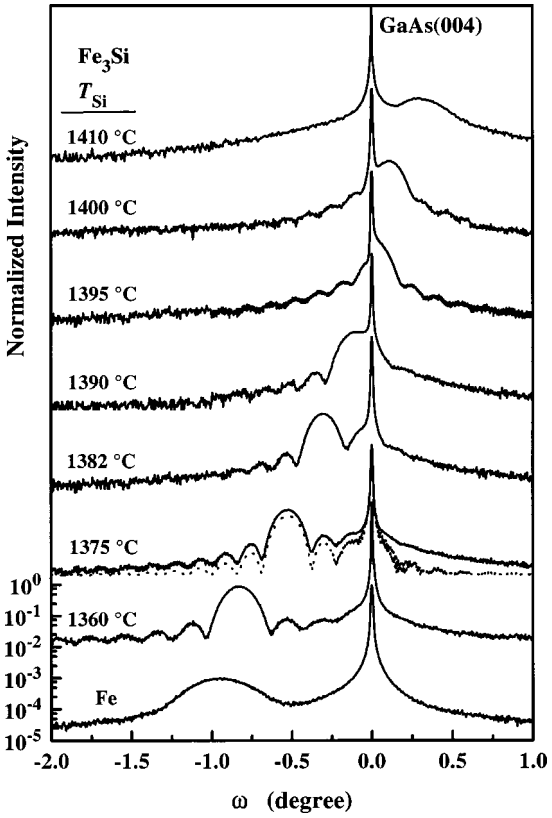

FIG. 1. Semi-logarithmic plots of the normalized intensity of DCXRD rocking curves of various $Fe_3Si/GaAs(001)$ layers grown at 200 °C dependent on the Si cell temperature T_{Si}. The bottom curve belongs to a Fe/GaAs(001) layer grown at 50 °C. The curves are normalized to the GaAs(004) reflection of the substrate. The rocking curves are shifted for clarity. The dotted line shows a simulation for $T_{Si}=1375$ °C.

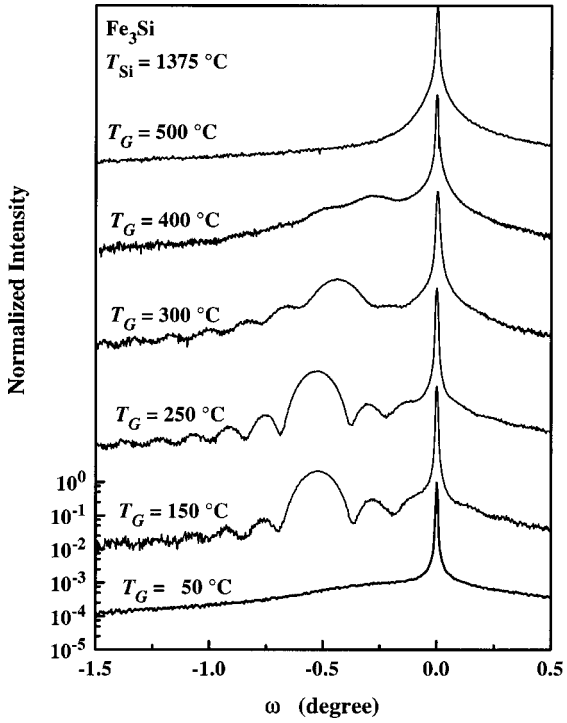

FIG. 2. Semi-logarithmic plots of the normalized intensity of DCXRD rocking curves for various $Fe_3Si/GaAs(001)$ layers grown at a fixed T_{Si} of 1375 °C dependent on the growth temperature T_G. The curves are normalized to the GaAs(004) reflection of the substrate. The rocking curves are shifted for clarity.

Second, both the structural quality and the interface abruptness of the layers first increase with increasing T_{Si} and then decrease above $T_{Si}=1400$ °C. This becomes evident by the appearance of distinct interference (Pendellösung) fringes up to the fifth order and very narrow Fe_3Si peaks. For a qualitative comparison, we have included a simulation of the rocking curve using the Takagi–Taupin formalism for the Fe_3Si layer with $T_{Si}=1375$ °C.[13] Fit parameters are the lattice mismatch $(\Delta a/a)_\perp$ and the layer thickness d, taking into account only the instrumental broadening of the diffractometer. The agreement with the experimental result is excellent, demonstrating high structural perfection as well as abrupt interfaces and very smooth surfaces of the layers. Note that interference fringes were never observed for pure Fe layers, as can be seen in Fig. 1. The full width at half-maximum for the layer with $T_{Si}=1375$ °C is as low as 0.14° compared to 0.39° of a pure Fe layer. The rms surface roughness as determined by atomic force microscopy (AFM) for the layer with $T_{Si}=1375$ °C is 4 Å (taken over 2×2 μm^2). Above $T_{Si}=1400$ °C, the interference fringes disappear and the peaks become much broader, accompanied by larger rms roughnesses $\geqslant 10$ Å.

Third, the optimum T_G to obtain single-crystal epitaxial Fe_3Si layers with high structural perfection is found to be between 150 and 250 °C, as can be seen in Fig. 2. For higher T_G, reactions of the Fe and/or Si with the Ga and/or As, similar to that observed for Fe epitaxy on GaAs,[3,6] are very likely to occur. This leads to a gradual disappearance of the Fe_3Si peak, accompanied by a broadening with increasing T_G. Note that for T_G around 500 °C, the growth front is no longer two-dimensional, but exhibits a large number of pyramidal-shaped nanocrystals, as evidenced by AFM. To get further inside any interface reactions and/or structural changes at higher T_G, detailed transmission electron microscopy studies are underway. For lower T_G, the Fe_3Si peak again disappears and only a rather broad profile is obtained, although the surface of the layers remains smooth (rms roughness ~4 Å). This is ascribed to an imperfect substitutional ordering and hence, an inhomogeneous composition of the layer due to the much smaller adatom mobility. It is worthwhile mentioning that the optimum T_G for Fe_3Si is considerably higher than that for Fe, Co, and Fe_xCo_{1-x} on GaAs(001). Hence, Fe_3Si is much more suitable for device processing steps after epitaxial growth, for which temperature cycling well above room temperature is often required.

An accurate determination of the exact stoichiometry of Fe_3Si layers from the DCXRD results is rather difficult due to the rather complex Fe–Si phase diagram and discrepancies in the published data of the relaxed lattice constants a_{Fe_3Si} of the Fe_3Si phase.[8,9,11,14] In Fig. 3, we have plotted a_{Fe_3Si} as a function of the Si content and have summarized results from the literature. In order to get an estimate of the composition of our layers, we have applied the following method. First, we calculated a_{Fe_3Si} using $(\Delta a/a)_\perp$ from the DCXRD rocking curves of Fig. 1, taking into account the elastic constants of Fe_3Si: $C_{11}=219$ GPa and $C_{12}=143$ GPa.[15] We then placed the values of a_{Fe_3Si} on the dashed line, which represents the mean value of the previously published data in the range between 10 and 30 at.% Si. From

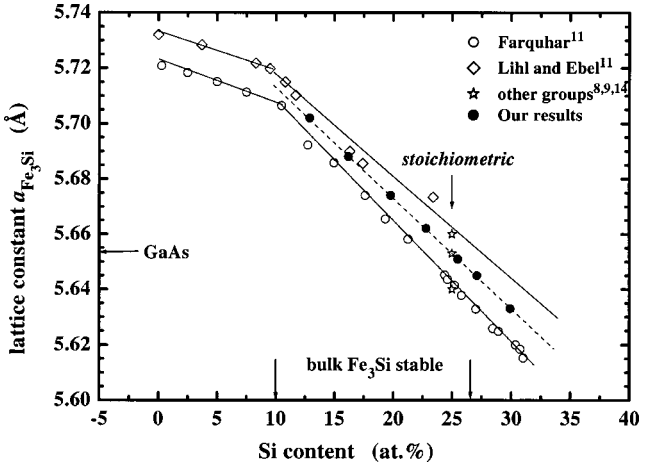

FIG. 3. Dependence of the relaxed lattice constant a_{Fe_3Si} on the Si content for the Fe_3Si phase. The solid lines are guides for the eye. The dashed line gives a mean value in the range of 10 to 30 at. % Si. The solid dots are taken from the results shown in Fig. 1. Note that a larger value of a_{Fe_3Si} belongs to a lower T_{Si} in Fig. 1.

Fig. 3, we can see that the Fe_3Si phase between 10 and 26 at. % Si is correlated with the range of high crystalline and interfacial perfection of the layers in Fig. 1 (namely, for $1360\,°C < T_{Si} < 1395\,°C$), in agreement with the RHEED results mentioned earlier.

The magnetic properties of the layers were measured using superconducting quantum interference device magnetometry at room temperature. Figure 4 shows the magnetization curves of a Fe_3Si layer close to exact stoichiometry, where the magnetic field H is applied in the film plane along the principal crystallographic axes. The layers are ferromagnetic at room temperature, where the easy axis of magnetization is in the film plane along the [100] direction, and the ⟨110⟩ directions are intermediate and slightly nonequivalent. As can be seen in Fig. 4, the magnetic anisotropy is rather small, with coercive fields $H_C \leqslant 1$ Oe (inset of Fig. 4) for all examined orientations. The magnetic moment amounts to 1050 emu/cm^3, which is close to the bulk value of Fe_3Si.[12] A detailed study of the distinct magnetic properties of the layers will be published elsewhere.

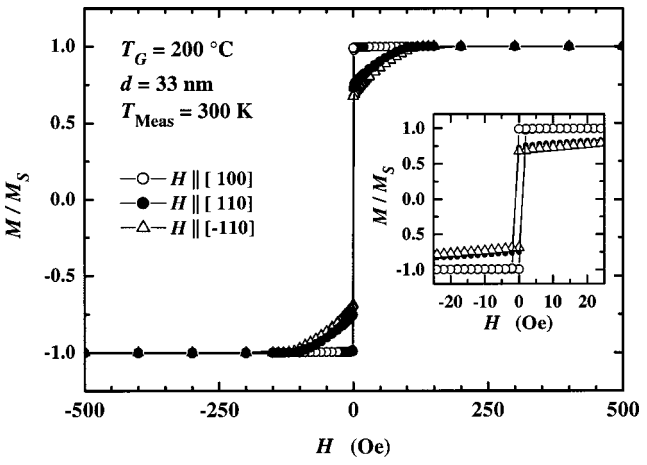

FIG. 4. Hysteresis curves measured at room temperature for a 33 nm Fe_3Si/GaAs(001) layer with the magnetic field H applied in the film plane along various crystallographic orientations. The magnetization M is normalized to the saturation magnetization M_S. The inset shows the hysteresis at very low fields.

In conclusion, we have established an optimized growth temperature range, that is, $150\,°C < T_G < 250\,°C$, in which ferromagnetic Fe_3Si/GaAs(001) hybrid structures with high crystalline and interfacial quality can be fabricated by molecular-beam epitaxy. The results are very promising for the application of Fe_3Si/GaAs(001) hybrid layers for future magnetoelectronics as this system combines high magnetic moments at room temperature with high crystalline and interfacial quality.

This work is partly supported by the German BMBF under contract no. 13N8255. The authors would like to thank O. Brandt for useful discussions.

[1] G. A. Prinz, Phys. Today **48**, 282 (1998).
[2] G. A. Prinz and J. J. Krebs, Appl. Phys. Lett. **39**, 397 (1981); C. Daboo, R. J. Hicken, E. Gu, M. Gester, S. J. Gray, D. E. P. Eley, E. Ahmad, and J. A. C. Bland, J. Appl. Phys. **51**, 15964 (1995); E. M. Kneedler, B. T. Jonker, P. M. Thibado, R. J. Wagner, B. V. Shanabrook, and R. J. Whitman, Phys. Rev. B **56**, 8163 (1997).
[3] H.-P. Schönherr, R. Nötzel, W. Ma, and K. H. Ploog, J. Appl. Phys. **89**, 169 (2001).
[4] K. G. Nath, F. Maeda, S. Suzuki, and Y. Watanabe, J. Appl. Phys. **90**, 1222 (2001).
[5] L. C. Chen, J. W. Dong, B. D. Schulz, B. D. Schultz, C. J. Palmstrom, J. Berezovsky, A. Isakovic, P. A. Crowell, and N. Tabat, J. Vac. Sci. Technol. B **18**, 2057 (2000); M. Dumm, B. Uhl, M. Zölfl, W. Kipferl, and G. Bayreuther, J. Appl. Phys. **91**, 8763 (2002).
[6] A. Fillipe, A. Schuhl, and P. Galtier, Appl. Phys. Lett. **70**, 129 (1997).
[7] H. J. Zhu, M. Ramsteiner, H. Kostial, M. Wassermeier, H.-P. Schönherr, and K. H. Ploog, Phys. Rev. Lett. **87**, 016601 (2001).
[8] M. Hong, H. S. Chen, J. Kwo, A. R. Kortan, J. P. Mannaerts, B. E. Weir, and L. C. Feldman, J. Cryst. Growth **111**, 984 (1991); S. H. Liou, S. S. Malhotra, J. X. Shen, M. Hong, J. Kwo, H. S. Chen, and J. P. Mannaerts, J. Appl. Phys. **73**, 6766 (1993).
[9] P. J. Webster and K. R. A. Ziebeck, *Landolt-Börnstein New Series III/19c* (Springer, Berlin, 1988), p. 104.
[10] R. A. de Groot, F. M. Mueller, P. G. van Engen, and K. H. Buschow, Phys. Rev. Lett. **50**, 2024 (1983); M. J. Otto, H. Feil, R. A. van Bruggen, and C. Haas, J. Magn. Magn. Mater. **70**, 33 (1987); S. Fujii, S. Sugimura, S. Ishida, and S. Asano, J. Phys.: Condens. Matter **43**, 8583 (1990).
[11] For the Fe–Si phase diagram, see M. Hansen, *Constitution of Binary Alloys* (McGraw-Hill, New York, 1958); R. P. Elliot, *Constitution of Binary Alloys, Suppl. 1* (McGraw-Hill, New York, 1965).
[12] W. A. Hines, A. H. Menotti, J. I. Budnick, T. Litrenta, V. Niculescu, and K. Raj, Phys. Rev. B **13**, 4060 (1976).
[13] O. Brandt, P. Waltereit, and K. H. Ploog, J. Phys. D **35**, 577 (2002).
[14] M. Fanciulli, G. Weber, H. van Känel, and N. Onda, Phys. Scr., T **54**, 16 (1994).
[15] G. Kötter, K. Nembach, F. Wallow, and E. Nembach, Mater. Sci. Eng., A **114**, 29 (1989).

Structural and magnetic properties of epitaxial $Fe_3Si/GaAs(001)$ hybrid structures

J. Herfort,[a] H.-P. Schönherr, K.-J. Friedland, and K. H. Ploog
Paul-Drude-Institut für Festkörperelektronik Berlin, Hausvogteiplatz 5-7, 10117 Berlin, Germany

(Received 9 February 2004; accepted 3 April 2004; published 19 August 2004)

The structural, electrical, and magnetic properties of $Fe_3Si/GaAs(001)$ hybrid structures with high crystalline and interfacial perfection are studied. The $Fe_3Si/GaAs(001)$ hybrid structures are fabricated by molecular beam epitaxy at 200 °C. The composition of the films, which can be regarded as a Heusler alloy, is tuned over a wide range of Si content. The high crystalline and interfacial perfection is correlated with the stable Fe_3Si phase. The resistivity of the films shows a strong minimum at almost exact stoichiometry which can be explained by the perfection of the ordering of the Si atoms within the Fe_3Si phase. The layers are ferromagnetic at room temperature with saturation magnetization values close to bulk Fe_3Si. The layers show very small coercive fields which again is correlated with high crystalline and interfacial perfection of the layers within the Fe_3Si phase. [DOI: 10.1116/1.1768528]

I. INTRODUCTION

An important step toward the integration of magnetism into microelectronics is a successful growth of high-quality epitaxial ferromagnetic films on semiconductor substrates.[1] For the epitaxy of ferromagnet/semiconductor (FM/SC) hybrid structures such as Fe,[2–6] Co,[7] and the binary alloy Fe_xCo_{1-x} (Refs. 8 and 9) on GaAs(001), the growth temperature has to be kept very low (close to room temperature), in order to prevent the formation of interfacial compounds[10] at the FM/SC interface. Since these interfacial compounds are adverse to spin injection it is highly desirable to obtain alternative materials which show improved interfacial perfection as well as a higher thermal stability of the FM/SC interface. Nevertheless, using optimized growth conditions of the Fe/GaAs(001) interface we have succeeded to demonstrate spin injection at room temperature.[11]

So far, only little work has been done on the epitaxial growth of Fe_3Si on GaAs(001) despite the fact that it is almost lattice matched to GaAs and is ferromagnetic up to 840 K.[12,13] Bulk Fe_3Si has the cubic DO_3 structure (Fig. 1) and the unit cell is composed of four interpenetrating fcc sublattices *A*, *B*, *C*, and *D*. Type *A*, *B*, and *C* sites are occupied by Fe atoms in a perfectly ordered Fe_3Si alloy and type *D* sites are occupied by Si atoms. Hence, Fe_3Si can be regarded as a Heusler alloy Fe_2FeSi as there are two distinct crystallographic and magnetic Fe sites.[14] The Fe(A,C) have four Fe(B) and four Si(D) as first nearest neighbors and carry a magnetic moment of $1.35\,\mu_B$ while the Fe(B) have eight Fe first nearest neighbors and carry a magnetic moment of $2.2\,\mu_B$.[15] Moreover, certain Heusler alloys are predicted to be 100% spin polarized at the Fermi level, i.e., they exhibit half-metallic behavior.[16–18]

Very recently, we succeeded to fabricate epitaxial single crystal Fe_3Si films grown by molecular beam epitaxy (MBE) on GaAs(001) substrates.[19] As evidenced by double crystal x-ray diffraction measurements (DCXRD) an optimized growth temperature regime, namely, $150\,°C < T_G < 250\,°C$, has been established, where ferromagnetic $Fe_3Si/GaAs(001)$ layers with high crystalline and interfacial perfection can be obtained.[19] It is worth mentioning that the optimum T_G for Fe_3Si is considerably higher than that for Fe, Co, and Fe_xCo_{1-x} on GaAs(001). Hence, Fe_3Si is much more suitable for device processing steps after epitaxial growth for which often temperature cycling well above room temperature is required. Here, we present a detailed study of the structural, electrical, and magnetic properties of $Fe_3Si/GaAs(001)$ hybrid structures grown within this optimized growth temperature range in dependence of the layer composition.

II. SAMPLE PREPARATION

GaAs(001) templates are prepared in a separate III–V growth chamber using standard GaAs growth techniques at 570 °C. Prior to the growth of Fe_3Si, an As-rich (2×1) reconstructed GaAs(001) surface is realized similar to our previous work[5] on Fe/GaAs(001) in order to avoid the formation of macroscopic defects. As controlled by reflection high-energy electron diffraction (RHEED) the As-rich (2×1) reconstructed GaAs(001) surface is obtained by cooling the substrate down to 400 °C under As_4 flux. After closing the As_4 shutter the GaAs template is further cooled down to room temperature. For Fe_3Si growth, the substrate is then transferred through ultrahigh vacuum into a As-free metal deposition chamber which is directly connected to the III–V growth chamber via an interlock. After transfer into the metal MBE chamber the actual surface reconstruction of the GaAs template is again confirmed by RHEED before the growth of Fe_3Si is initiated. Fe and Si are codeposited from high temperature effusion cells at a growth temperature of 200 °C at a growth rate of 0.4 nm/min with a base pressure of 1×10^{-10} Torr. The growth temperature is measured with a thermocouple which was calibrated in a conventional manner using the oxide desorption temperature of an epiready GaAs wafer. The evaporation rates are controlled by the cell tem-

[a]Electronic mail: herfort@pdi-berlin.de

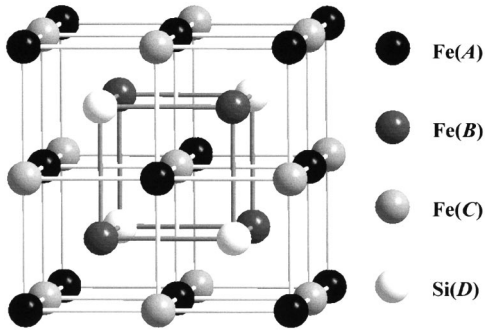

FIG. 1. DO_3 unit cell of the intermetallic alloy Fe_3Si. The sites are represented by *A*, *B*, *C*, and *D*. The *A* and *B* sites are equivalent and are occupied with Fe atoms, the *C* site is also occupied by Fe atoms, and the *D* site by Si atoms.

peratures and adjusted by measuring the beam equivalent pressure using a Bayard–Alpert ionization gauge. To change the composition we kept the Fe cell temperature $T_{\mathrm{Fe}} = 1350\,^{\circ}\mathrm{C}$ constant and changed the Si cell temperature T_{Si} in the range between 1360 and 1410 °C. For simplicity we kept the growth time (2 h) constant. This results in layer thicknesses which increase with raising T_{Si} and are determined using x-ray reflectivity measurements to be between 30 and 45 nm for all layers. This thickness range is a compromise to obtain bulk like layers within reasonable growth time.

The growth is monitored *in situ* using RHEED. Figure 2 shows a typical RHEED patterns of a Fe_3Si layer taken after the growth along the [110] and [010] directions, respectively. Immediately upon deposition of about 1 ML Fe_3Si, a sharp streaky (2×2) RHEED pattern emerges and is maintained throughout the further growth. After a few MLs sharp Kikuchi lines are observed. This is an indication of a two-dimensional growth mode and implies a smooth surface of the films. The epitaxial orientation relationship is determined to be $Fe_3Si(001)\langle 110\rangle \| GaAs(001)\langle 110\rangle$ by RHEED, which was later confirmed by DCXRD. However, the RHEED pattern changes from a 2× to a more complex 5× pattern along the [110] direction for T_{Si} above 1400 °C, indicating the appearance of a different Fe_xSi_y phase due to the higher Si flux.

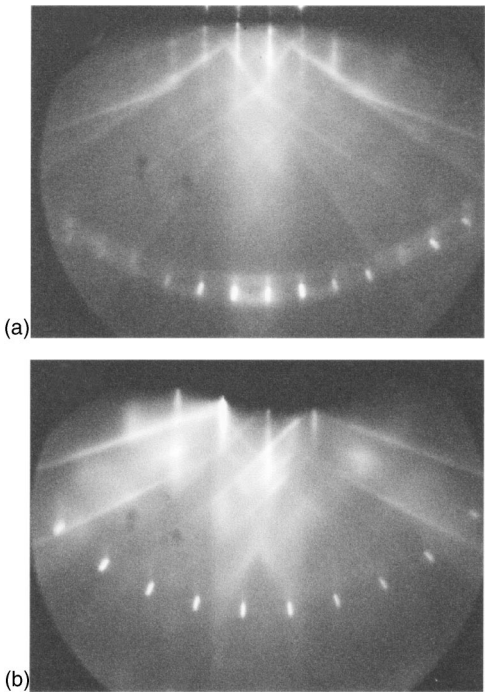

FIG. 2. RHEED pattern taken immediately after the MBE growth of 30 nm Fe_3Si on GaAs(001) along the (a) [110] and (b) [010] crystallographic directions.

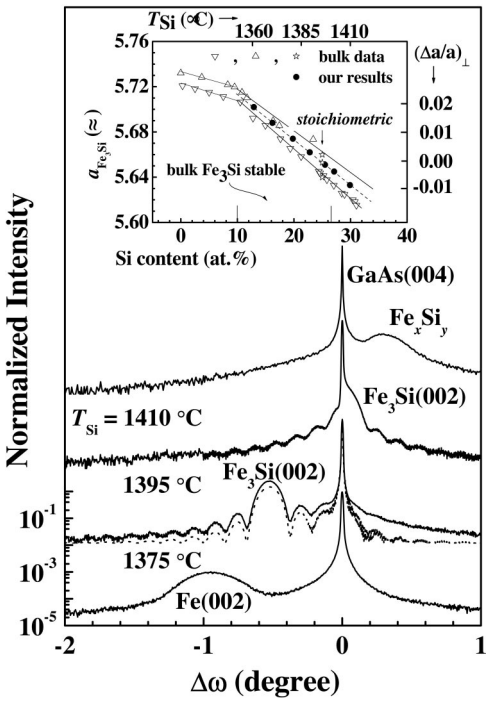

FIG. 3. Semilogarithmic plots of the normalized intensity of DCXRD rocking curves of various Fe_3Si/GaAs(001) layers grown at 200 °C in dependence of the Si cell temperature T_{Si}. The bottom curve belongs to a Fe/GaAs(001) layer grown at 50 °C. The curves are normalized to the GaAs(004) reflection of the substrate. The rocking curves are shifted for clarity. The dotted line shows a simulation for $T_{\mathrm{Si}} = 1375\,^{\circ}\mathrm{C}$. The inset shows the correlation between the relaxed lattice constant a_{Fe_3Si}, the Si cell temperature T_{Si}, the perpendicular lattice mismatch $(\Delta a/a)_\perp$ and the Si content and summarizes results from the literature (Refs. 12–14, 20, and 22).

III. RESULTS AND DISCUSSION

A. Double crystal x-ray diffraction

Figure 3 summarizes the results of DCXRD measurements on Fe_3Si films having different composition, i.e., different T_{Si}. The rocking curves are recorded with a wide open detector and normalized with respect to the symmetric GaAs(004) reflection of the substrate. The second reflection is due to the Fe_3Si layer. For comparison we have included in Fig. 3 the rocking curve of a pure Fe film ($d = 35$ nm) grown at 50 °C, which is the optimized T_G for Fe epitaxy on GaAs(001).[5,6] With increasing T_{Si} the Fe_3Si peak systematically shifts with respect to the GaAs main peak, indicating the different composition of the layers. Note that the Fe_3Si

phase covers a range from 10 to 26.6 at. % Si.[20] As the Fe/Si ratio is varied around stoichiometry, any excess Fe will substitute into Si lattice sites and vice versa, leading to different lattice constants of the layers.[15] From the peak separation the perpendicular lattice mismatch $(\Delta a/a)_\perp$ of the layers is determined, which varies between $+2\%$ and -0.85% for T_{Si} between 1360 and 1410 °C, respectively. The layers are pseudomorph and tetragonally distorted with the parallel lattice mismatch smaller than 0.01%, as evidenced by DCXRD profiles of asymmetric Bragg reflections (not shown here).

In general, both the structural quality and the interface abruptness of the layers initially improve with increasing T_{Si} and then deteriorate above $T_{Si}=1400$ °C. This is evidenced by the appearance of distinct interference (Pendellösung) fringes up to the fifth order and very narrow Fe_3Si peaks. For a qualitative comparison, we have included in Fig. 3 a simulation of the rocking curve using the Takagi–Taupin formalism[21] for the Fe_3Si layer with $T_{Si}=1375$ °C. Fit parameters are the lattice mismatch $(\Delta a/a)_\perp$ and the layer thickness d taking into account only the instrumental broadening of the diffractometer. The agreement with the experimental result is excellent, demonstrating high structural perfection as well as abrupt interfaces and very smooth surfaces of the layers. Note that interference fringes were never observed for pure Fe layers, as can be seen in Fig. 3. The full width at half maximum of the $Fe_3Si(002)$ reflection for the layer with $T_{Si}=1375$ °C is as low as 0.14° compared to 0.39° of a pure Fe layer. The rms surface roughness as determined by atomic force microscopy for the layer with $T_{Si}=1375$ °C is 4 Å (taken over an area of 2×2 μm^2). Above $T_{Si}=1400$ °C the interference fringes disappear and the peaks become much broader accompanied by larger rms roughnesses $\geqslant 10$ Å.

An accurate determination of the exact stoichiometry of Fe_3Si layers from the DCXRD results is difficult due to the rather complex Fe-Si phase diagram and discrepancies among the published data of the relaxed lattice constants a_{Fe_3Si} of the Fe_3Si phase.[12–14,20,22] In the inset of Fig. 3 we have plotted a_{Fe_3Si} as a function of the Si content and summarized results from the literature. In order to estimate the composition of our layers we have applied the following method. First, we calculated a_{Fe_3Si} using $(\Delta a/a)_\perp$ from the DCXRD rocking curves of Fig. 3, taking into account the elastic constants of Fe_3Si, i.e., $C_{11}=219$ GPa and $C_{12}=143$ GPa.[23] Then, we have placed the values of a_{Fe_3Si} on the dashed line which represents the mean value of the previously published data in the range between 10 and 30 at. % Si. From the inset of Fig. 3 we can see that the Fe_3Si phase between 10 and 26 at. % Si is correlated with the range of high crystalline and interfacial perfection of the layers, namely, for $1360\,°C < T_{Si} < 1395\,°C$, in agreement with the RHEED results mentioned above.

B. Resitivity measurements

Figure 4 displays the dependence of the resistivity R_S of several Fe_3Si layers on the composition of the layers. The resistance of the layers is measured by van der Paw and Hall bar structures at temperatures 77 and 300 K. The resistivity does not substantially change for lower temperatures down to 4.2 K. The thickness of the films determined by DCXRD was used in calculating R_S. The composition of the layers is expressed in the form of the perpendicular lattice mismatch $(\Delta a/a)_\perp$. The upper scale in Fig. 4 gives the composition of the films within the Fe_3Si range which has been determined from the inset of Fig. 3. As can be seen in Fig. 4, irrespective of the temperature, R_S first increases with increasing Si content. Beyond about 20 at. % Si, however, R_S strongly decreases with further increase of the Si content. A deep minimum is reached around the exact stoichiometry. For even higher Si contents R_S drastically increases again. The values at room temperature are slightly larger than those for bulk Fe_3Si, but the composition dependence is very similar.[24] The inset of Fig. 4 shows the ratio of the sheet resistance values at 300 and 77 K, $R_S^{300\,K}/R_S^{77\,K}$, as a function of the composition. As can be seen from the inset of Fig. 4, $R_S^{300\,K}/R_S^{77\,K}$ peaks sharply around the exact stoichiometry, in correspondence with the observed minimum in R_S. This indicates that the dominating scattering mechanisms are different within and outside the strong minimum in R_S.

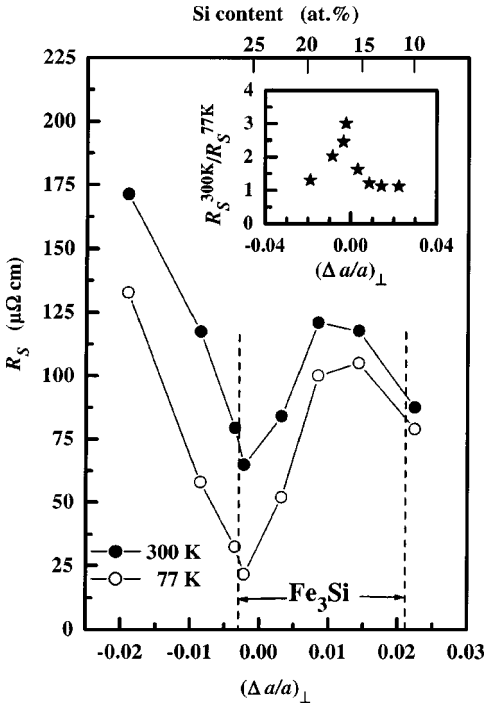

FIG. 4. Sheet resistance R_S of several Fe_3Si layers in dependence of the composition of the layers expressed in the form of the perpendicular lattice mismatch $(\Delta a/a)_\perp$ of the films for two different temperatures. The upper scale gives the composition of the films within the Fe_3Si range as determined from the inset of Fig. 3. The inset shows the ratio of the resistance values at 300 and 77 K, $R_S^{300\,K}/R_S^{77\,K}$, in dependence of the composition.

The above results can be qualitatively understood by considering the ordering of the Si atoms within the Fe_3Si phase. The resistivity of pure Fe will rapidly increase with an addition of Si since the Si atoms will act as random impurities and lead to an enhancement of ''alloy'' scattering in the lay-

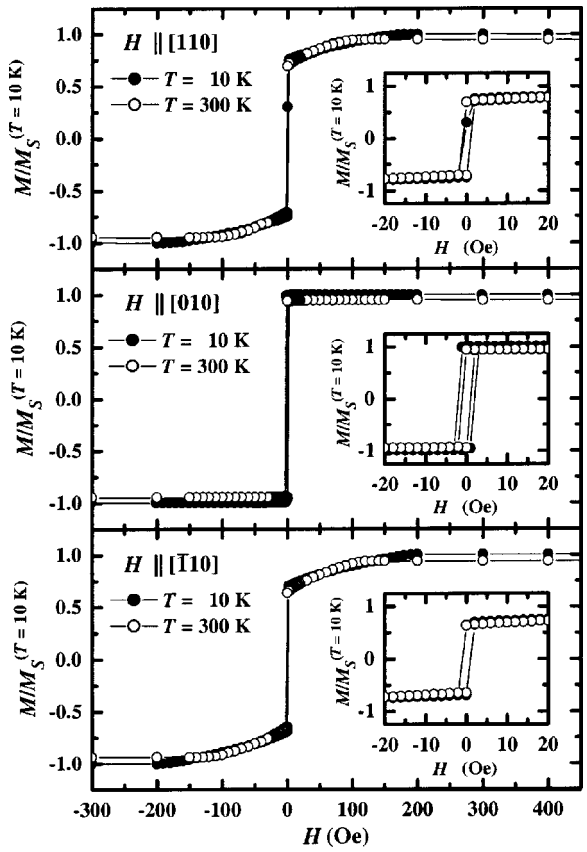

FIG. 5. Magnetization curves for a 33 nm Fe_3Si/GaAs(001) layer (T_{Si} = 1375 °C, $(\Delta a/a)_\perp = 1.41\%$) with the magnetic field H applied in the film plane along various crystallographic orientations. The measurements have been performed at room temperature (300 K) and low temperature (10 K), respectively. The magnetization M is normalized to the saturation magnetization $M_S^{(T=10\ \mathrm{K})}$. The inset shows the magnetization curves at very low fields.

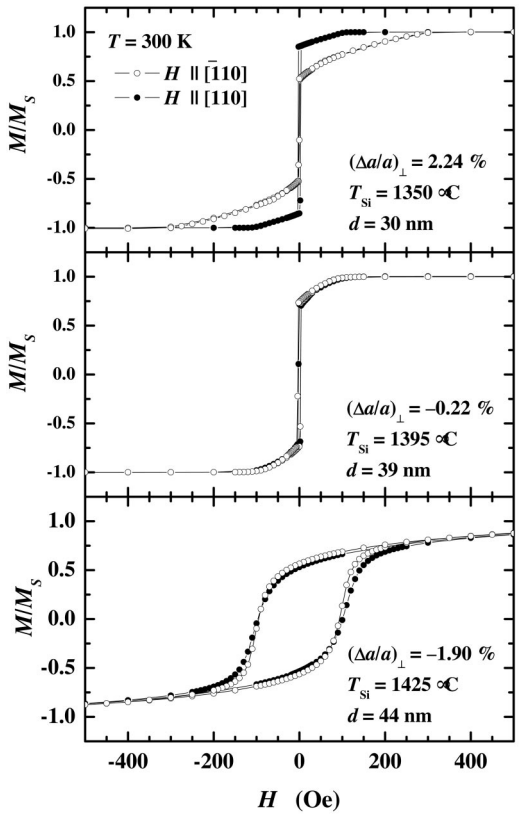

FIG. 6. Magnetization curves at room temperature along the [110] and [$\bar{1}$10] directions for three layers having different composition. The data are normalized to the saturation magnetization.

ers which exhibits weak temperature dependence. The increase in the resistivity is suppressed beyond 10 at. % of Si, when atomic ordering begins to occur. While the ordering is established the resistivity turns from the local maximum (around 20 at. %) to the minimum at the perfect ordering for stoichiometric Fe_3Si. Since in this case ''alloy'' scattering is strongly reduced and phonon scattering which is more strongly temperature dependent, come into play. The strong increase of the resistivity for even higher Si content is attributed to the deviation from the perfect ordering, as a consequence of the appearence of a new Fe_xSi_y phase identified by RHEED and DCXRD.

C. Magnetic properties

The magnetic properties of the layers are measured using superconducting quantum interference device (SQUID) magnetometry and are summarized in Figs. 5–7. Figure 5 shows the magnetization curves of a Fe_3Si layer where the magnetic field H is applied in the film plane along three principal crystallographic axes for two different temperatures 10 and 300 K, respectively. The magnetization curves have been corrected for a small diamagnetic contribution of the GaAs substrate and normalized to the saturation magnetization M_S at 10 K. The layers are ferromagnetic in the whole available temperature range of the SQUID magnetometer (2 to 400 K). The easy axis of magnetization is in the film plane along the [010] direction and the ⟨110⟩ directions are intermediate or hard axis. However, the in-plane anisotropy fields along the ⟨110⟩ directions are rather small, i.e., about 100 Oe at T = 300 K and about 200 Oe at T = 10 K. The temperature dependence of the saturation magnetization (≤5%) is weak as can be expected since the measurements are performed at temperatures far below the Curie temperature. As can be seen in the inset of Fig. 5 small, temperature independent coercive fields $H_C \leq 1$ Oe are obtained for all examined orientations.

Figure 6 shows the magnetization curves at room temperature along the [110] and [$\bar{1}$10] directions for three layers having different composition. As indicated by the values of $(\Delta a/a)_\perp$ the Si content of the layers increases from the top to the bottom in Fig. 6. Two main conclusions can be deduced in Fig. 6. First, the nonequivalence of the magnetization along the [110] and [$\bar{1}$10] directions observed for low Si content (topmost layer in Fig. 6) and pure Fe films (not shown here) in this thickness range is lifted for higher Si content leading to almost identical magnetization curves along both ⟨110⟩ directions. The nonequivalence of the ⟨110⟩ directions for pure Fe is due to the contribution of the very strong uniaxial magnetic anisotropy (UMA) observed in Fe/GaAs(001) films to the effective magnetic anisotropy.[25] The

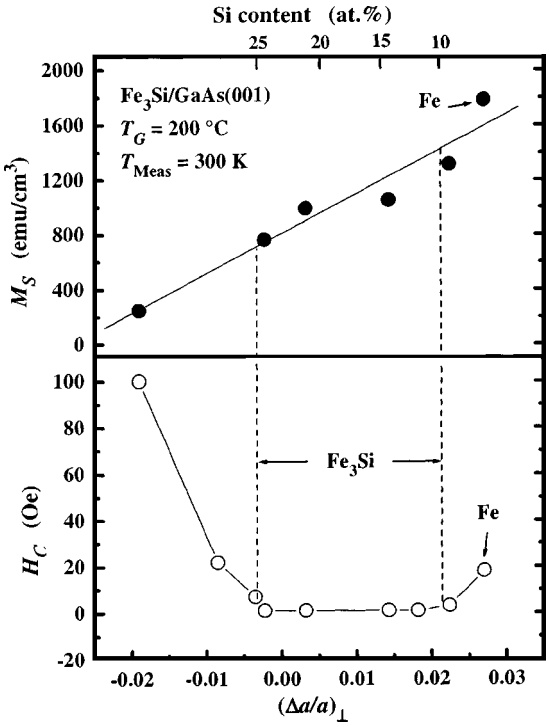

FIG. 7. Saturation magnetization M_S and coercive field H_C of several Fe_3Si layers in dependence of the composition of the layers expressed in the form of the perpendicular lattice mismatch $(\Delta a/a)_\perp$ of the films. The upper scale gives the composition of the films within the Fe_3Si range as determined from the inset of Fig. 3.

UMA is a pure interface related term with the uniaxial hard axis along the $[\bar{1}10]$ direction.[25,26] Hence, the nearly identical magnetization curves along both $\langle 110\rangle$ directions indicate that the contribution of the UMA to the effective magnetic anisotropy is significantly reduced for the Fe_3Si layers. This suggests that the anisotropic Fe–As bonding structure, which is considered to be responsible for the strong UMA in the Fe/GaAs(001) system,[27,28] is strongly modified for Fe_3Si/GaAs(001) layers. However, to get further insight, a detailed study of the thickness dependence of the magnetic anisotropy, which is currently underway, and the exact atomic configuration at the Fe_3Si/GaAs(001) interface are required.

Second, in addition to the structural properties mentioned in Sec. III A, the magnetic properties are significantly modified for Fe_xSi_y layers, i.e., for films grown at $T_{Si}>1400\,^\circ$C. As can be seen for the bottom curves in Fig. 6 the magnetization curves show a much more rounded shape with strongly increased in-plane anisotropy fields and coercive fields.

Figure 7 summarizes the values for the saturation magnetization M_S and the coercive fields H_C obtained from the experimental magnetization curves of several Fe_3Si layers in dependence of the composition of the layers. M_S decreases almost linearly with increasing the Si content of the layers. Although the scatter of the data is rather large (most likely due to the uncertainty in determining the exact volume of the ferromagnetic films) the values are very close to the bulk values for Fe_3Si.[14,24] In addition, Fig. 7 reveals that the observation of very small coercive fields is restricted to the Fe_3Si phase between 10 and 26 at. % Si. We would like to point out that any structural degradation of the layer and the interface will increase the coercive field. Hence, this provides further evidences that the Fe_3Si phase is correlated with the range of high crystalline and interfacial perfection of the layers, i.e., for $1360\,^\circ\text{C}<T_{Si}<1395\,^\circ\text{C}$, in agreement with the RHEED and DCXRD results mentioned above.

IV. CONCLUSIONS

In conclusion, we have shown that Fe_3Si/GaAs(001) hybrid structures with high crystalline and interfacial perfection can be fabricated by molecular beam epitaxy at 200 °C. The composition of the films, which can be regarded as a Heusler alloy, can be tuned within the stable Fe_3Si phase. The strong minimum in the resistivity of the films at almost exact stoichiometry can be explained by the perfection of the ordering of the Si atoms within the Fe_3Si phase. The layers are ferromagnetic at room temperature with saturation magnetization values close to that of bulk Fe_3Si. The layers show very small coercive fields which is correlated with the high crystalline and interfacial perfection of the layers within the Fe_3Si phase. The results are promising for the application of Fe_3Si/GaAs(001) hybrid layers for future magnetoelectronics as this system combines high magnetic moments at room temperature with high crystalline and interfacial perfection. Moreover, the possibility of tuning the composition within the Fe_3Si phase provides a higher degree of freedom for the design of ferromagnet/semiconductor devices.

ACKNOWLEDGMENTS

This work is partly supported by the Bundesministerium für Bildung und Forschung (BMBF) of the Federal Republic of Germany under Contract No. 13N8255. The authors would like to thank A. Riedel for technical assistance during the resistivity measurements, O. Brandt for useful discussions, and Y. Takagaki for a careful reading of the manuscript.

[1] G. A. Prinz, Phys. Today **48**, 282 (1998).
[2] G. A. Prinz and J. J. Krebs, Appl. Phys. Lett. **39**, 397 (1981).
[3] C. Daboo, R. J. Hicken, E. Gu, M. Gester, S. J. Gray, D. E. P. Eley, E. Ahmad, and J. A. C. Bland, Phys. Rev. B **51**, 15964 (1995).
[4] E. M. Kneedler, B. T. Jonker, P. M. Thibado, R. J. Wagner, B. V. Shanabrook, and R. J. Whitman, Phys. Rev. B **56**, 8163 (1997).
[5] H.-P. Schönherr, R. Nötzel, W. Ma, and K. H. Ploog, J. Appl. Phys. **89**, 169 (2001).
[6] J. Herfort, W. Braun, A. Trampert, H.-P. Schönherr, and K. H. Ploog, Appl. Surf. Sci. (in press).
[7] K. G. Nath, F. Maeda, S. Suzuki, and Y. Watanabe, J. Appl. Phys. **90**, 1222 (2001).
[8] L. C. Chen, J. W. Dong, B. D. Schulz, B. D. Schultz, C. J. Palmstrom, J. Berezovsky, A. Isakovic, P. A. Crowell, and N. Tabat, J. Vac. Sci. Technol. B **18**, 2057 (2000).
[9] M. Dumm, B. Uhl, M. Zölfl, W. Kipferl, and G. Bayreuther, J. Appl. Phys. **91**, 8763 (2002).
[10] A. Fillipe, A. Schuhl, and P. Galtier, Appl. Phys. Lett. **70**, 129 (1997).
[11] H. J. Zhu, M. Ramsteiner, H. Kostial, M. Wassermeier, H.-P. Schönherr, and K. H. Ploog, Phys. Rev. Lett. **87**, 016601 (2001).

[12]M. Hong, H. S. Chen, J. Kwo, A. R. Kortan, J. P. Mannaerts, B. E. Weir, and L. C. Feldman, J. Cryst. Growth **111**, 984 (1991).
[13]S. H. Liou, S. S. Malhotra, J. X. Shen, M. Hong, J. Kwo, H. S. Chen, and J. P. Mannaerts, J. Appl. Phys. **73**, 6766 (1993).
[14]P. J. Webster and K. R. A. Ziebeck, *Landolt-Börnstein New Series III/19c* (Springer, Berlin, 1988), p. 104.
[15]W. A. Hines, A. H. Menotti, J. I. Budnick, T. J. Burch, T. Litrenta, V. Niculescu, and K. Raj, Phys. Rev. B **13**, 4060 (1976).
[16]R. A. de Groot, F. M. Mueller, P. G. van Engen, and K. H. Buschow, Phys. Rev. Lett. **50**, 2024 (1983).
[17]M. J. Otto, H. Feil, R. A. van Bruggen, and C. Haas, J. Magn. Magn. Mater. **70**, 33 (1987).
[18]S. Fujii, S. Sugimura, S. Ishida, and S. Asano, J. Phys.: Condens. Matter **43**, 8583 (1990).
[19]J. Herfort, H.-P. Schönherr, and K. H. Ploog, Appl. Phys. Lett. **83**, 3912 (2003).
[20]For the Fe-Si phase diagram, see M. Hansen, *Constitution of Binary Alloys* (McGraw-Hill, New York, 1958); R. P. Elliot, *Constitution of Binary Alloys, Suppl. 1* (McGraw-Hill, New York, 1965).
[21]O. Brandt, P. Waltereit, and K. H. Ploog, J. Phys. D **35**, 577 (2002).
[22]M. Fanciulli, G. Weber, H. van Känel, and N. Onda, Phys. Scr., T **54**, 16 (1994).
[23]G. Kötter, K. Nembach, F. Wallow, and E. Nembach, Mater. Sci. Eng., A **114**, 29 (1989).
[24]R. M. Bozorth, *Ferromagnetism* (IEEE Press, New York, 1993).
[25]M. Brockmann, M. Zölfl, S. Miethaner, and G. Bayreuther, J. Magn. Magn. Mater. **198/199**, 384 (1999).
[26]R. Moosbühler, F. Bensch, M. Dumm, and G. Bayreuther, J. Appl. Phys. **91**, 8757 (2002).
[27]O. Thomas, Q. Shen, P. Schieffer, N. Tournier, and B. Lepine, Phys. Rev. Lett. **90**, 017205 (2003).
[28]J. W. Freeland, I. Coulthard, W. J. Antel, and A. P. J. Stampfl, Phys. Rev. B **63**, 193301 (2001).

Spin injection from Fe_3Si into GaAs

A. Kawaharazuka,[a] M. Ramsteiner, J. Herfort, H.-P. Schönherr, H. Kostial, and K. H. Ploog
Paul-Drude-Institut für Festkörperelektronik, Hausvogteiplatz 5–7, 10117 Berlin, Germany

(Received 25 February 2004; accepted 17 August 2004)

We demonstrate room-temperature spin injection from the epitaxially grown ferromagnetic metal Fe_3Si into the semiconductor GaAs. The injection efficiency is comparable to values previously obtained for the Fe/GaAs and MnAs/GaAs hybrid systems using the emission of similar (In,Ga)As/GaAs light-emitting diodes for the detection of spin polarization. The temperature dependence of the detected polarization is explained by taking into account spin relaxation inside the semiconductor device. © *2004 American Institute of Physics*. [DOI: 10.1063/1.1807014]

Electrical spin injection into semiconductors at room temperature has become a crucial issue for the realization of spin-electronic devices.[1,2] Hybrid structures consisting of a ferromagnetic metal layer on a semiconductor (FM/SC) are suitable for room-temperature operation. Actually, spin injection from epitaxially grown FM layers into SC has been demonstrated for Fe on GaAs,[3] Fe on (Al,Ga) As,[4] and MnAs on GaAs.[5] The growth temperature for Fe on (Al,Ga) As has to be kept low (close to room temperature) to prevent the formation of interfacial compounds, which are unfavorable for spin injection.[6] The drawback of MnAs is the Curie temperature of 40 °C, which is rather close to room temperature.[7,8] Regarding processing aspects as well as the heat dissipation in semiconductor devices, it is desirable to establish a FM/SC hybrid system for spin injection, which exhibits a high thermal stability. In this respect, Fe_3Si,[9,10] which is ferromagnetic up to 840 K[11] and almost lattice matched to GaAs, is a promising material for spin injection. Very recently, epitaxial growth of Fe_3Si on GaAs(001) was achieved with high crystalline and interfacial perfection at a growth temperature of $T_G=200$ °C, which is much higher than the one for Fe growth.[12] Moreover, Fe_3Si can be regarded as a Heusler alloy Fe_2FeSi and is therefore a candidate for being half-metallic,[13–15] which should be advantageous concerning the spin-injection efficiency.

In this letter, we demonstrate room-temperature spin injection for the Fe_3Si/GaAs hybrid system. Spin-polarized electrons are electrically injected from the ferromagnetic Fe_3Si layer and detected via the circular polarization of the electroluminescence (EL) intensity emitted by an *n-i-p* light-emitting diode (LED) on the semiconductor side.

The LED device structure consisting of a Fe_3Si injection layer on a $In_{0.1}Ga_{0.9}As$/GaAs LED structure (see Ref. 3) was grown by molecular-beam epitaxy (MBE). From the bottom, a 500 nm-thick *p*-GaAs buffer layer, a 50-nm-thick undoped GaAs barrier, a 4-nm-thick undoped $In_{0.1}Ga_{0.9}As$ quantum well (QW), a 50-nm-thick undoped GaAs barrier, and a 70-nm-thick *n*-GaAs layer were successively grown on the *p*-type GaAs(001) substrate. The doping concentration is 2×10^{18} cm^{-3} for both *n* and *p*-GaAs layers. After growing the LED structure, the substrate was transferred into the As-free metal deposition chamber through ultrahigh vacuum, and then the 35-nm-thick Fe_3Si layer was grown on the *n*-GaAs layer at $T_G=200$ °C For details about the growth of the Fe_3Si layer, we refer to Ref. 12. The epitaxial wafer was processed into LED devices with mesas of 230 μm diameter patterned by dry etching. We also prepared a reference sample from the same wafer by removing the Fe_3Si layer by wet etching and depositing the nonferromagnetic metal Ti. We measured the EL intensity from the back side of the LED structures placed in a superconducting magnet system. The degree of circular polarization of the EL was analyzed by using a photoelastic modulator. Details of the EL measurements are given in Ref. 3.

The low-temperature (25 K) EL spectrum reveals one peak at 1.427 eV due to the recombination of electrons with heavy holes. The linewidth of 11 meV is clearly smaller than the estimated heavy-hole/light-hole splitting of about 45 meV. The degree of circular polarization is determined by $P=(I_+-I_-)/(I_++I_-)$, where $I_+(I_-)$ denotes the intensity of right (left) circularly polarized light integrated over the width determined by the full width at half maximum of the spectrum. The absolute value of the polarization degree P is identical to the spin polarization of the radiatively recombining electrons, if the heavy holes are assumed to be unpolarized. The magnetic-field dependence of the circular polarization degree obtained at 25 K is shown in Fig. 1 (open squares). Successful spin injection must be accompanied by a circular polarization degree that follows the out-of-plane magnetization curve of Fe_3Si (solid line) independently obtained by using superconducting-quantum-interference-device (SQUID) magnetometry. Indeed, the steep increase of the polarization degree in the lower magnetic field region

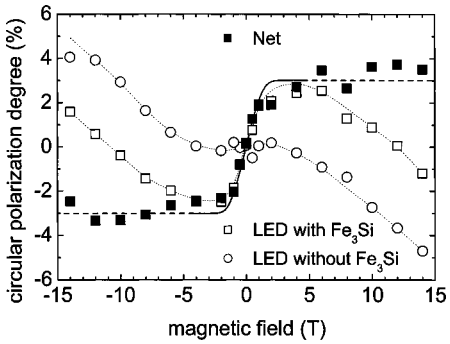

FIG. 1. Circular polarization degree as a function of external magnetic field at 25 K from LEDs with (open squares) and without (open circles) Fe_3Si. Dotted lines are guides to the eyes. The net polarization (closed squares) is plotted together with the magnetization curve measured by SQUID in arbitrary units (solid line, dashed line is a continuation as guide to the eyes).

[a]Electronic mail: kawaha@pdi-berlin.de

($|B|<2$ T) indicates the injection of spin-polarized electrons from Fe_3Si. However, the decrease at higher magnetic fields ($|B|>4$ T) does not correspond to the saturation observed for the out-of-plane magnetization. This discrepancy is due to the contribution of the polarization, which originates from carrier thermalization into the lowest of the Zeeman-split spin-up and spin-down states in the present semiconductor structure (see Ref. 5 for QWs with an In content of 0.1). The contribution of the Zeeman effect to the EL polarization is superimposed on the polarization induced by spin injection at the $Fe_3Si/GaAs$ interface and becomes more pronounced in the higher magnetic-field region. The bare Zeeman-induced polarization in the semiconductor structure can be determined from the EL of the reference LED without a ferromagnetic injection layer. The obtained degree of circular polarization P_{ref} (open circles) decreases monotonously as expected from the contribution due to the Zeeman effect. In order to eliminate the Zeeman contribution, the polarization curve obtained from the reference sample P_{ref} has been subtracted from the total polarization P_{tot} obtained from the sample with Fe_3Si injection layer. This subtraction eliminates the Zeeman contribution for small EL polarizations as can be seen by a first-order approximation of the theoretical expression given in Ref. 16 [Eq. 5]. The resulting net polarization $P_{\mathrm{net}}=P_{\mathrm{tot}}-P_{\mathrm{ref}}$ (closed squares) indeed follows the Fe_3Si out-of-plane magnetization curve obtained from SQUID measurements. This result provides evidence for the successful spin injection from the ferromagnetic metal Fe_3Si into the semiconductor GaAs. The net polarization degree in the saturation region is about 3%, which is comparable to the values previously reported for the injection from Fe and MnAs into similar semiconductor LED structures.[3,5] The similar polarization degrees obtained for the three different FM/SC hybrid systems indicates that the spin polarization is strongly influenced by spin relaxation processes inside the semiconductor device. Therefore, in order to determine the injection mechanism and efficiency at the FM/SC interface, it is essential to understand the spin relaxation processes.

In order to study the influence of the spin relaxation in the semiconductor structure, we investigated the spin injection at higher temperatures. The total and net EL polarizations are shown in Figs. 2(a) and 2(b), respectively. The magnetic-field dependencies of the net polarization degree obtained at 150 and 295 K [Fig. 2(b)] clearly exhibit the signature of spin injection. However, the saturation value decreases with increasing temperature. This observation can be explained by taking into account the carrier lifetime τ_R of the recombining electrons and the spin-relaxation time τ_S in the QW. From a simple rate equation model,[16] the EL polarization degree P is obtained as

$$P=\frac{\eta+r(1-\nu)}{1+r(1+\nu)}, \tag{1}$$

where η denotes the injection efficiency at the $Fe_3Si/GaAs$ interface, $r=\tau_R/2\tau_S$ the ratio between carrier lifetime and spin-relaxation time, and ν the ratio of the electron population between upper and lower Zeeman levels given by Fermi–Dirac distribution functions. In the following we will discuss the dependence of P on the ratio r, which characterizes the semiconductor structure by spin relaxation time and carrier lifetime. Due to their very fast spin relaxation, holes are assumed to be in quasi-equilibrium, i.e., the spin polarization of holes is regarded to be independent of r. Since, consequently, only the spin relaxation time of electrons enters in the ratio r, we eliminated the Zeeman contribution of holes for the sake of simplicity ($\pi=1$ in Ref. 16). When the spin-relaxation time is much longer than the carrier lifetime ($r\ll 1$), the measured EL polarization represents the spin polarization due to electrical injection: $P\approx\eta$. In contrast, when the spin-relaxation time is much shorter than the carrier lifetime ($r\gg 1$), the spin polarization in the QW approaches the quasi-equilibrium state defined by Zeeman splitting. Consequently, the contribution of the Zeeman effect to the observed polarization is significant: $P\approx(1-\nu)/(1+\nu)$.

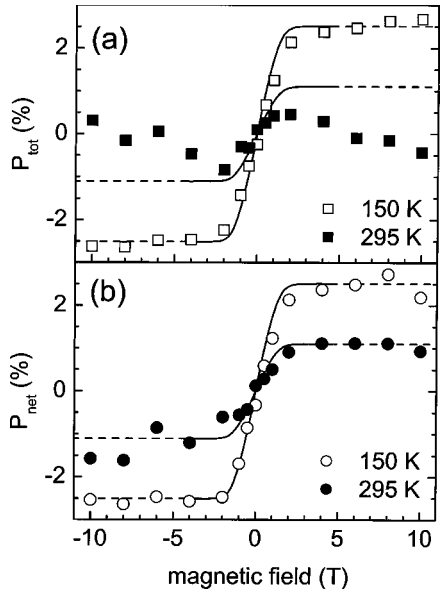

FIG. 2. (a) Total polarization P_{tot} obtained at 150 (open squares) and 295 K (closed squares). (b) Net polarization P_{net} obtained at 150 (open circles) and 295 K (closed circles). Solid lines are magnetization curves measured by SQUID normalized to the net polarization in the saturation region for each temperature. Dashed lines are continuations as guides for the eyes.

The total polarization shown in Fig. 2(a) reveals that the saturation polarization due to spin injection strongly decreases with increasing temperature, whereas the contribution of the Zeeman polarization exhibits a minimum around 150 K. Assuming a constant spin-injection efficiency η (Fe_3Si is ferromagnetic up to 840 K), the spin polarization due to electrical injection does not explicitly depend on temperature. This fact can be deduced from Eq. (1), since a vanishing Zeeman polarization ($\nu\approx 1$) results in

$$P\approx\frac{\eta}{1+2r}=\frac{\eta}{1+\tau_R/\tau_R}. \tag{2}$$

Therefore, the decreasing polarization due to spin injection can be explained only by a temperature-dependent ratio $r=\tau_R/2\tau_S$. Indeed, r has been found to strongly increase above 150 K for QWs with an In content of 0.1 (see Ref. 5). The Zeeman polarization, however, is assumed to decrease monotonously with increasing temperature, since the population ratio ν approaches unity. Without spin injection ($\eta\approx 0$), we obtain

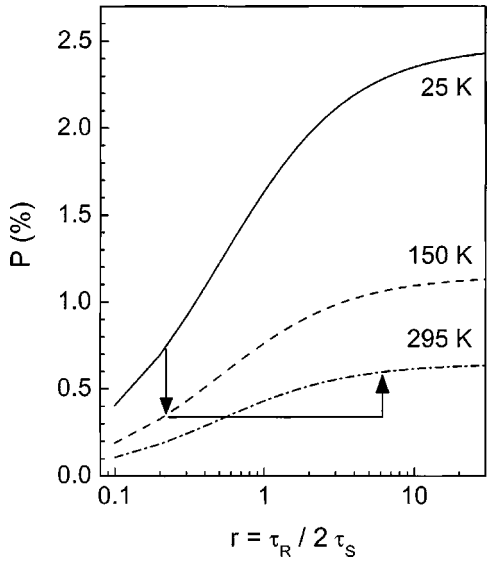

FIG. 3. Zeeman polarization calculated by Eq. (3) as a function of the ratio r for temperatures of 25 (solid line), 150 (dashed line), and 295 K (dash-dotted line). The changes from 25 to 150 K and 150 to 295 K are indicated by arrows. ν is calculated as described in Ref. 16.

$$P \approx \left(\frac{1}{r}\frac{1}{1+\nu}+1\right)^{-1}\frac{1-\nu}{1+\nu}. \tag{3}$$

Consequently, the increasing Zeeman contribution for temperatures above 150 K has to be explained again by a temperature-dependent ratio $r=\tau_R/2\tau_S$. The Zeeman polarization according to Eq. (3) is shown in Fig. 3 as a function of r for different temperatures (at a fixed magnetic field of 14 T). As reasonable parameters, we used a Zeeman splitting of 0.5 meV (observed EL peak splitting at 14 T) and a Fermi energy of 10 meV. The changes from 25 to 150 K as well as from 150 to 295 K are indicated by arrows in Fig. 3 and explain the observed behavior at least qualitatively. We assume r to be almost constant between 25 and 150 K and to increase by about one order of magnitude between 150 to 295 K (cf. Ref. 5). Altogether, the complete temperature dependence of the EL polarization can be explained in a consistent way by an increasing carrier lifetime τ_R (or decreasing spin-relaxation time τ_S) at temperatures above 150 K. According to Eq. (2), the net polarization represents the lower limit of the spin-injection efficiency at the $Fe_3Si/GaAs$ interface. The estimated spin-injection efficiency is about 10% at 25 K by assuming the spin-relaxation time and carrier lifetime obtained from a similar semiconductor structure (Ref. 5). For a more quantitative consideration, carrier lifetimes and spin-relaxation processes in the actual semiconductor LED device have to be studied in more detail.

Note that the observed temperature dependence of the EL polarization cannot be explained by artifacts due to a possible magnetic circular dichroism (MCD), which in principle could influence the polarization of the EL light reflected at the $Fe_3Si/GaAs$ interface.[17] Such a MCD effect would indeed be proportional to the magnetization of the ferromagnetic layer. However, the magnetic properties of the Fe_3Si injection layer do not change below room temperature as shown in Ref. 18, since the Curie temperature of Fe_3Si is much higher.

In conclusion, injection of spin-polarized electrons up to room temperature has been demonstrated in a FM/SC hybrid structure $Fe_3Si/GaAs$. The spin-injection efficiency is comparable to values obtained for the Fe/GaAs and MnAs/GaAs hybrid systems, but Fe_3Si is, in particular, promising for device applications because of its high thermal stability. The temperature dependence of the detected polarization can be consistently explained by spin-relaxation processes in the semiconductor LED.

The authors would like to thank E. Wiebicke for sample processing. This work was partly supported by the German BMBF under Contract No. 13N8255.

[1] G. A. Prinz, Phys. Today **48**, 58 (1995).
[2] S. A. Wolf, D. D. Awschalom, R. A. Buhrman, J. M. Daughton, S. von Molnár, M. L. Roukes, A. Y. Chtchelkanova, and D. M. Treger, Science **294**, 1488 (2001).
[3] H. J. Zhu, M. Ramsteiner, H. Kostial, M. Wassermeier, H.-P. Schönherr, and K. H. Ploog, Phys. Rev. Lett. **87**, 016601 (2002).
[4] A. T. Hanbicki, B. T. Jonker, G. Itskos, G. Kioseoglou, and A. Petrou, Appl. Phys. Lett. **80**, 1240 (2002).
[5] M. Ramsteiner, H. Y. Hao, A. Kawaharazuka, H. J. Zhu, M. Kästner, R. Hey, L. Däweritz, H. T. Grahn, and K. H. Ploog, Phys. Rev. B **66**, 081304 (2002).
[6] H.-P. Schönherr, R. Nötzel, W. Q. Ma, and K. H. Ploog, J. Appl. Phys. **89**, 169 (2001).
[7] M. Tanaka, J. P. Harbison, T. Sands, T. L. Cheeks, V. G. Keramidas, and G. M. Rothberg, J. Vac. Sci. Technol. B **12**, 1091 (1994).
[8] T. Plake, M. Ramsteiner, V. M. Kaganer, B. Jenichen, M. Kästner, L. Däweritz, and K. H. Ploog, Appl. Phys. Lett. **80**, 2523 (2002).
[9] M. Hong, H. S. Chen, J. Kwo, A. R. Kortan, J. P. Mannaerts, B. E. Weir, and L. C. Feldman, J. Cryst. Growth **111**, 984 (1991).
[10] S. H. Liou, S. S. Malhotra, J. X. Shen, M. Hong, J. Kwo, H. S. Chen, and J. P. Mannaerts, J. Appl. Phys. **73**, 6766 (1993).
[11] Y. Nakamura, *Landolt-Börnstein*, New Series III/19c (Springer, Berlin, 1988), p. 26.
[12] J. Herfort, H.-P. Schönherr, and K. H. Ploog, Appl. Phys. Lett. **83**, 3912 (2003).
[13] R. A. de Groot, F. M. Mueller, P. C. van Engen, and K. H. Buschow, Phys. Rev. Lett. **50**, 2024 (1983).
[14] M. J Otto, H. Feil, R. A. van Bruggen, and C. Haas, J. Magn. Magn. Mater. **70**, 33 (1987).
[15] S. Fujii, S. Sugimura, S. Ishida, and S. Asano, J. Phys.: Condens. Matter **43**, 8583 (1990).
[16] M. Ramsteiner, J. Supercond. **16**, 661 (2003).
[17] J. Zak, E. R. Moog, C. Liu, and S. D. Bader, Phys. Rev. B **43**, 6423 (1991).
[18] J. Herfort, H.-P. Schönherr, K.-J. Friedland, and K. H. Ploog, J. Vac. Sci. Technol. B **22**, 2073 (2004).

Available online at www.sciencedirect.com
SCIENCE DIRECT®
Journal of Crystal Growth 278 (2005) 666–670
JOURNAL OF CRYSTAL GROWTH
www.elsevier.com/locate/jcrysgro

Epitaxial growth of Fe_3Si/GaAs(0 0 1) hybrid structures for spintronic application

J. Herfort*, H.-P. Schönherr, A. Kawaharazuka, M. Ramsteiner, K.H. Ploog

Paul-Drude-Institut für Festkörperelektronik Berlin, Hausvogteiplatz 5-7, Berlin 10117, Germany

Available online 2 February 2005

Abstract

Fe_3Si/GaAs(0 0 1) hybrid structures of high crystal and interfacial perfection are fabricated by molecular beam epitaxy at 200 °C. The composition of the films can be tuned over a wide range of Si content. The Fe_3Si/GaAs(0 0 1) films are robust against thermal annealing up to 425 °C. Room-temperature spin injection is demonstrated from the ferromagnetic metal Fe_3Si into the semiconductor GaAs by analyzing the circular polarization of the electroluminescence intensity emitted by an n–i–p light-emitting diode.

PACS: 68.55.−a; 72.25.Hg; 81.15.Hi

Keywords: A1. Spin injection; A3. Molecular beam epitaxy; B2. Ferromagnet/semiconductor hybrid structures

An important step toward the integration of magnetism into microelectronics is the successful growth of high-quality epitaxial ferromagnetic films on semiconductor substrates [1]. Spin injection from epitaxially grown ferromagnet (FM) layers into a semiconductor (SC) has been demonstrated at room temperature (RT) for Fe on GaAs [2], Fe on (Al,Ga)As [3], and MnAs on GaAs [4]. However, for the epitaxy of FM/SC hybrid structures such as Fe on GaAs(0 0 1) [5–9], the growth temperature has to be kept low (close to RT), in order to prevent the formation of interfacial compounds at the FM/SC interface [10], which are considered to be adverse to spin injection. The drawback of MnAs is the Curie temperature of 45 °C, which is rather close to RT [11]. Therefore, it is highly desirable to obtain alternative materials which show improved interfacial perfection as well as a higher thermal stability of the FM/SC interface.

In this respect, Fe_3Si, which is ferromagnetic up to 840 K [12], is a promising candidate for spin injection. Bulk Fe_3Si has the cubic $D0_3$ structure and can be regarded as a Heusler alloy Fe_2FeSi as there are two distinct crystallographic and magnetic Fe sites [12]. Very recently, we succeeded in

*Corresponding author. Tel.: +49 30 20377 344; fax: +49 30 20377 515.
E-mail address: herfort@pdi-berlin.de (J. Herfort).

0022-0248/$ - see front matter © 2005 Elsevier B.V. All rights reserved.
doi:10.1016/j.jcrysgro.2004.12.124

fabricating epitaxial single-crystal Fe_3Si films grown by molecular beam epitaxy (MBE) on GaAs(0 0 1) substrates [13,14]. As evidenced by double-crystal X-ray diffraction measurements (DCXRD), an optimized growth temperature regime, namely $150\,^{\circ}C < T_G < 250\,^{\circ}C$, has been established, where ferromagnetic Fe_3Si/GaAs(0 0 1) layers with high crystalline and interfacial perfection can be obtained [13]. It is important to note that the optimum T_G for Fe_3Si is considerably higher than RT and hence higher than that for Fe, Co, and Fe_xCo_{1-x} on GaAs(0 0 1). Hence, Fe_3Si is much more suitable for device processing steps after epitaxial growth for which temperature cycling well above RT is often required.

GaAs(0 0 1) templates are prepared in a separate III–V growth chamber using standard GaAs growth technique at 580 °C. Prior to the growth of Fe_3Si, an As-rich (2×1) reconstructed GaAs(0 0 1) surface is realized similar to our previous work [8,9] on Fe/GaAs(0 0 1) in order to avoid the formation of macroscopic defects. For Fe_3Si growth, the substrate is then transferred through ultrahigh vacuum (UHV) into an As-free metal deposition chamber which is directly connected to the III–V growth chamber via an interlock. Fe and Si are codeposited from high-temperature effusion cells at a growth temperature of 200 °C with a base pressure of 1×10^{-10} Torr. The evaporation rates are controlled by the cell temperatures and adjusted by measuring the beam equivalent pressure using a Bayard-Alpert ionization gauge. To change the composition we keep the Fe cell temperature constant and change the Si cell temperature T_{Si}. For simplicity we keep the growth time (2 h) constant. This results in layer thicknesses which increase with raising T_{Si} and are obtained using X-ray reflectivity measurements to be between 30 and 45 nm for all layers. The epitaxial orientation relationship is determined to be $Fe_3Si(0\,0\,1)\langle 1\,1\,0\rangle \| GaAs(0\,0\,1)\langle 1\,1\,0\rangle$ by in situ reflection high-energy electron diffraction, and is later confirmed by DCXRD.

Fig. 1 summarizes the results of DCXRD measurements on $Fe_{3+x}Si_{1-x}$ films having different compositions, i.e. different T_{Si}. Here, x reflects the deviation from the exact stoichiometry. The rocking curves are recorded with a wide open detector and normalized with respect to the symmetric GaAs(0 0 4) reflection of the substrate. The second reflection is due to the $Fe_{3+x}Si_{1-x}$ layer. The high structural quality and the interface abruptness of the layers is evidenced by the appearance of distinct interference (Pendellösung) fringes up to the fifth order and very narrow $Fe_{3+x}Si_{1-x}$ peaks. The layers are pseudomorph and tetragonally distorted with the parallel lattice mismatch smaller than 0.01%, as evidenced by DCXRD profiles of asymmetric Bragg reflections (not shown here). With increasing T_{Si} the Fe_3Si peak systematically shifts with respect to the GaAs main peak, indicating the different compositions of the layers. As the Fe/Si ratio is varied around stoichiometry, any excess Fe will substitute into Si lattice sites and vice versa, leading to different lattice constants of the layers [15]. From the peak separation the perpendicular lattice mismatch $(\Delta a/a)_\perp$, and by taking into account the elastic constants of

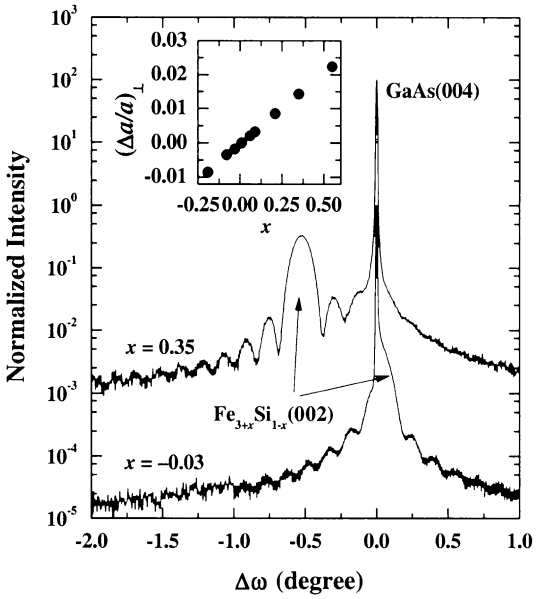

Fig. 1. Semilogarithmic plots of the normalized intensity of DCXRD rocking curves of two different Fe_3Si/GaAs(0 0 1) layers grown at 200 °C. The curves are normalized to the GaAs(0 0 4) reflection of the substrate and shifted for clarity. The inset shows the correlation between the perpendicular lattice mismatch $(\Delta a/a)_\perp$ and the deviation x from the exact stoichiometry as determined from the DCXRD results [14].

$Fe_{3+x}Si_{1-x}$ the relaxed lattice constants of the layers a_L are determined. From a comparison of a_L with the bulk lattice constants (taken from the literature) the composition of the films within the stable Fe_3Si phase can be estimated [13]. Note that the Fe_3Si phase covers a range from 10 to 26.6 at% Si [16], which corresponds to $0.6 \geqslant x \geqslant -0.07$. The correlation between $(\Delta a/a)_\perp$ and the composition of the layers is shown in the inset of Fig. 1. Here, the composition of the layers is expressed in the form of the deviation x from the exact stoichiometry. It is important to note that the exact stoichiometry, i.e. $x = 0$, can be achieved for almost lattice-matched films.

In order to study the thermal stability of the FM/SC hybrid structure we have performed rapid thermal annealing (RTA) on several pieces of an $Fe_{3+x}Si_{1-x}$/GaAs(0 0 1) sample ($T_G = 200\,^\circ C$, $d = 33\,nm, x = 0.35$) at various temperatures T_A between 275 and 575 °C. The RTA has been carried out for 10 min in a nitrogen ambient with a constant heating rate of 20 K/s using a Jetfirst 100 furnace. The dependence of the RTA on the structural properties of the layers has been studied by DCXRD and atomic force microscopy (AFM). Fig. 2 summarizes the results of DCXRD measurements on Fe_3Si films with different T_A. Almost identical rocking curves are observed for the *as-grown* sample and for samples with $T_A \leqslant 425\,^\circ C$, indicating that the structural perfection within the detection limit of DCXRD is not altered by RTA in this temperature range. However, for $T_A \geqslant 500\,^\circ C$ the structural perfection clearly degrades. For the sample with $T_A = 500\,^\circ C$, although interference fringes are still visible, the intensity of the Fe_3Si(0 0 2) reflection is reduced. This is accompanied by the appearance of rectangular-shaped holes with a lateral size of about 1 μm on the surface of the film as observed by AFM. The root mean square (rms) roughness of the films taken over $5 \times 5\,\mu m^2$ is constant with a value of 3–6 Å up to $T_A = 425\,^\circ C$ and then drastically increases (>100 Å) above 500 °C. For the sample with $T_A = 575\,^\circ C$, the Fe_3Si(0 0 2) reflection has completely disappeared and a new peak occurs at $\Delta\omega \approx 4^\circ$ with respect to the GaAs(0 0 4) reflection. Although the chemical composition of the reaction layer is not yet known,

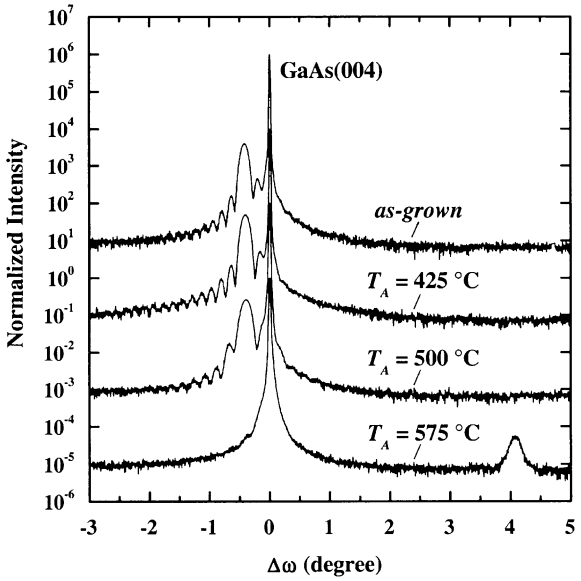

Fig. 2. Semilogarithmic plots of the normalized intensity of DCXRD rocking curves of Fe_3Si/GaAs(0 0 1) layers annealed at different temperatures T_A. The curves are normalized to the GaAs(0 0 4) reflection of the substrate and shifted for clarity.

we speculate from the azimuthal position of the peak with respect to the GaAs(0 0 4) reflection that it is most likely due to the Fe_2As(2 2 0) reflection [17]. Nevertheless, the above results indicate that the Fe_3Si/GaAs(0 0 1) films are robust against thermal annealing up to 425 °C, which is much higher than for Fe/GaAs(0 0 1). However, further investigations like transmission electron microscopy and the electrical characterization of the FM/SC Schottky barrier are required to prove the thermal stability, especially within the distinct interface region.

Spin injection from Fe_3Si into GaAs was investigated by analyzing the electroluminescence (EL) signal of an underlying n–i–p GaAs/(In,-Ga)As light-emitting diode (LED). More details of these investigations are published elsewhere [18]. The LED was grown by MBE on a p-type GaAs substrate with a 500 nm thick p-type GaAs buffer layer. The active region consists of a 4 nm thick $In_{0.1}Ga_{0.9}As$ quantum well (QW) sandwiched between two 50 nm thick undoped GaAs spacer layers. On top of this intrinsic region, a 70 nm thick n-type GaAs layer was grown. The doping

concentration is $2 \times 10^{18}\,\mathrm{cm}^{-3}$ for both n- and p-type GaAs layers. Finally, the 35 nm thick $Fe_{3+x}Si_{1-x}$ ($x = 0.35$) injection layer was deposited on the n-type GaAs in the connected As-free metal deposition MBE chamber at $T_G = 200\,^{\circ}\mathrm{C}$. The EL measurements were carried out in Faraday geometry with the LED mounted in a superconducting magnet system. The magnetic field B is applied out-of-plane which corresponds to a hard axis of magnetization. The EL signal was collected from the backside of the transparent substrate. Details of the EL measurement are given in Ref. [2].

The degree of circular polarization is determined by $P = (I_+ - I_-)/(I_+ + I_-)$, where $I_+(I_-)$ denotes the intensity of right (left) circularly polarized light integrated over the full-width at half-maximum of the EL spectrum. The magnetic field dependence of P obtained at 25 K from LEDs with (solid circles) and without (open circles) Fe_3Si injection layer is shown in Fig. 3(a). We observe a steep increase of the polarization degree in the lower magnetic field region ($|B| < 2$ T) in case of the Fe_3Si injection layer which is not observed in the reference sample (Fe_3Si is replaced by a non-magnetic Ti layer). The decrease of P at higher magnetic fields ($|B| > 4$ T), which is found in both cases, can be attributed to the Zeeman effect inside the semiconductor structure (see Ref. [4] for QWs with a In content of 0.1). In order to eliminate the Zeeman contribution, the polarization curve obtained from the reference sample has been subtracted from the one with Fe_3Si injection layer. The resulting net polarization P_{Net} is shown in Fig. 3(b) for three different temperatures. Successful spin injection must be accompanied by a circular polarization degree that follows the out-of-plane magnetization curve of the Fe_3Si layer. The resulting net polarization indeed follows the out-of-plane magnetization curve independently obtained from superconducting quantum interference device (SQUID) magnetometry. The net polarization degree in the saturation region at 25 K is about 3%, which is comparable to the values previously reported for the injection from Fe and MnAs into similar SC LED structures [2,4]. The magnetic field dependencies of the net polarization degree at higher temperatures, i.e. 150 and 295 K, clearly exhibit the signature of spin

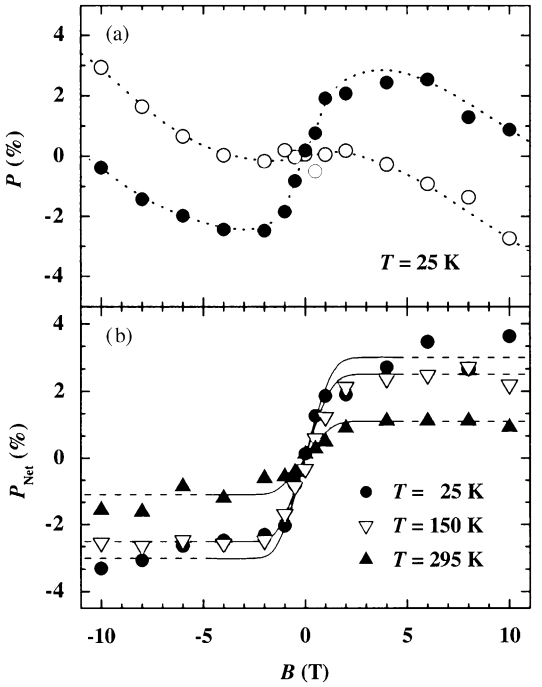

Fig. 3. (a) Circular polarization degree P as a function of the external magnetic field B at 25 K from LEDs with (solid circles) and without (open circles) Fe_3Si. Dotted lines are guides to the eye. (b) The net polarization degree P_{Net} for three different temperatures. Solid lines are magnetization curves measured by SQUID normalized to the net polarization in the saturation region for each temperature. Dashed lines are continuations as guides to the eye.

injection, too. However, the saturation value decreases with increasing temperature.

The similar polarization degrees obtained for three different FM/SC hybrid systems indicate that the spin polarization is strongly influenced by spin relaxation processes inside the SC device. This becomes even more apparent in the temperature dependence of the net polarization degree, which can be explained by taking into account the carrier lifetime τ_R of the recombining electrons and the spin-relaxation time τ_S in the QW. An analysis of a simple rate equation model reveals for the injection efficiency of the $Fe_3Si/GaAs$ interface $\eta = -(1 + \tau_R/\tau_S)P_{Net}$, which follows the temperature dependence of the ratio τ_R/τ_S [18]. Taking into account the results of the temperature dependence of τ_R and τ_S as obtained by time-resolved transmission spectroscopy, the resulting spin

injection efficiency η is about 18% at low temperatures and 10% at high temperatures [19]. Since the magnetic properties of the Fe_3Si injection layer do not change in this temperature range [14], the origin of the remaining temperature dependence of η is not yet clear. Further detailed work has to be done to completely understand the injection mechanism at the FM/SC interface.

In conclusion, we have shown that Fe_3Si/GaAs(0 0 1) hybrid structures of high crystal and interfacial perfection can be fabricated by molecular beam epitaxy at 200 °C. The composition of the films can be tuned over a wide range of Si content. Fe_3Si/GaAs(0 0 1) films are found to be robust against thermal annealing up to 425 °C. Room-temperature spin injection can be achieved from the ferromagnetic metal Fe_3Si into the semiconductor GaAs.

Acknowledgements

The authors would like to thank H. Kostial and E. Wiebicke for sample processing. This work is partly supported by the German BMBF under contract number 13N8255.

References

[1] G.A. Prinz, Physics Today 48 (1998) 282.
[2] H.J. Zhu, M. Ramsteiner, H. Kostial, M. Wassermeier, H.-P. Schönherr, K.H. Ploog, Phys. Rev. Lett. 87 (2001) 016601.
[3] A.T. Hanbicki, B.T. Jonker, G. Itskos, G. Kiseoglou, A. Petrou, Appl. Phys. Lett. 80 (2002) 1240.
[4] M. Ramsteiner, H.Y. Yao, A. Kawaharazuka, H.J. Zhu, M. Kästner, R. Hey, L. Däweritz, K.H. Ploog, Phys. Rev. B 66 (2002) 081304.
[5] G.A. Prinz, J.J. Krebs, Appl. Phys. Lett. 93 (1981) 397.
[6] C. Daboo, R.J. Hicken, E. Gu, M. Gester, S.J. Gray, D.E.P. Eley, E. Ahmad, J.A.C. Bland, J. Appl. Phys. 51 (1995) 15964.
[7] E.M. Kneedler, B.T. Jonker, P.M. Thibado, R.J. Wagner, B.V. Shanabrook, R.J. Whitman, Phys. Rev. B 56 (1997) 8163.
[8] H.-P. Schönherr, R. Nötzel, W. Ma, K.H. Ploog, J. Appl. Phys. 89 (2001) 169.
[9] J. Herfort, W. Braun, A. Trampert, H.-P. Schönherr, K.H. Ploog, Appl. Surf. Sci. 237 (2004) 181.
[10] A. Fillipe, A. Schuhl, P. Galtier, Appl. Phys. Lett. 70 (1997) 129.
[11] C. Guiland, J. Phys. Radium 12 (1951) 223.
[12] Y. Nakamura, Landoldt-Börnstein, New Series III/19c, Springer, Berlin, Heidelberg, 1988, p. 26.
[13] J. Herfort, H.-P. Schönherr, K.H. Ploog, Appl. Phys. Lett. 83 (2003) 3912.
[14] J. Herfort, H.-P. Schönherr, K.-J. Friedland, K.H. Ploog, J. Vac. Sci. Technol. B 22 (2004) 2073.
[15] W.A. Hines, A.H. Menotti, J.I. Budnick, T.J. Burch, T. Litrenta, V. Niculescu, K. Raj, Phys. Rev. B 13 (1976) 4060.
[16] O. Kubaschewski, Iron—Binary Phase Diagrams, Springer, Berlin, Heidelberg, 1982, p. 137.
[17] B. Lepine, S. Ababou, A. Guivarc'h, G. Jezequel, S. Depurtier, R. Guerin, A. Fillipe, A. Schuhl, F. Abel, C. Cohen, A. Rocher, J. Crestou, J. Appl. Phys. 83 (1998) 3077.
[18] A. Kawaharazuka, M. Ramsteiner, J. Herfort, H.-P. Schönherr, H. Kostial, K.H. Ploog, Appl. Phys. Lett. 85 (2004) 3492.
[19] A. Kawaharazuka, M. Ramsteiner, J. Herfort, H.-P. Schönherr, H. Kostial, K.H. Ploog, L. Schreiber, N. Müsgens, K. Schmalbuch, B. Beschoten, unpublished.

Order-driven contribution to the planar Hall effect in Fe_3Si thin films

M. Bowen,* K.-J. Friedland, J. Herfort, H.-P. Schönherr, and K. H. Ploog
Paul Drude Institute for Solid State Electronics, Hausvogteiplatz 5-7, 10117 Berlin, Germany
(Received 3 February 2005; published 4 May 2005)

We report on an intrinsic origin to the planar Hall effect through experiments on the Heusler alloy $Fe_{3+x}Si_{1-x}$ in the range $-0.08 \leqslant x \leqslant +0.06$. Both structural ordering around exact Fe_3Si stoichiometry and thermally regulated magnetic ordering of interpenetrating fcc Fe sublattices drive the planar Hall effect from a conventional to an ordered intrinsic magnetotransport regime. The transition is marked by a change in sign of ρ_{xy} but not of $\Delta\rho_{xx}$. A microscopic model which extends anisotropic magnetoresistance theory correctly describes this regime.

DOI: 10.1103/PhysRevB.71.172401 PACS number(s): 75.47.Np, 72.15.Eb, 73.43.−f, 75.50.Bb

Both the anomalous Hall effect[1] (AHE) and anisotropic magnetoresistance[2] (AMR)—studied intensively over the past several decades—relate to the magnetization of a ferromagnetic thin film in an external magnetic field applied perpendicular and parallel to the film plane, respectively. An early intrinsic description ascribed the anomalous Hall resistivity to a spin-orbit interaction of spin-polarized conduction electrons,[3] while extrinsic models involved scattering potentials due to impurities and defects.[4,5]

The past five years have seen a surge in research on an intrinsic origin to the AHE. According to a recent theory[6] on the prototypical ferromagnet Fe, the AHE arises due to conduction of carriers from a very narrow portion of the Fermi surface which is split by the spin-orbit interaction. The near degeneracy of spin up and spin down states at such points in the band structure may thus induce a nontrivial spin topology throughout the ferromagnet's lattice. Due to a Berry phase[7,8] connection of wavefunctions, this leads to a transverse resistivity, which is intrinsic to the ferromagnetic material. However, while the AHE and the planar Hall effect (PHE) both originate from the spin-orbit interaction,[9] the PHE has not yet been described in a similar framework, despite a conjunction of PHE experiments[10] on and AHE Berry phase theory[11] of dilute magnetic semiconductors. While PHE measurements on Fe have evidenced a deviation from AMR theory,[9,12] a Berry phase description was not applied.

In this paper, we present experimental results on $Fe_{3+x}Si_{1-x}$ thin films with $D0_3$ crystal structure and composition x near Fe_3Si [see Fig. 1(a)], which also reveal an additional contribution to the PHE as compared to the straightforward AMR model. A microscopic model functionally reproduces this PHE term, which we ascribe to topological defects in the spin density distribution. In support of our model, both thermal and structural disorder drive magnetotransport into a conventional regime by destroying the coherence of spin fluctuations between Fe sublattices.

Epitaxial $Fe_{3+x}Si_{1-x}$ thin films of high crystalline and interfacial quality were grown by molecular-beam epitaxy on GaAs(001) substrates.[13] With thicknesses in the 30–50 nm range, these fully strained films are sufficiently thick to quench any significant uniaxial anisotropy.[14] $Fe_{3+x}Si_{1-x}$ films with nearly exact stoichiometry $x=0$ are almost lattice-matched to the GaAs(001) substrate and exhibit a nearly complete magnetization remanence along a [100] easy axis as well as coercive fields of 1 Oe.[14]

Within AMR and AHE theory, the electric field **E** resulting from a current density **j** applied through a ferromagnetic thin film with magnetization vector of unit length **m** is given by

$$\mathbf{E} = \rho_\perp \mathbf{j} + (\rho_\parallel - \rho_\perp)(\mathbf{j}\cdot\mathbf{m})\mathbf{m} + \rho_{HS}(\mathbf{m}\times\mathbf{j}). \quad (1)$$

With sample resistivities $\rho_\parallel$ and $\rho_\perp$ for configurations of current parallel and perpendicular to **m**, respectively, the first term embodies in part longitudinal magnetoresistance and the second one AMR theory. ρ_{HS} describes the normal Hall effect and the AHE resulting from the out-of-plane component of magnetization. Thus, upon rotating a film with a single magnetization domain in a fixed in-plane magnetic field, the longitudinal and transverse resistivities $\Delta\rho_{xx}$ and ρ_{xy}^{AMR} evolve as

$$\Delta\rho_{xx} = (\rho_\parallel - \rho_\perp)\cos^2(\theta_M), \quad (2)$$

$$\rho_{xy}^{AMR} = \frac{1}{2}(\rho_\parallel - \rho_\perp)\sin(2\theta_M), \quad (3)$$

where θ_M denotes the angle between magnetization and current. ρ_{xy}^{AMR} is also called the planar Hall effect.

Magnetotransport experiments in the planar Hall geometry were performed on rectangular samples with Ohmic contacts such that a homogeneous current was directed along the [-110] hard axis. In this crystallographic direction, the angle of in-plane applied magnetic field θ_H is 0. When the magnetic field is directed along an easy magnetization axis, i.e. for $\theta_H=45°$, the directions of applied field and magnetization coincide ($\theta_H=\theta_M$). As the sample is rotated away from $\theta_H=45°$, θ_M begins to lag behind θ_H. Figure 2 presents the evolution of ρ_{xx} and ρ_{xy} with θ_H on a nearly stoichiometric $Fe_{3+x}Si_{1-x}$ sample ($x=+0.01$; 44 nm thick) at $T=77$ K and $T=300$ K. For an applied field $H=25$ Oe which does not overcome the film's fourfold anisotropy energy,[14] sweeping θ_H through a hard axis induces a jump in θ_M toward the next easy axis and consequently a kink (jump) in ρ_{xx} (ρ_{xy}) data. Such behavior indicates single-domain magnetization reversal. As the crucial observation of this paper, an inversion in the angular traces of ρ_{xy} has occurred between $T=77$ K and $T=300$ K, while the angular dependence of ρ_{xx} remains unchanged. The implied sign change of $\rho_{xy}(\theta_H)$ takes place at

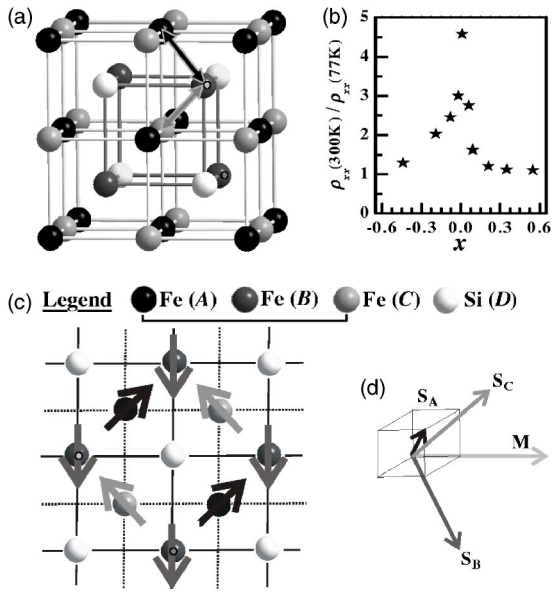

FIG. 1. (a) $D0_3$ structure of Fe_3Si. Arrows indicate magnetic interactions between Fe(B) and Fe(A,C) sites. (b) Evolution of $\rho_{xx}(300\ \mathrm{K})/\rho_{xx}(77\ \mathrm{K})$ with x for $Fe_{3+x}Si_{1-x}$. (c) One spin configuration in a (100) plane for magnetization $\mathbf{M}\|[100]$, with chirality $\chi>0$ due to noncoplanar orientations of Fe(A,B,C) spins which compose $\mathbf{M}$ as schematized in (d).

$T_{\mathrm{ord}}=251$ K for this sample and persists even for a moderate applied field which has overcome the fourfold anisotropy energy. Significantly nonstoichiometric samples do not show this sign change.

Figure 3 presents magnetic field sweeps of ρ_{xx} and ρ_{xy} at a fixed angle θ_H away from the hard axis at $T=300$ K. Our measurements on Fe_3Si down to $T=77$ K show that $\rho_\| < \rho_\perp$, an unusual but not unique result.[2] As the field is lowered, all ρ_{xx} curves [Fig. 3(a)] converge toward the same low-field resistivity, which reflects the rotation of sample magnetization toward an easy axis as identified by the measurement for $\theta_H=45°$. Given Eq. (2), one cannot distinguish between different easy axes from ρ_{xx} data. Correspondingly, ρ_{xy} data

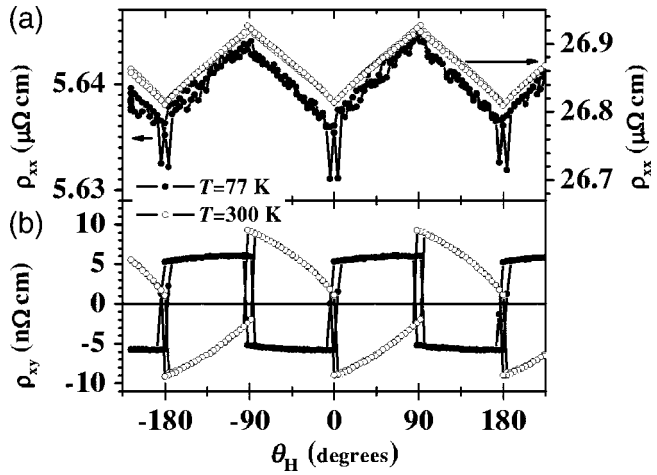

FIG. 2. (a) ρ_{xx} and (b) ρ_{xy} vs θ_H at $T=77$ K (dots) and $T=300$ K (circles) for a sample with $x=+0.01$ at $H=25$ Oe.

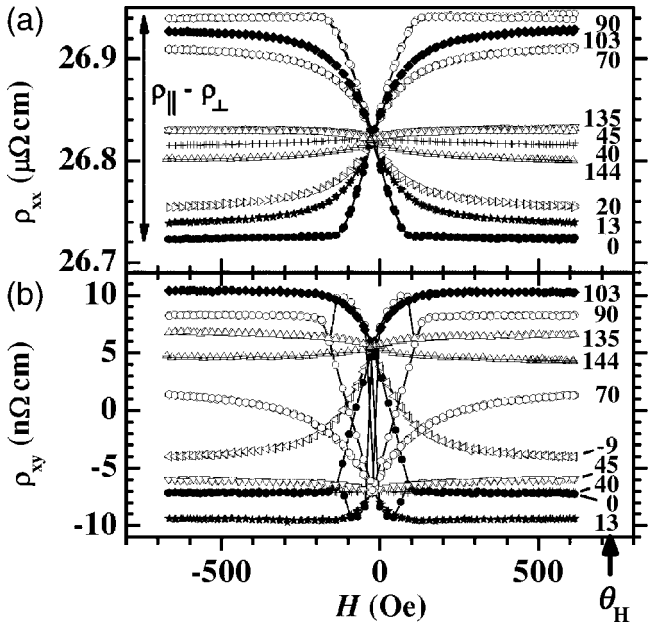

FIG. 3. (a) ρ_{xx} and (b) ρ_{xy} vs applied field H for specific angles θ_H (in degrees), at $T=300$ K for $x=+0.01$.

[Fig. 3(b)] converge to the 45°/135° points in a vanishing applied field, and ρ_{xy} may exhibit two switching events as θ_M jumps from one easy axis to another during magnetization reversal. However, the 45°/135° orientations of magnetization do not represent an extremum as expected within AMR theory from Eq. (3).

To simplify the complex magnetization behavior presented in Figs. 2 and 3, we assume to first order that ρ_{xx} fulfills AMR theory and extract θ_M[12] from Eq. (2). We may then plot ρ_{xy} as a function of θ_M as shown in Fig. 4 for $T=300$ K and $T=77$ K. Relative to AMR theory, $\rho_{xy}(\theta_M)$ also exhibits the expected fourfold anisotropic behavior but is phase-shifted by $\Delta\theta_M(T=300\ \mathrm{K})=-22.5°$ and $\Delta\theta_M(T=77\ \mathrm{K})=+95°$ with respect to these axes. Furthermore, $\Delta\rho_{xy}(\theta_M)$ is generally much lower than the value predicted by AMR theory. We therefore introduce[12] a *compensating* term to ρ_{xy}

$$\rho_{xy}=\sigma_{xy}^{\mathrm{AMR}}+\rho_{xy}^{\mathrm{Comp}}$$
$$=\frac{1}{2}(\rho_\|-\rho_\perp)\sin(2\theta_M)+\rho_{\mathrm{Comp}}\frac{1}{2}\sin(2\theta_M+\theta), \quad (4)$$

which can correct AMR theory above and below T_{ord} (see insets of Fig. 4) using $T=300$ K: $\rho_{\mathrm{Comp}}=-0.95(\rho_\|-\rho_\perp)$, $\theta=2.1°$; $T=77$ K: $\rho_{\mathrm{Comp}}=-1.49(\rho_\|-\rho_\perp)$, $\theta=-3.3°$.

Effects due to domain wall boundaries, atomic disorder, and electron localization could explain our results within AMR theory only if both ρ_{xx} and ρ_{xy} behaved similarly. Also, AMR theory cannot account for $|\rho_{xy}| \ll \rho_\|-\rho_\perp$. A change in sign of the cubic anisotropy constant K_1 (Ref. 15) may be ruled out since the angular position of the jump in ρ_{xy} remains unchanged. A systematic error in the in-plane angular position has been corrected to within ±2°, and the fourfold symmetry of ρ_{xy} jumps precludes any dominant contribution

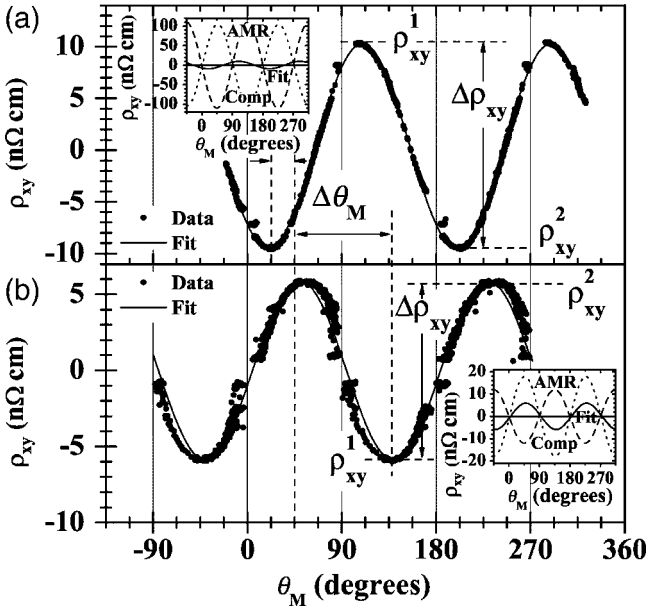

FIG. 4. ρ_{xy} vs θ_M obtained within AMR theory from ρ_{xx} data, at (a) $T=300$ K and (b) $T=77$ K, and fit to Eq. (4) for $x=+0.01$. Insets: $\rho_{xy}^{\mathrm{Comp}}$, ρ_{xy}^{AMR}, and fit vs θ_M.

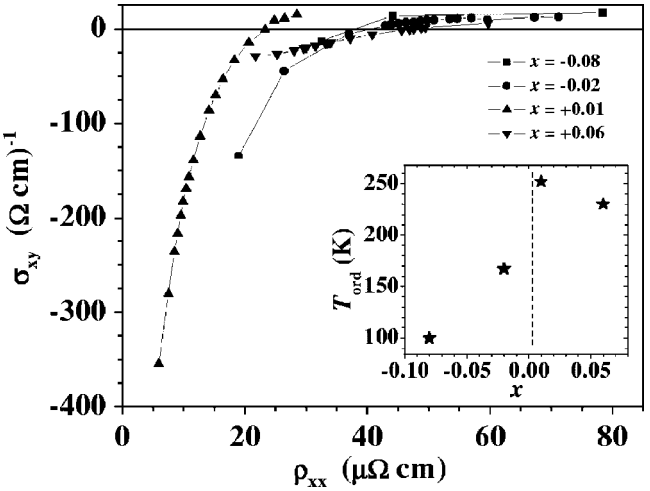

FIG. 5. σ_{xy} vs ρ_{xx} for all samples. Inset: T_{ord} vs x.

from uniaxial anisotropy, in agreement with other measurements.[13] Any small out-of-plane misalignment would induce an antisymmetric angular response from the AHE and was carefully avoided. An intrinsic out-of-plane magnetization was not observed. In addition, such considerations are already excluded through the data analysis contained in Fig. 4, which now narrows the problem exclusively to the dependence of the PHE on θ_M. Altogether, our results demonstrate the existence of an additional contribution to the PHE.

Toward a microscopic model for the additional PHE observed in ordered Fe_3Si with $D0_3$ symmetry, we analyze the ensemble of collective spin fluctuations on the different sublattices given the intra-lattice spin density distribution[16] and a two-spin interaction between the Fe(A,C) and Fe(B) sublattices.[17] The Fe(B) site lies in a cubic magnetic environment of Fe(A,C) sites, so that its spin is unconstrained in rotation. In contrast, the inversion symmetry of the Fe(A,C) spin sublattices is broken due to a tetrahedral Fe(B) environment, resulting in preferred spin orientations. Without any loss of generality to our model, we assume that their on-site spins tend to align along $\langle 111\rangle$ directions containing the magnetically stronger Fe(B) nearest neighbor sites [see arrows in Fig. 1(a)]. Using this constraint, configurations of spins $\mathbf{S}_A,\mathbf{S}_B,\mathbf{S}_C$ at lattice sites Fe(A), Fe(B), and Fe(C) may be found such that the spin chirality $\chi_{ABC}=\mathbf{S}_A\cdot(\mathbf{S}_B\times\mathbf{S}_C)\neq 0$. An example of such a collective spin configuration, which conserves the orientation of mean magnetization $\mathbf{m}\|[100]$ and yields $\chi_{ABC}>0$, is demonstrated in Figs. 1(c) and 1(d). We thus describe collective spin fluctuations in a normal ferromagnet with no frustrated steady spin state.

Spin chirality acts as the gauge flux for the charged carriers which evolve in the background of fluctuating spins, thus describing the AHE as due to a Berry phase connection of the wave function.[18] It was already demonstrated theoretically that a finite AHE may exist in systems with more than two non-coplanar spin sublattices.[19] Due to the high symmetry of the Fe_3Si system, multiply degenerate contributions to a PHE from the ensemble of possible spin configurations for a given $\mathbf{m}$ will cancel each other out. However, this cancellation, which is also typical for the AHE, may be lifted by topological defects at the boundary between clusters of such configurations[20] and by higher-order spin interactions (see Ref. 19 and references therein). Such defects are known to lead to an intrinsic AHE.[21,22] Also, as shown for other systems,[6,22] spin orbit interaction will lift these degeneracies, resulting in Berry phase contributions at narrowly defined regions in k space away from the high-symmetry directions considered here.

Another consequence of the spin orbit interaction is a spin scattering asymmetry between different spin sublattices.[19] Defining such a scattering ratio α_i with $i=A$, B, or C, scattering of an electron with momentum $\mathbf{p}$ at a lattice site with an out-of-plane spin component leads to an in-plane field $H_{\mathrm{SO}}^{\mathrm{planar}}\approx\Sigma_{i=A,B,C}\alpha_i(\mathbf{S}_i\times\mathbf{p})$ which is perpendicular to the electron's momentum $\mathbf{p}$. In addition, an angular analysis of the spin chirality $\chi_{\mathrm{A,B,C}}(\theta_M)$ straightforwardly results in a functional form $H_{\mathrm{SO}}^{\mathrm{planar}}=\sin(\theta_M+\theta)\cos(\theta_M+\theta)$ which corresponds to our experimental observation [see Eq. (4)]. Detailed theoretical calculations beyond the scope of this paper will determine which topological defects and which electrons at the Fermi surface are participating in this angular- and phase-dependent PHE.

Recent calculations[6] for Fe of the AHE in a Berry phase framework yield a large value $\sigma_{xy}\sim 751\ (\Omega\ \mathrm{cm})^{-1}$ from the saturated magnetization. Accordingly, in the planar Hall geometry, we define σ_{xy} to be

$$\sigma_{xy}=\frac{\Delta\rho_{xy}}{\rho_{xx}^2+\Delta\rho_{xy}^2}, \tag{5}$$

where $\Delta\rho_{xy}=\rho_{xy}^1-\rho_{xy}^2$, and ρ_{xy}^1,ρ_{xy}^2 denote the maximum planar Hall resistivities due to the fully saturated magnetiza-

tion (see Fig. 4). For $x=+0.01$ at $T=77$ K, $\sigma_{xy} \sim -350\ (\Omega\,\mathrm{cm})^{-1}$—an extremely large value compared to AMR theory which suggests an intrinsic magnetotransport regime in our ordered alloy.

As seen in Fig. 1(b), metallic conduction in $Fe_{3+x}Si_{1-x}$ is drastically reduced with increasing deviation x from stoichiometry.[14] We may thus *control* structural disorder, while retaining the $D0_3$ crystal structure, and use $\rho_{xx}(T)$ as an ordering parameter. Figure 5 presents the dependence of σ_{xy} on ρ_{xx} for 77 K$\leqslant T \leqslant$300 K. Within $-0.08 \leqslant x \leqslant +0.06$, σ_{xy} exhibits two magnetotransport regimes. In the high-temperature regime, i.e., $T > T_{\mathrm{ord}}$, σ_{xy} is of same sign and comparable amplitude $\sim +20\ (\Omega\,\mathrm{cm})^{-1}$ as for Fe[12] and almost independent of ρ_{xx}. For $T < T_{\mathrm{ord}}$, σ_{xy} changes sign and increases, for low values of x and ρ_{xx}, by over one order of magnitude relative to $\sigma_{xy}(T > T_{\mathrm{ord}})$. No such crossover was observed at $T=4$ K for samples with $x \leqslant -0.19$ and $x +0.09$, i.e., farther from $x=0$. In addition, T_{ord} decreases with increasing $|x|$ (see inset of Fig. 5).[23] The T_{ord} range is in good agreement with the exchange energy $J_{ex}[B \leftrightarrow (A,C)] = 145$ K between Fe(A,C) and Fe(B) sublattices as experimentally determined by Stearns,[17] thus supporting our model. From this we infer that spin-chirality effects between Fe(B) and Fe(A,C) sublattices with coupled spin fluctuations below T_{ord} drive this *ordered intrinsic* magnetotransport regime. In addition, since only our extension to AMR theory can explain our results above T_{ord}, we presume that similar considerations may apply to this conventional regime at high temperature, in related fashion to the case of Fe.[12]

In conclusion, we have observed an additional contribution to the planar Hall effect through experiments on $Fe_{3+x}Si_{1-x}$ films. A microscopic model based on Berry phase effects shows how this extra term reflects magnetic interactions with reduced crystal symmetry for certain Fe sublattices in the ordered Fe_3Si Heusler alloy. Both structural disorder in $Fe_{3+x}Si_{1-x}$ across the $-0.08 \leqslant x \leqslant +0.06$ stoichiometry range and thermal disorder above a correlated temperature T_{ord} destroy the coherent spin density fluctuations and drive the system into a conventional magnetotransport regime. Our results call for an *ab initio* theory on an intrinsic origin of the planar Hall effect, in particular for Fe_3Si.

We thank A. Riedel for technical assistance, H. T. Grahn for a critical reading of the manuscript, and Y. Takagaki, P. Kleinert, P. K. Muduli, R. Engel-Herbert, and S. L. Lu for stimulating discussions.

*Electronic address: mbowen@pdi-berlin.de

[1] T. R. McGuire and R. I. Potter, IEEE Trans. Magn. **11**, 1018 (1975).
[2] I. A. Campbell and A. Fert, in *Ferromagnetic Materials*, edited by E. P. Wohlfarth (North-Holland, Amsterdam, 1982), Vol. 3, p. 797.
[3] R. Karplus and J. Luttinger, Phys. Rev. **95**, 1154 (1954).
[4] J. Smit, Physica (Amsterdam) **21**, 877 (1955).
[5] L. Berger, Phys. Rev. B **2**, 4559 (1970).
[6] Y. Yao, L. Kleinman, A. H. MacDonald, J. Sinova, T. Jungwirth, D. S. Wang, E. Wang, and Q. Niu, Phys. Rev. Lett. **92**, 037204 (2004).
[7] M. V. Berry, Proc. R. Soc. London, Ser. A **392**, 45 (1984).
[8] B. Simon, Phys. Rev. Lett. **51**, 2167 (1983).
[9] K.-J. Friedland, R. Nötzel, H. P. Schönherr, A. Riedel, H. Kostial, and K. H. Ploog, Physica E (Amsterdam) **10**, 442 (2000).
[10] H. X. Tang, R. K. Kawakami, D. D. Awschalom, and M. L. Roukes, Phys. Rev. Lett. **90**, 107201 (2003).
[11] T. Jungwirth, Q. Niu, and A. H. MacDonald, Phys. Rev. Lett. **88**, 207208 (2003).
[12] K.-J. Friedland, J. Herfort, P. K. Muduli, H. P. Schönherr, and K. H. Ploog, J. Supercond. (to be published).
[13] J. Herfort, H.-P. Schönherr, and K. Ploog, Appl. Phys. Lett. **83**, 3912 (2003).
[14] J. Herfort, K.-P. Schönherr, K.-J. Friedland, and K. H. Ploog, J. Vac. Sci. Technol. B **22**, 2073 (2004).
[15] M. Goto and T. Kamimori, J. Phys. Soc. Jpn. **52**, 3710 (1983).
[16] J. Moss and P. J. Brown, J. Phys. F: Met. Phys. **2**, 358 (1972).
[17] M. B. Stearns, Phys. Rev. **168**, 588 (1968).
[18] J. Ye, Y. B. Kim, A. J. Millis, B. I. Shraiman, P. Majumdar, and Z. Tešanović, Phys. Rev. Lett. **83**, 3737 (1999).
[19] R. Shindou and N. Nagaosa, Phys. Rev. Lett. **87**, 116801 (2001).
[20] Y. Lyanda-Geller, S. H. Chun, M. B. Salamon, P. M. Goldbart, P. D. Han, Y. Tomioka, A. Asamitsu, and Y. Tokura, Phys. Rev. B **63**, 184426 (2001).
[21] Y. Taguchi, Y. Oohara, H. Yoshizawa, N. Nagaosa, and Y. Tokura, Science **291**, 2573 (2001).
[22] Z. Fang, N. Nagaosa, K. S. Takahashi, A. Asamitsu, R. Mathieu, T. Ogasawara, H. Yamada, M. Kawasaki, Y. Tokura, and K. Terakura, Science **302**, 92 (2003).
[23] The asymmetry in $T_{\mathrm{ord}}(x)$ could reflect the proximity of Fe_3Si to the $D0_3$ phase boundary at $x<0$. Strain could also play a role.

Long-range order in thin epitaxial Fe_3Si films grown on GaAs(001)

B. Jenichen,* V. M. Kaganer, J. Herfort, D. K. Satapathy, H. P. Schönherr, W. Braun, and K. H. Ploog
Paul-Drude-Institut für Festkörperelektronik, Hausvogteiplatz 5-7, D-10117 Berlin, Germany
(Received 17 March 2005; published 11 August 2005)

As-grown thin epitaxial Fe_3Si films fabricated by molecular beam epitaxy on GaAs(001) are studied by grazing incidence x-ray diffraction. The long-range order parameters of the films of different stoichiometry are determined by measuring fundamental and superlattice crystal truncation rods and comparing them to simulations in dynamical approximation. Two order parameters, associated with the degree of migration of Si atoms into different Fe sublattices, are obtained. A residual intermixing of the sublattices is found, even near complete stoichiometry. The relative positions of the Fe_3Si and GaAs lattices are determined. Fe atoms in Fe_3Si are located at the positions of the Ga atoms in GaAs, with an additional shift of 0.1 ± 0.04 Å of the tetragonally distorted Fe_3Si lattice normal to the interface.

DOI: 10.1103/PhysRevB.72.075329 PACS number(s): 81.15.Hi, 61.10.Nz, 68.55.Nq, 75.50.Cc

I. INTRODUCTION

The combination of magnetic and semiconducting materials opens up new pathways in the development of semiconductor devices utilizing the spin of the carriers.[1] From the viewpoint of such spintronic device structures, it is highly desirable to explore epitaxial ferromagnet/semiconductor heterostructures that possess a rather perfect interface[2] structure as well as high thermal stability. Fe_3Si on GaAs is a promising candidate for spintronics applications.[3–5] It can be grown by molecular beam epitaxy at GaAs substrate temperatures near 200 °C.[6] The Curie temperature of Fe_3Si is as high as 840 °C.[7] Spin injection at room temperature has been already demonstrated.[8] The lattice misfit between stoichiometric Fe_3Si and GaAs is very low.[6] The interface between Fe_3Si and GaAs is found to be smooth and of good structural perfection: Fe_3Si on GaAs can be grown without misfit dislocations at the heterointerface.

Fe_3Si has the face-centered cubic $D0_3$ structure.[9,10] This structure (see Fig. 1) can be considered as four interpenetrating fcc sublattices A, B, C, and D with origins at A(0, 0, 0), B(0.25, 0.25, 0.25), C(0.5, 0.5, 0.5), and D(0.75, 0.75, 0.75). In the ordered Fe_3Si crystal, Fe atoms occupy the three sublattices A, B, and C, while Si atoms fill the sublattice D. Bulk Fe_3Si crystals acquire a long-range order of the sublattices after an annealing in vacuum at 600 °C for about two hours.[11] The ordered alloy can be regarded as a magnetic Heusler alloy $Fe(B)Fe(A,C)_2Si(D)$ with the two distinct Fe sites (A,C) and (B).[10,12] The order in Heusler alloys[13] has a significant influence on their electric and magnetic properties: the magnetic moments of the Fe atoms at the positions Fe(A,C) linearly depend on the number of nearest Fe neighbors.[14,15] Thus, the magnetic properties can be tuned: some of the local Fe magnetic moments are almost as large as in pure bcc iron, while others are reduced due to the presence of Si. Moreover, the introduction of small amounts of transition metal impurities into the Fe_3Si matrix opens up new possibilities[11,16] to tune the magnetic properties. Impurities to the left of Fe in the periodic table prefer the Fe(B) site with eight first-neighbor Fe atoms. Those beneath and to the right of Fe in the periodic table enter the Fe(A, C) site with four Fe and four Si atoms as nearest neighbors. A highly ordered and stoichiometric Fe_3Si matrix is the starting point for most experiments with bulk Fe_3Si.

In as-grown thin epitaxial films of Fe_3Si on GaAs, the lattice mismatch and the long-range order depend on the stoichiometry. Significant changes of the saturation magnetization and the resistivity with film stoichiometry have been observed.[17] While the saturation magnetization changes almost linearly with composition and the coercive field remains unchanged over a wide range of compositions, a clear minimum of the resistivity R_S near stoichiometric conditions is found. It has been suspected that the minimum is due to alloy scattering, which is smallest for an ordered crystal structure, but detection of the degree of the order has been lacking. Moreover, an additional contribution to the planar Hall effect was recently found, which reflects magnetic in-

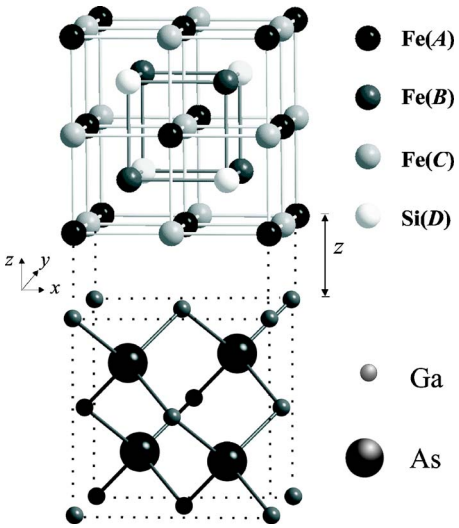

FIG. 1. (Color online) Schematic view of the $D0_3$ unit cell of Fe_3Si grown epitaxially on GaAs. The A and C sites are equivalent and are occupied by Fe. The B sites are also occupied by Fe, whereas the D sites are occupied by Si. In the epitaxial system, the first layer of Fe atoms is located at the positions of the Ga atoms in the GaAs lattice. The vertical shift z is enlarged for clarity. The choice of the radii of the atoms is arbitrary.

TABLE I. Structural parameters and the low temperature resistivities of the samples under investigation.

Sample	Si cell temperature (°C)	Si content in Fe_3Si (%)	Layer thickness (nm)	Misfit (%)	Order parameters α to Fe (B)	Order parameters β to Fe (A, C)	Relaxation z Å	Resistivity (μΩ cm)
1	1395	25.5	32.6	−0.06	0	0.3	0.14	23
2	1390	22.5	28.4	0.15	0.25	0.28	0.06	50
3	1375	16.5	28.2	0.62	0.25	0.5	0.08	103

teractions with reduced crystal symmetry for certain Fe sublattices in ordered Fe_3Si on GaAs.[18]

Our aim in the present work is the determination of long range order in thin Fe_3Si films by grazing incidence x-ray diffraction (GID) measurements. We use the same measurements for a precise determination of position of the Fe_3Si unit cell with respect to the GaAs substrate. We utilize the method of grazing incidence diffraction that is ideally suited for thin film investigation, since it gives access even to those reflections that cannot be measured by conventional diffraction methods.

II. EXPERIMENTAL

The Fe_3Si films were grown by solid source molecular beam epitaxy (MBE). The GaAs(001) templates were prepared in a separate III-V growth chamber using standard GaAs growth techniques. The sample was then transferred into an As-free chamber through UHV for the Fe_3Si deposition. The Fe_3Si layers were grown[6] on the As-rich GaAs surface at 200 °C with a growth rate of 24 nm h^{-1}. The Si cell temperature was varied in order to obtain different degrees of stoichiometry of the films. The Si content of the film was obtained[6] from the position of the Fe_3Si layer peak on the x-ray diffraction curve. For the present study, we have chosen three samples with different Si contents; see Table I. Samples 1 and 2 are nearly stoichiometric, sample 1 with a small Si surplus, sample 2 with a slight Fe excess. Sample 3 is clearly nonstoichiometric.

The x-ray measurements were performed at the wiggler beamline U125/2 KMC (PHARAO) at the storage ring BESSY in Berlin, Germany. A double crystal Si(111) monochromator was used. The energy of the radiation was 10 keV. A six-circle x-ray diffractometer[19] was used for grazing incidence diffraction measurements. The incidence angle was 1.2°. The acceptance angle of the detector was 0.1° perpendicular to the surface and 1° (open slits) parallel to the surface. Additional conventional coplanar x-ray diffraction measurements were made using a Panalytical X-Pert system with Ge (220) hybrid monochromator and CuKα_1 radiation.

III. THEORY

The stoichiometric compound Fe_3Si possesses three types of reflections. Fundamental reflections, which are not influenced by disorder, are given by $H+K+L=4n$, where n is an integer and (HKL) are the Miller indices of the diffracting net planes. The structure amplitude of these reflections is

$$F_0 = 4(f_{Si} + 3f_{Fe}), \tag{1}$$

where f_{Si} and f_{Fe} are the atomic scattering factors of the respective elements.

The disorder is described by two order parameters α and β, which are fractions of Si atoms occupying the Fe(B) and Fe(A,C) sites, respectively. There are two distinct types of superlattice reflections.[9] Reflections with odd H,K,L are sensitive to both types of disorder, the structure amplitude being

$$F_1 = 4i(1 - 2\alpha - \beta)(f_{Si} - f_{Fe}). \tag{2}$$

Reflections given by $H+K+L=2n$ (where n is an integer) are sensitive to disorder in the Fe(A,C) sublattice,

$$F_2 = -4(1 - 2\beta)(f_{Si} - f_{Fe}). \tag{3}$$

In order to obtain the order parameters α and β, we measure diffraction curves of all three types of reflections and fit them by dynamical diffraction calculations. They are obtained for each sample by a simultaneous fit of the diffracted intensities of all the measured Fe_3Si peaks. The epitaxial layers themselves are thin enough and their diffraction peaks can be well fitted in the kinematical approximation. However, we want to fit simultaneously the layer and the substrate peaks, the latter serving as an internal reference to obtain the absolute values of the structure amplitudes (1)–(3). The dynamical calculation automatically solves this problem.

The dynamical diffraction theory for layer structures is well established, and we use the well-known algorithm described in Ref. 20 and references therein. One point of the dynamical calculations needs a special discussion. The scattering properties of each layer are described by the Fourier components of the polarizability $\chi_{\mathbf{H}}$. In the computer programs for the analysis of x-ray diffraction experiments available so far, the coefficients $\chi_{\mathbf{H}}$ are considered as eigenproperties of each layer. That means that the origin of the unit cell to calculate $\chi_{\mathbf{H}}$ is chosen independently for each layer, usually according to the symmetry of the respective layer. The phase factor $\exp(i\mathbf{H}\cdot\mathbf{R})$ that arises if the origin is shifted by a real-space distance $\mathbf{R}$ is not taken into consideration. Such a phase factor does not appear if all epitaxial layers have a similar structure (an AlAs/GaAs superlattice would be a simple example). However, if the structures are different, the relative positions of the unit cells are not known in advance and an additional phase factor in the polarizability of one layer with respect to another may appear.

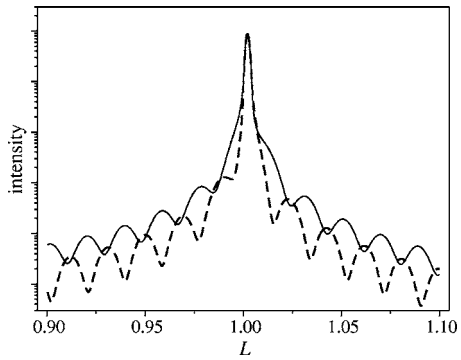

FIG. 2. Calculated CTRs at the 111 reflection from a stoichiometric fully ordered Fe_3Si layer (30 nm thick) on GaAs(001) for the lattice registry shown in Fig. 1 (full line) and for the case of the Fe_3Si structure shifted by 1/2 of the unit cell in the (100) direction (broken line).

The problem is resolved by choosing a common origin for all structures. This is a commonplace in surface diffraction,[21,22] but not taken into consideration in practical dynamical diffraction calculations. Figure 2 shows the influence of the relative shift of the crystal lattices on the diffraction curves. We compare a crystal truncation rod (CTR) scan at the 111 reflection calculated for relative positions of the Fe_3Si and GaAs lattices shown in Fig. 1 with the same scan for the case when the Fe_3Si lattice is shifted by 1/2 of the unit cell in the interfacial plane. The corresponding shift of the layer thickness oscillations is obvious. Thus, we have included the relative positions of the layer and the substrate crystal lattices in the fits to obtain the registry of the layer on the substrate. The z component (normal to the interface) of the shift is a relaxation at the interface. A similar analysis is commonly performed in x-ray surface structure studies to obtain the registry of a reconstructed layer with respect to the bulk structure, but has not been applied to studies of epitaxial layers so far.

IV. RESULTS

Figure 3 combines CTR scans performed on sample 1 at different bulk reflections. The width of the GaAs substrate peak is limited by the resolution of the experimental setup. The Fe_3Si layer peak is broadened due to the small thickness of the layer, and evidencing periodic side maxima thanks to the high quality of its top and bottom interfaces (see Table I). The layer peak is fairly close to the substrate peak, indicating that the sample is nearly stoichiometric. The 004 and 022 reflections are not sensitive to disorder. The 002 and 222 reflections are influenced by disorder in the Fe(A,C) sublattice, see Eq. (3), and the 111, 311, and 113 reflections are sensitive to disorder in both sublattices Fe(B) and Fe(A,C), as given by Eq. (2). A well-pronounced Fe_3Si layer reflection in all these scans indicates a high degree of long-range structural order in the layer.

All measured curves were fitted simultaneously by the dynamical diffraction calculations. We obtain the order parameters α and β from the relative intensities of the layer peaks (with the substrate peak serving as an internal reference), the layer thickness from the oscillation period and the registry of the lattices from the phase of the oscillations. The order parameters are found to be $\alpha=0$ and $\beta=0.3$ (see Table I) with an accuracy of ± 0.05. Thus, the as-grown Fe_3Si layer of sample 1 is not fully ordered, although it is nearly stoichiometric. Approximately 30% of Si has left its sublattice D and exchanged with the Fe(A,C) atoms. The Si atoms did not exchange with Fe(B) atoms. This is an unexpected result, since in Fe_3Si powder samples an excess of Si was found to replace the Fe(B) sites.[9–11]

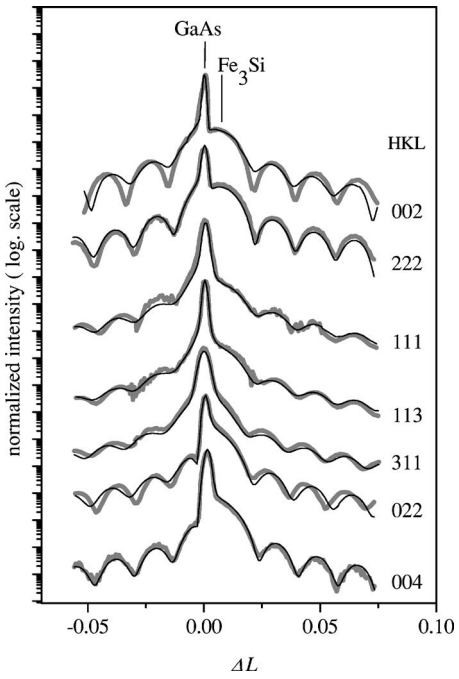

FIG. 3. Measured (thicker gray lines) and fitted (fine black lines) CTRs of sample 1 near different reciprocal lattice points. The fits of all curves are performed simultaneously with one and the same set of parameters. The sample is nearly stoichiometric with a slight surplus of Si and exhibits an ordered structure with some disorder due to the migration of Si atoms into the Fe(A,C) sublattice. The coordinate L along the CTRs has its origin at the respective GaAs peak.

From the positions of the intensity oscillations, we find that the Fe_3Si and GaAs lattices are positioned with respect to each other, as shown schematically in Fig. 1, i.e., the Fe(A) atoms at the positions of Ga atoms. The Fe_3Si unit cell is found to be shifted up vertically along z by 0.14Å with respect to the GaAs unit cell. No signatures of an interface reconstruction are found.

Figure 4 shows the CTR scans of sample 2. The Fe_3Si film of sample 2 contains 22.55% Si, i.e., it is nearly stoichiometric with a small deficit of Si. The fundamental 022 and 004 reflections are similar to those of sample 1, as expected. A large amplitude of the thickness oscillations in the 002 reflection and weak contrast in the 111 reflection indicates that the disorder mainly involves the order parameter α. The simultaneous fit of all experimental curves gives $\alpha=0.25$ and $\beta=0.28$ with an accuracy of ± 0.05. Thus, sample 2 still shows some long-range order with considerable disorder. In this case about 25% of the Si atoms migrate into the

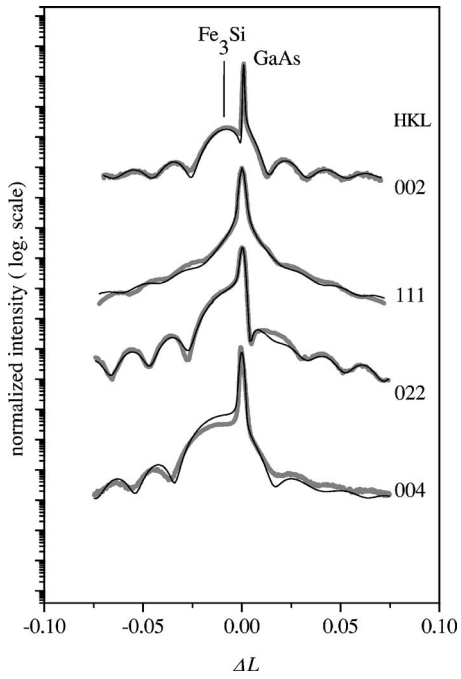

FIG. 4. Measured (thicker gray lines) and fitted (fine black lines) CTRs of sample 2 near different reciprocal lattice points. The sample is nearly stoichiometric with a slight excess of Fe. Long-range order is found as well. In contrast to sample 1, the misfit is of opposite sign, and the Si atoms migrate to all the Fe sublattices.

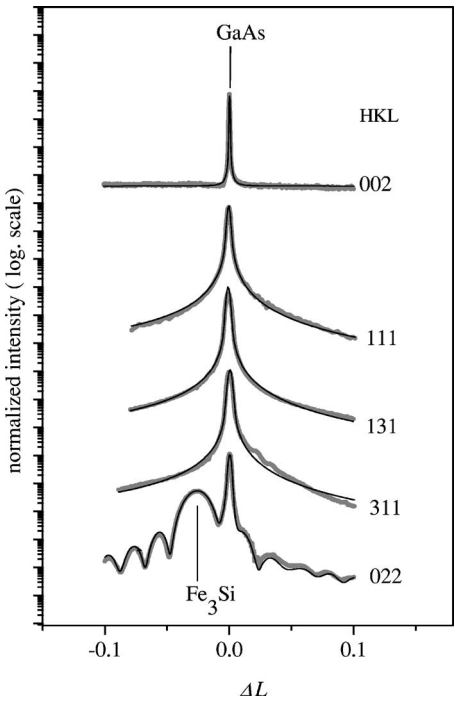

FIG. 5. Measured (thicker gray lines) and fitted (fine black lines) CTRs of sample 3 near different reciprocal lattice points. The sample is nonstoichiometric and exhibits a highly disordered structure.

Fe(B) sublattice, whereas 28% of the Si atoms migrate into the Fe(A,C) sublattices.

Figure 5 shows analogous scans of sample 3. The film contains only 16.5% Si, i.e., it is highly nonstoichiometric. The fundamental reflection 022 shows the layer peak with the adjacent thickness oscillations. All the measured superlattice reflections (002, 111, 131, and 311) of the layer vanish and only the GaAs substrate peaks remain. The fits to the experimental curves give $\alpha=0.25$ and $\beta=0.5$, i.e., a complete intermixing of Fe and Si in the sublattices. The film does not show any long-range order.

Thus, the long-range order in Fe_3Si epitaxial layers strongly depends on their stoichiometry. Near stoichiometry the layers are ordered. It is important to note that the almost complete long-range order is observed without additional thermal treatment, which is usually required for the preparation of bulk samples. The slight remaining disorder may be due to the relatively low growth temperature, which has been chosen to avoid the possible intermixing of Fe and/or Si with Ga and/or As at the ferromagnet/semiconductor interface. Figure 6 illustrates the resistivity R_S of several Fe_3Si films measured at 77 K as a function of the composition. The parameter x is the deviation from stoichiometric composition. Samples investigated in the present work by grazing incidence diffraction are marked by full circles. The ordered Fe_3Si films (samples 1 and 2) have a lower resistivity R_S than the fully disordered film (see also Table I). Sample 1, which exhibits the highest order, has the smallest R_S, indicating that the alloy scattering is indeed an important factor.

V. SUMMARY

In conclusion, we analyzed MBE-grown Fe_3Si films on GaAs using grazing incidence x-ray diffraction. We characterized the relative positions of the film and the substrate lattices as well as the long-range order in films with different stoichiometry. The Fe(A) atoms are positioned above the Ga atoms, as shown in Fig. 1. The Fe_3Si lattice is shifted with

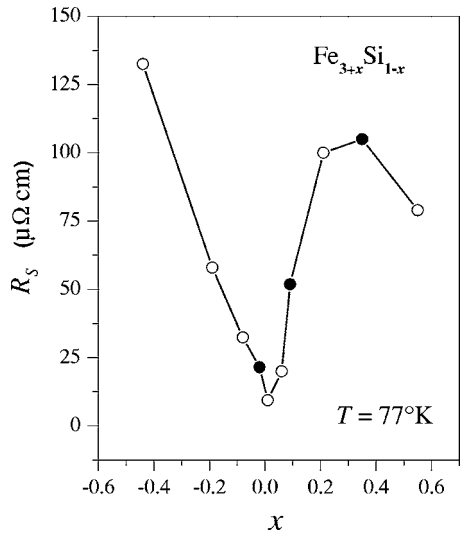

FIG. 6. Resistivity R_S of several Fe_3Si films measured at 77 K as a function of the deviation x from stoichiometric composition. The three samples investigated by grazing incidence diffraction are marked by full circles.

respect to the GaAs lattice by 0.1 ± 0.04 Å normal to and away from the interface. Long-range order is observed in the nearly stoichiometric as-grown films without additional thermal treatment, which seems to be required for the preparation of bulk samples. A slight deficit of Fe in the epitaxial Fe_3Si layer leads to the intermixing of Si and Fe from the Fe(A,C) sites. A small excess of Fe gives rise to the intermixing of Si and Fe on all the Fe sublattices. Better long-range order in the Fe_3Si films leads to lower resistivity R_S.

ACKNOWLEDGMENTS

The authors thank Sergey Stepanov (Argonne National Laboratory) for a helpful discussion and L. Däweritz for a critical reading of the manuscript. Part of this work was sponsored by the Bundesministerium für Bildung und Forschung of the Federal Republic of Germany.

*Electronic address: jen@pdi-berlin.de

[1] G. A. Prinz, Science **54**, 17638 (1996).
[2] S. J. Hashemifar, P. Kratzer, and M. Scheffler, Phys. Rev. Lett. **94**, 096402 (2005).
[3] M. Hong, H. S. Chen, J. Kwo, A. R. Kortan, J. P. Mannaerts, B. E. Weir, and L. C. Feldman, J. Cryst. Growth **111**, 984 (1991).
[4] S. H. Liou, S. S. Malhotra, J. X. Shen, M. Hong, J. Kwo, H. S. Chen, and J. P. Mannaerts, J. Appl. Phys. **73**, 6766 (1993).
[5] A. Ionescu, C. A. F. Waz, T. Trypiniotis, C. M. Gürtler, H. Garcia-Miquel, J. A. C. Bland, M. E. Vickers, R. M. Dalgliesh, C. Langridge, Y. Bugoslavsky, Y. Miyoshi, L. F. Cohen, and K. R. A. Ziebeck, Phys. Rev. B **71**, 094401 (2005).
[6] J. Herfort, H.-P. Schönherr, and K. H. Ploog, Appl. Phys. Lett. **83**, 3912 (2003).
[7] Y. Nakamura, *Landolt-Börnstein New Series III/19c* (Springer-Verlog, Berlin, Germany, 1988).
[8] A. Kawaharazuka, M. Ramsteiner, J. Herfort, H.-P. Schönherr, H. Kostial, and K. H. Ploog, Appl. Phys. Lett. **85**, 3492 (2004).
[9] V. Niculescu, K. Raj, J. I. Budnick, T. J. Burch, W. A. Hines, and A. H. Menotti, Phys. Rev. B **14**, 4160 (1976).
[10] W. A. Hines, A. H. Menotti, J. I. Budnick, T. J. Burch, T. Litrenta, V. Niculescu, and K. Raj, Phys. Rev. B **13**, 4060 (1976).
[11] T. J. Burch, T. Litrenta, and J. I. Budnick, Phys. Rev. Lett. **33**, 421 (1974).
[12] N. I. Kulikov, D. Fristot, J. Hugel, and A. V. Postnikov, Phys. Rev. B **66**, 014206 (2002).
[13] R. A. de Groot, F. M. Müller, P. G. van Engen, and K. H. J. Buschow, Phys. Rev. Lett. **50**, 2024 (1983).
[14] V. Niculescu, T. J. Burch, and J. I. Budnick, J. Magn. Magn. Mater. **39**, 223 (1983).
[15] J. Kudrnovsky, N. E. Christensen, and O. K. Andersen, Phys. Rev. B **43**, 5924 (1991).
[16] S. Pickart, T. Litrenta, T. J. Burch, and J. I. Budnick, Phys. Lett. **53**, 321 (1975).
[17] J. Herfort, H.-P. Schönherr, K.-J. Friedland, and K. H. Ploog, J. Vac. Sci. Technol. B **22**, 2073 (2004).
[18] M. Bowen, K. -J. Friedland, J. Herfort, H.-P. Schönherr, and K. H. Ploog, Phys. Rev. B **71**, 172401 (2005).
[19] B. Jenichen, W. Braun, V. M. Kaganer, A. G. Shtukenberg, L. Däweritz, C. G. Schulz, and K. H. Ploog, Rev. Sci. Instrum. **74**, 1267 (2003).
[20] S. A. Stepanov, E. A. Kondrashkina, R. Köhler, D. V. Novikov, G. Materlik, and S. M. Durbin, Phys. Rev. B **57**, 4829 (1998).
[21] R. Feidenhans'l, Surf. Sci. Rep. **10**, 105 (1989).
[22] I. K. Robinson and D. J. Tweet, Rep. Prog. Phys. **55**, 599 (1992).

Magnetic anisotropy and resonance linewidth of Fe_3Si/GaAs(001)

K. Lenz[*1], **E. Kosubek**[1], **K. Baberschke**[1], **J. Herfort**[2], **H.-P. Schönherr**[2], and **K. H. Ploog**[2]

[1] Institut für Experimentalphysik, Freie Universität Berlin, Arnimallee 14, D-14195 Berlin, Germany
[2] Paul-Drude-Institut für Festkörperelektronik, Hausvogteiplatz 5-7, D-10117 Berlin, Germany

Key words Fe_3Si/GaAs(001), Magnetic anisotropy, Ferromagnetic resonance, Linewidth
PACS 76.50.+g, 75.30.Gw, 75.50.Bb, 75.70.Ak

The magnetic anisotropy energy and the resonance linewidth of epitaxial Fe_3Si grown on GaAs(001) is studied by ferromagnetic resonance (FMR) technique. For a nearly stoichiometric sample (25.5% Si-content) a clear fourfold anisotropy is observed which is modulated by a small contribution of an uniaxial in-plane anisotropy. This uniaxial component is found to increase with the Fe concentration in the intermetallic compound. The samples show an exceptional narrow resonance linewidth of only 17 Oe at 9 GHz excitation frequency confirming the very high structural quality.

1 Introduction

The major criterion for a successful combination of ferromagnets (FM) with semiconductor (SC) substrates like GaAs, InAs, or Si is the epitaxial growth [1], while in terms of applicability the decisive factors are of course the magnetic properties. A promising candidate is the intermetallic compound Fe_3Si which is of cubic $D0_3$ structure resembling a binary Heusler alloy [2–5]. This structure is almost lattice matched to the GaAs(001) substrate yielding the desired epitaxial growth and high interfacial perfection [3]. The FM/SC interface of Fe_3Si/GaAs(001) is thermally stable up to 700 K [6]. Moreover, a known feature of Heusler alloys is their high Curie temperature which is 840 K in this case [7].

The Fe_3Si/GaAs(001) samples have been prepared by molecular beam epitaxy (MBE) as described elsewhere [4]. The epitaxial growth was monitored *in situ* by reflection high-energy electron diffraction and the high structural quality was confirmed by double crystal x-ray diffraction measurements [4]. In the following, two samples (A and B) with different thickness (39 nm and 33 nm, respectively) and different Si content of 25.5% Si for sample A and 16.5% for sample B are discussed. Magnetic hysteresis loops recorded using superconducting quantum interference device magnetometry have shown a slight non-equivalence for the [110] and [$\bar{1}$10] in-plane directions depending on the Fe concentration of the compound [4]. To clarify and to study this in detail, ferromagnetic resonance (FMR) experiments were carried out.

2 Experimental results and discussion

The FMR experiments were performed with ν= 1.1, 4.1 and 9.2 GHz microwave frequency at ambient temperature. The measurements at three different frequencies allow for cross-checking the obtained anisotropy values. The FMR signal has been detected as a function of the orientation of the externally applied static magnetic field **H**. For this, the sample has been rotated either in the film plane, varying the azimuth φ_H with the [100] axis being the origin. Or the sample has been rotated in the vertical plane spanned by [001] ($\theta_H = 0°$) and [110] axis, i.e. varying the polar angle θ_H keeping φ_H fixed at 45°. The corresponding angles

* Corresponding author: e-mail: babgroup@physik.fu-berlin.de, Phone: +00 49 30 838-53342, Fax: +00 49 30 838-53646

of the magnetization $\mathbf{M}$ are θ and φ. From the angular dependent measurement of the resonance field the anisotropy fields can be determined by applying the Smit and Beljers [8] formalism using the free energy density F given by

$$\begin{aligned} F &= -MH[\sin\theta\sin\theta_H\cos(\varphi-\varphi_H)+\cos\theta\cos\theta_H]-(2\pi M^2-K_{2\perp})\sin^2\theta \\ &\quad -K_{2\parallel}\sin^2\theta\cos^2(\varphi-45^\circ)-\frac{1}{2}K_{4\perp}\cos^4\theta-\frac{1}{8}K_{4\parallel}(3+\cos 4\varphi)\sin^4\theta. \end{aligned} \quad (1)$$

The individual terms correspond to the Zeeman energy, $K_{2\perp}$ ($K_{2\parallel}$) are the uniaxial out-of-plane (in-plane) anisotropy constants, and $K_{4\parallel}$ and $K_{4\perp}$ are the fourfold anisotropy constants, respectively. The shape anisotropy enters with $2\pi M^2$ leading to an effective magnetization of $4\pi M_{\rm eff} = 4\pi M - 2K_{2\perp}/M$. The resulting rather long resonance equations can be found elsewhere [9].

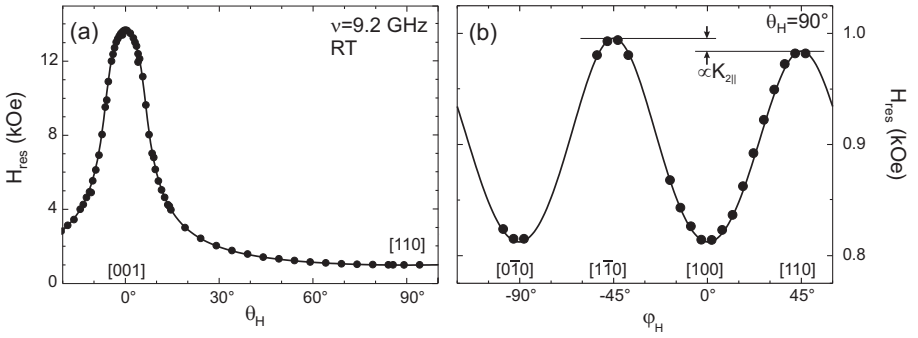

Fig. 1 a) Polar and b) azimuthal angular dependence of the resonance field for sample A. Measurements were done at ν= 9.2 GHz and ambient temperature. The solid lines are fits according to the resonance equation. The crystallographic directions are given in square brackets.

In Fig. 1 the polar and azimuthal angular dependence of the resonance field $H_{\rm res}$ of sample A measured at ν= 9.2 GHz is shown. The solid lines are fits according to the resonance equation. From Fig. 1a the effective magnetization can be well determined. The fit yields $4\pi M_{\rm eff}$= 10.1 kOe. The positive value denotes a hard axis of magnetization along the sample's normal, i.e. the [001] direction. The easy axis of magnetization can be deduced from the in-plane angular dependence. In Fig. 1b a 90-degree symmetry of the fourfold anisotropy is obvious with the in-plane <100> being the easy axes. But there is a small uniaxial in-plane contribution superimposed on that, visible by the lower lying maximum in [110] direction. This means, that the easy axis of $K_{2\parallel}$ is rotated by 45° with respect to the easy axis of $K_{4\parallel}$. The fourfold anisotropy field is $K_{4\parallel}/M$= 47 Oe and the uniaxial in-plane anisotropy field corresponds to $K_{2\parallel}/M$= 3 Oe for sample A. Thus, the <110> in-plane directions are intermediate axes.

In Fig. 2 the corresponding measurements on sample B are shown. Here, a smaller microwave frequency of ν= 4.1 GHz was used which shifts the resonance fields to lower values. Moreover, two resonance modes are observable now. The solid symbols depict the saturated resonance mode, where the static magnetic field and the magnetization are aligned parallel and the open symbols correspond to the unsaturated mode, where $\mathbf{M}$ is no more aligned along the direction of $\mathbf{H}$. Due to the lower excitation frequency the minima in the azimuthal angular dependence (Fig. 2b) are missing. Nevertheless, it is still possible to extract the anisotropy fields from the fit curves. Compared with sample A the uniaxial contribution in sample B is strongly increased, leading to a 5 times larger uniaxial in-plane anisotropy field of $K_{2\parallel}/M$= 16 Oe, although the Fe content is only 12% higher in sample B. The other anisotropy contributions have increased only by 30 to 50%. Table 1 summarizes the anisotropy fields of both samples determined by FMR. The value of the fourfold anisotropy field for sample A is in good agreement to the bulk value of 55 Oe [10] or the value determined by Ionescu *et al.* for a 21 nm thick stoichiometric sample [5]. In contrast, the uniaxial in-plane anisotropy is by a factor of 10 larger than the value found by Ionescu. For pure Fe/GaAs(001)

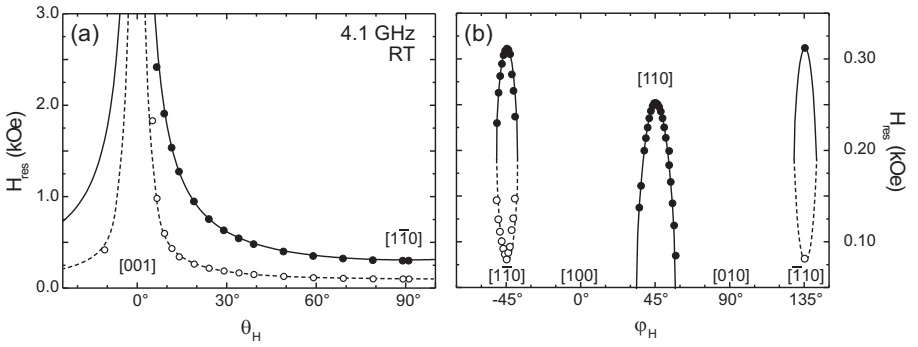

Fig. 2 (a) Polar and azimuthal angular dependence of the resonance field for sample B measured at ν= 4.1 GHz. The solid circles depict the position of the saturated mode, open circles depict the unsaturated mode. The solid lines are fits, whereas dashed lines are guides to the eye only.

Table 1 Anisotropy fields of the 39 and 33 nm thick samples A and B. The Fe_3Si bulk-value is $K_{4\|}/M$= 55 Oe [10].

	$4\pi M - 2K_{2\perp}/M$	$K_{2\|}/M$	$K_{4\perp}/M$	$K_{4\|}/M$
sample A (25.5% Si)	10.10(2)	3(1)	-20(3)	47(1)
sample B (16.5% Si)	13.50(2)	16(1)	0(1)	70(1)

an even stronger and dominating $K_{2\|}$ contribution is well-known [11–14], where the origin of $K_{2\|}$ is an anisotropic Fe-As bonding structure of the FM/SC interface [13, 14].

The resonance linewidth is the manifestation of the damping of the precessional motion of $\mathbf{M}$. It's angular dependence can be written as [15]:

$$\Delta H_{pp}(\theta) = \left|\frac{\partial H_{\rm res}}{\partial \theta}\right| \Delta\theta + \frac{2}{\sqrt{3}}\frac{G}{\gamma^2 M}\frac{\omega}{\cos(\theta - \theta_H)}, \tag{2}$$

where the first term describes the mosaicity of the sample, i.e. some in-plane spread of the crystallographic axes, and the second term is the intrinsic Gilbert damping with the Gilbert damping constant G and γ being the gyromagnetic ratio. Fig. 3 shows the polar angular dependence of $\Delta H_{\rm pp}$ for sample A measured

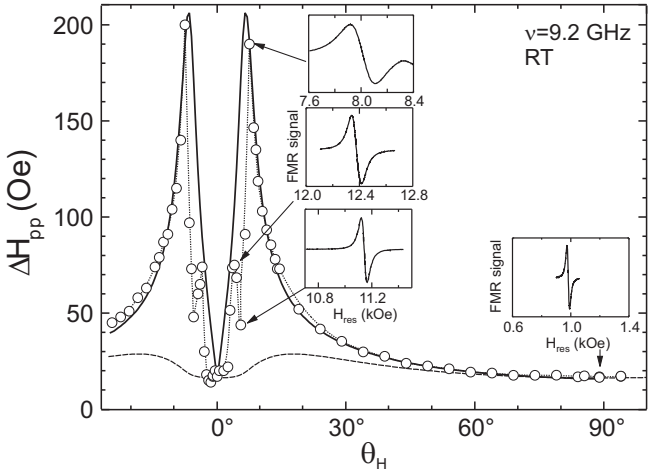

Fig. 3 Polar angular dependence of the resonance linewidth for sample A. The solid curve is a fit according to Eq. (2) with the parameters G= 0.6×10^8 s^{-1} and $\Delta\theta_H$= 0.14°. The dashed line is the contribution due to Gilbert-damping only. The dotted line is a guide to the eye. The insets show the FMR signal of selected data points marked with an arrow.

at 9 GHz. The insets show FMR spectra taken at different angles marked with arrows. For θ_H= 90° the linewidth is as small as $\Delta H_{\rm pp}$= 17 Oe (sample A) and 13 Oe (sample B, not shown), which is even

smaller than what is known for pure Fe [16–19]. The solid line is a fit according to Eq. (2) with the parameters $\Delta\theta_H = 0.14^\circ$ and $G = 0.6\times10^8\ s^{-1}$. The very small angular spread below 0.5° is an indication of a very good epitaxial growth [20] and homogeneity of the samples. Since the Gilbert damping has a very weak angular dependence (dashed line) it is a minor contribution and an accurate determination of G should only be derived from the frequency dependence of G [21]. The fit describes the overall angular dependence quite well, although, there is an unusual deviation around $\theta_H = \pm5^\circ$. The decrease toward $\theta_H = 0$ is not monotonic as one would expect but the reason for this behavior is not fully understood. At least a superposition or crossing of two resonances can be ruled out, since this would broaden the linewidth, making the unperturbed line in turn even smaller.

3 Conclusions

The FMR has enabled us to determine precisely the various contributions of the anisotropy fields of epitaxial Fe_3Si/GaAs(001) hybrid structures. With increasing Fe content an uniaxial in-plane component appears. The samples show an exceptionally small linewidth of only 17 Oe and a very small mosaicity corroborating the high structural quality.

Acknowledgements This work was supported by the DFG (Sfb290 TP A2) and partly by BMBF (13N8255).

References

[1] G. A. Prinz, Phys. Today **48**, 282 (1998).
[2] S. H. Liou, S. S. Malhotra, J. X. Shen, M. Hong, J. Kwo, H. S. Chen, and J. P. Mannaerts, J. Appl. Phys. **73**, 6766 (1993).
[3] J. Herfort, H.-P. Schönherr, and K. H. Ploog, Appl. Phys. Lett. **83**, 3912 (2003).
[4] J. Herfort, H.-P. Schönherr, K.-J. Friedland, and K. H. Ploog, J. Vac. Sci. Technol. B **22**, 2073 (2004).
[5] A. Ionescu, C. A. F. Vaz, T. Trypiniotis, C. M. Gürtler, H. García-Miquel, J. A. C. Bland, M. E. Vickers, R. M. Dalgliesh, S. Langridge, Y. Bugoslavsky, Y. Miyoshi, L. F. Cohen, and K. R. A. Ziebeck, Phys. Rev. B **71**, 094401 (2005); A. Ionescu, C. A. F. Vaz, T. Trypiniotis, C. M. Gürtler, M. E. Vickers, H. García-Miquel, and J. A. C. Bland, J. Magn. Magn. Mater **286**, 72 (2005).
[6] J. Herfort, H.-P. Schönherr, A. Kawaharazuka, M. Ramsteiner, and K. H. Ploog, J. Cryst. Growth **278**, 666 (2005).
[7] Y. Nakamura, *Landolt-Börnstein, New Series III/19c* (Springer, Berlin, 1988), p. 26.
[8] J. Smit, H.-G. Beljers, Philips Res. Rep. **10**, 113 (1955).
[9] T. Toliński, K. Lenz, J. Lindner, E. Kosubek, K. Baberschke, D. Spoddig, and R. Meckenstock, Solid State Commun. **128**, 385 (2003).
[10] M. Goto and T. Kamimori, J. Phys. Soc. Jap. **52**, 3710 (1983).
[11] A. A. Veselov, A. G. Veselov, S. L. Vysotsky, A. S. Dzhumaliev, and Yu. A. Filimonov, Tech. Phys. **47**, 1067 (2002).
[12] M. Brockmann, M. Zölfl, S. Miethaner, and G. Bayreuther, J. Magn. Magn. Mater. **198-199**, 384 (1999); M. Zölfl, M. Brockmann, M. Köhler, S. Kreuzer, T. Schweinböck, S. Miethaner, F. Bensch, and G. Bayreuther, J. Magn. Magn. Mater. **175**, 16 (1997).
[13] R. Moosbühler, F. Bensch, M. Dumm, and G. Bayreuther, J. Appl. Phys. **91**, 8757 (2002).
[14] O. Thomas, Q. Shen, P. Schieffer, N. Tournerie, and B. Lépine, Phys. Rev. Lett. **90**, 017205 (2003).
[15] Yu. V. Goryunov, N. N. Garif'anov, G. G. Khaliullin, I. A. Garifullin, L. R. Tagirov, F. Schreiber, Th. Mühge, and H. Zabel, Phys. Rev. B **52**, 13450 (1995).
[16] S. M. Bhagat and M. S. Rothstein, Solid State Commun. **11**, 1535 (1972).
[17] S. A. Oliver, C. Vittoria, E. Schloemann, H. J. Van Hook, and R. W. Tustison, J. Appl. Phys. **63**, 3802 (1988).
[18] G. A. Prinz, G. T. Rado, and J. J. Krebs, J. Appl. Phys. **53**, 2087 (1982).
[19] Z. Celinski and B. Heinrich, J. Appl. Phys. **70**, 5935 (1991).
[20] T. Toliński and J. Baszyński, J. Phys. IV France **8**, Pr2-229 (1998).
[21] J. Lindner, K. Lenz, E. Kosubek, K. Baberschke, D. Spoddig, R. Meckenstock, J. Pelzl, Z. Frait, and D. L. Mills, Phys. Rev. B **68**, 060102(R) (2003).